

POLITECNICO DI MILANO

Scuola di Architettura Urbanistica Ingegneria delle  
Costruzioni

Corso di studi di Laurea Magistrale in Ingegneria dei  
Sistemi Edilizi



"Self-healing efficiency evaluation of UHPFRC  
enhanced with Crystalline Admixtures and  
Nanomaterials"

Relatore: Prof. Liberato Ferrara

Correlatore: Prof. Pedro Serna Ros

Tesi di Laurea:

Negrini Alberto

Matricola N° 873740

Anno accademico 2017/2018



*Per Aspera Ad Astra*





## Abstract

Concrete has a natural self-healing capability to seal small cracks, named autogenous healing, which is mainly produced by continuing hydration and carbonation. This capability is highly limited and is activated only when in direct contact with water. Studies published in the literature report that Ultra-High-Performance Fibre-Reinforced Concrete and Engineered Cementitious Composites are able to heal cracks for low damage levels, due to their cracking pattern with multiple micro-cracks and high cement content. While their superior self-healing behaviour compared to traditional concrete classes is frequently assumed, this study aims to have a direct comparison to move a step forward in durability quantification. In this research, reinforced beams of the size of  $150 \times 100 \times 750 \text{ mm}^3$  have been casted, made of traditional concrete, high-performance concrete and two types of ultra-high-performance concrete reinforced with steel fibres. In particular, these last two types of concretes have been studied incorporating crystalline admixtures and two different species of nanomaterials. All the beams were pre-cracked through a four-point bending test up to a fixed strain level in the tension zone, to allow the analysis of the effect of the different cracking patterns. Afterwards, water permeability tests were performed, before and after healing exposure, using as healing condition the immersion of the specimens in water for a period of 28 days. A modification of the water permeability test was also explored using chlorides to evaluate the potential protection of the healing in aggressive chloride-rich environments. The results show the superior durability and self-healing performance of Ultra-High-Performance Fibre-Reinforced Concrete elements.

## Sinossi

Il calcestruzzo è dotato di una naturale capacità di autoriparazione in grado di sigillare piccole fessure, chiamata autoguarigione autogena, la quale viene principalmente prodotta per continua idratazione e carbonatazione. Questa capacità è assai limitata e si attiva solo in contatto diretto con acqua. Gli studi pubblicati in letteratura riportano che Calcestruzzi Fibro-Rinforzati ad Ultra-Alta Resistenza e Compositi Cementizi Ingegnerizzati sono in grado di guarire le fessure per un basso livello di danno, grazie al loro modello di fessurazione caratterizzato da molteplici micro-fessure e alto contenuto di cemento. Mentre la loro superiore capacità di autoguarigione è considerata ormai assodata in comparazione alle classi di calcestruzzi ordinari, questo studio mira a realizzare un confronto diretto al fine di poter quantificare il loro grado di durabilità. In questo progetto sono state fabbricate travi armate della dimensione di 150×100×750 mm<sup>3</sup> con calcestruzzo tradizionale, calcestruzzo ad alta resistenza e due tipologie di calcestruzzi ad ultra-alta resistenza rinforzati con fibre di acciaio. In particolare, queste ultime due tipologie di calcestruzzi sono state studiate incorporando additivi cristallini e due diverse specie di nanomateriali. Tutte le travi sono state pre-fessurate mediante un test a flessione a quattro punti fino al raggiungimento di un livello fisso di deformazione nell'area soggetta a tensione, al fine di consentire l'analisi dell'effetto dei diversi modelli di fessurazione. Successivamente, sono stati realizzati test di permeabilità all'acqua, prima e dopo la fase di autoguarigione, utilizzando come condizione di guarigione l'immersione dei campioni in acqua per un periodo di 28 giorni. Infine, una modifica del test di permeabilità all'acqua è stata analizzata, usando cloruri al fine di valutare il grado di protezione garantito dall'autoguarigione in ambienti aggressivi. I risultati mostrano la superiore durabilità e capacità di autoguarigione dei Calcestruzzi Fibro-Rinforzati ad Ultra-Alta Resistenza.

## Resumen

El hormigón tiene una capacidad natural de autosanado para sellar pequeñas fisuras, llamada sanación autógena, que se produce principalmente por hidratación continua y carbonatación. Esta capacidad es muy limitada y se activa solo en contacto directo con el agua. Los estudios publicados en la literatura reportan que los materiales de Hormigón de Ultra Altas Prestaciones Reforzado con Fibras son capaces de sanar las fisuras para bajos niveles de daño, debido a su patrón con múltiples fisuras y alto contenido de cemento. Con frecuencia se asume su superior respuesta de autosanado en comparación con las clases de hormigones tradicionales. Este estudio pretende llevar a cabo una comparación directa entre estos tipos de hormigones para avanzar en la cuantificación de la durabilidad. En este trabajo se fabricaron vigas armadas con un tamaño de 150×100×750 mm<sup>3</sup>, fabricadas con hormigón tradicional, hormigón de alta resistencia y dos tipos de hormigón de ultra altas prestaciones reforzado con fibras de acero. Además, estos dos últimos tipos se estudiaron también incorporando aditivos cristalinos y dos tipos de nanoadiciones. Todas las vigas se prefisuraron mediante un ensayo a flexión a cuatro puntos hasta un nivel de deformación fijo en la zona de tensión, para permitir el análisis del efecto de los diferentes patrones de fisuras. Posteriormente, se realizaron ensayos de permeabilidad al agua, antes y después del proceso de autosanado, utilizando como condición de sanado la inmersión en agua durante 28 días. Además, se analizó una modificación del ensayo de permeabilidad al agua, utilizando cloruros para evaluar la potencial protección de la autocuración en ambientes agresivos ricos en cloruro. Los resultados demuestran la superior durabilidad y capacidad de autosanado de los elementos de Hormigón de Ultra Altas Prestaciones Reforzado con Fibras.

## Acknowledgements

First of all, I would like to thank my supervisor of Politecnico di Milano, Professor Liberato Ferrara, for the trust and the opportunity given to me to carry out this training period at the *Universitat Politècnica de València* (UPV). It has been an unforgettable period of my life, both for the professional and personal growth. I really appreciated the interest shown by prof. Ferrara on the performance of my work during the period abroad. I would also like to express my gratitude to my supervisor of Valencia, Professor Pedro Serna, who has always believed in me entrusting me with assignments of great importance. He approached me to the world of the research, working alongside me and giving to me the right advices during the whole project. I learned a lot from him and I owe him most of my current knowledge about concrete. Very important was the motivational ambience of all the investigation group of the Instituto de Ciencia y Tecnología del Hormigón (ICITECH) as well. Especially, I want to sincerely thank Marta Roig Flores for all her support, the advices and for having shared with me a great experience, namely, the attendance at the international “SARCOS” (Self-healing as preventive repair of concrete structures) PhD Meeting, organised in Novi Sad (Serbia) by the COST association, where the opportunity to present my thesis work was given to me. I would also like to thank Eduard Mezquida Alcaraz, a great workmate, for all the good time spend inside and outside the laboratory. And a big thanks to the laboratory technician Paco who helped me from the beginning in carrying out the experimental activities. A special thanks goes to my dear family who never stopped supporting me and encouraging me from Italy, and to my friends of course who have always been present. At last but not least, I want to thank two special people I met in Valencia who have always been by my side, Michelle and Olain. I would really like to thank them for everything because they have made of Valencia an unforgettable experience.

# Table of contents

Abstract .....	I
Sinossi .....	II
Resumen .....	III
Acknowledgements .....	IV
List of figures .....	VIII
List of tables.....	XIV
1. Introduction.....	1
1.1 Background .....	2
1.2 Objectives.....	2
1.3 Outline of the document .....	3
2. State of the art .....	4
2.1 Introduction to self-healing .....	4
2.2 Autogenous healing .....	5
2.2.1 Continuing hydration effect on autogenous healing .....	7
2.2.2 Carbonation effect on autogenous healing .....	8
2.2.3 Effect of various parameters on autogenous healing.....	10
2.3 Autonomous healing.....	17
2.3.1 Crystalline admixtures as healing agent .....	18
2.3.2 Comparison of autonomous healing methods .....	21
2.4 Experimental tests to evaluate self-healing .....	22
2.5 Nanomaterials in concrete technology.....	26
2.5.1 Nano-cellulose.....	26
2.5.2 Nano-alumina .....	29

3. Experimental phase.....	31
3.1 Introduction .....	31
3.2 Experimental program .....	32
3.3 Materials .....	34
3.3.1 Cement .....	35
3.3.2 Silica Fume.....	35
3.3.3 Water.....	36
3.3.4 Aggregates.....	38
3.3.5 Silica Flour .....	38
3.3.6 Superplasticizer .....	39
3.3.7 Fibres .....	40
3.3.8 Penetron Admix.....	40
3.3.9 Cellulose Nano-Crystals and Cellulose Nano-Fibres .....	42
3.3.10 Alumina Nano-Fibres.....	43
3.4 Methodology.....	44
3.4.1 Mix design .....	44
3.4.2 Mixing process.....	53
3.4.3 Compressive strength tests.....	55
3.4.4 Inverse analysis .....	56
3.5 Self-healing methodology .....	61
3.5.1 Preliminary tests.....	63
3.5.2 Pre-cracking.....	64
3.5.3 Cracks analysis.....	69
3.5.4 Sawing .....	71
3.5.5 High-pressure water permeability test .....	72

3.5.6 Low-pressure water permeability test.....	76
3.5.7 Chloride penetration test.....	77
3.5.8 Self-healing.....	80
4. Test results and discussion.....	82
4.1 Compressive strength results .....	82
4.2 Tensile strength results.....	85
4.3 Pre-cracking results.....	87
4.4 Cracks analysis results.....	92
4.5 High-pressure water permeability test results .....	96
4.6 Low-pressure water permeability test results.....	99
4.7 Chloride penetration test results.....	101
4.8 Outcomes after Self-healing .....	106
5. Conclusions and Future lines .....	112
5.1 Conclusions .....	112
5.2 Future lines .....	113
References.....	115
Appendix 1. Pre-cracking results .....	122
Appendix 2. Chloride penetration results .....	142

## List of figures

Figure 2–1. Processes causing autogenous healing (De Rooij et al., 2013) .....	7
Figure 2–2. Carbonation process in a crack produced in a water tank (Edvardsen, 1999) .....	9
Figure 2–3. Surface and diffusion healing process by carbonation (Edvardsen, 1999) .	10
Figure 2–4. Correlation between water flow and time for different crack widths (Edvardsen, 1999).....	14
Figure 2–5. Self-healing evolution for NSC and FRC samples (Desmettre & Charron, 2012).....	15
Figure 2–6. Old healed crack and new cracks produced (Yang et al., 2009).....	15
Figure 2–7. Partial crack healing after water exposure (Qian et al., 2009).....	16
Figure 2–8. Process of release of the healing agent (left) and a broken microcapsule (right) (White et al., 2001).....	18
Figure 2–9. Comparison of permeability reduction achieved by different PRA (ACI Committee 212, 2010).....	19
Figure 2–10. Methodology procedure for self-healing evaluation (adapted from M. Roig Flores, 2018) .....	23
Figure 2–11. Correlation between water flow and crack area (a) and average crack width (b) for control concrete and concrete with crystalline admixtures (Roig-Flores et al., 2015) .....	24
Figure 2–12. CNF production process (Nippon Paper Group).....	27
Figure 2–13. CNC production process (CelluForce).....	28
Figure 3–1. Reinforced beam model .....	33
Figure 3–2. Experimental program.....	34
Figure 3–3. Binder materials and aggregates used in the UHPFRC mix.....	34
Figure 3–4. Cement used in concrete mix .....	35
Figure 3–5. Silica Fume used in UHPFRC mix .....	36
Figure 3–6. Fine and coarse silica sand used in UHPFRC mix.....	38
Figure 3–7. Silica Flour used in UHPFRC mix .....	39
Figure 3–8. Superplasticizer used in concrete mix.....	39



Figure 3–9. Fibres used in concrete mix.....	40
Figure 3–10. Crystalline Admixtures from Penetron used as addition in UHPFRC mix .	41
Figure 3–11. Dilution of Nanocellulose in tap water.....	43
Figure 3–12. Alumina Nano-Fibres from Nafen used as addition in concrete mix .....	43
Figure 3–13. Preparation of the materials for UHPFRC mixes .....	48
Figure 3–14. Casting into the moulds of base concrete HB3 with self-compacting property.....	52
Figure 3–15. Mini-cone workability test in UHPFRC base mixes.....	52
Figure 3–16. Lack of workability when using HB3 + 2.4% of Penetron Admix.....	53
Figure 3–17. Concrete cast into the moulds .....	55
Figure 3–18. Compressive strength test.....	56
Figure 3–19. Specimen size and degrees of freedom FPBT .....	57
Figure 3–20. Displacement measurement at mid-span by means of two LVDTs .....	58
Figure 3–21. Measurement of the distance of the crack from the mid-span (d) .....	58
Figure 3–22. Definition of the 4 key points on the experimental $\sigma - \delta$ curve .....	59
Figure 3–23. Constitutive model for UHPFRC proposed .....	60
Figure 3–24. Methodology procedure .....	62
Figure 3–25. Scheme of self-healing methodology .....	62
Figure 3–26. Shear crack appeared during pre-cracking.....	64
Figure 3–27. Reinforced beams with rebars and stirrups .....	65
Figure 3–28. Visible crack in the bending area.....	65
Figure 3–29. Displacement sensor used in the pre-cracking stage.....	66
Figure 3–30. DEMEC points glued to the beam to measure strain .....	67
Figure 3–31. DEMEC intervals displacement as a function of the load .....	68
Figure 3–32. Strain target for "large crack" and "small crack" .....	69
Figure 3–33. Crack Width Meter .....	70
Figure 3–34. PCE-MM200 Microscope .....	70
Figure 3–35. Sawing scheme .....	71
Figure 3–36. Specimens A and B obtained after sawing .....	72

Figure 3–37. Permeabilimeter used for performing high-pressure water permeability tests .....	73
Figure 3–38. High-pressure water permeability test methodology.....	74
Figure 3–39. Drops of water from a 0.05 mm crack during high-pressure water permeability test .....	75
Figure 3–40. Leakage of water from a side crack during the high-pressure water permeability test in a traditional concrete.....	75
Figure 3–41. Low-pressure water permeability test methodology.....	77
Figure 3–42. Chloride penetration test methodology.....	77
Figure 3–43. Specimen transversely sawn after chloride penetration test .....	78
Figure 3–44. Sawn specimens in oven to dry .....	79
Figure 3–45. Chloride penetration through the specimen thickness (HB4).....	79
Figure 3–46. Attempt of chloride penetration test with a HPC with 0.3 mm of crack width.....	80
Figure 3–47. Specimens in a tank of water during healing exposure .....	81
Figure 4–1. Broken sample after a compressive strength test .....	82
Figure 4–2. Average compressive strength H0, H1, HB3 and HB4 .....	83
Figure 4–3. Average compressive strength HB3 functionalized batches .....	84
Figure 4–4. Average compressive strength HB4 functionalized batches.....	84
Figure 4–5. Average tensile strength HB3 functionalized batches .....	87
Figure 4–6. Average tensile strength HB4 functionalized batches .....	87
Figure 4–7. UHPFRC Load-Displacement graph .....	88
Figure 4–8. UHPFRC Load-Strain graphs.....	89
Figure 4–9. Traditional concrete Load-Displacement graph .....	90
Figure 4–10. Traditional concrete Load-Strain graphs .....	90
Figure 4–11. Traditional concrete cracking pattern with few localized cracks .....	91
Figure 4–12. UHPFRC cracking pattern with multiple micro-cracks .....	91
Figure 4–13. Comparison between a crack of 0.01 mm in a UHPFRC and a crack of 0.1 mm in a traditional concrete at the same magnification (200X) .....	93
Figure 4–14. Panorama of a 0.01 mm UHPFRC crack.....	93

Figure 4–15. Crack closed before the healing exposure .....	96
Figure 4–16. Bottom of a UHPFRC specimen during a water permeability test in 2 bar pressure .....	97
Figure 4–17. Cracks made visible by the water permeability test .....	98
Figure 4–18. Specimens after low-pressure water permeability test .....	101
Figure 4–19. Visible chloride penetration in UHPFRC specimens after the spray of silver nitrate .....	101
Figure 4–20. Comparison between chloride penetration in HB3 and HB4 .....	102
Figure 4–21. Comparison between chloride penetration in HB3 and HB4 with addition of Penetron .....	103
Figure 4–22. Comparison between chloride penetration in HB3 and HB4 with addition of Penetron and Alumina Nano-Fibres .....	103
Figure 4–23. Comparison between chloride penetration in HB3 and HB4 with addition of Penetron and Cellulose Nano-Crystals .....	104
Figure 4–24. . Comparison between chloride penetration in HB3 and HB3 with addition of Penetron .....	105
Figure 4–25. Comparison between chloride penetration in HB4 and HB4 with addition of Penetron .....	105
Figure 4–26. Photo of chloride penetration taken with the optical microscope at a 200X magnification .....	106
Figure 4–27. Cracks closure detected in UHPFRCs after 28 days of healing exposure	107
Figure 4–28. Comparison between chloride penetration in HB3 before and after the healing exposure .....	109
Figure 4–29. Comparison between chloride penetration in HB4 before and after the healing exposure .....	109
Figure 4–30. Comparison between chloride penetration in HB3 with addition of Penetron (0.8%) before and after the healing exposure .....	110
Figure 4–31. Comparison between chloride penetration in HB3 with addition of Nanocellulose before and after the healing exposure .....	110

Figure 4–32. Comparison between chloride penetration in HB3 with addition of Penetron (1.6%) and Alumina Nano-Fibres before and after the healing exposure ...	111
Figure 4–33. Comparison between chloride penetration in HB4 with addition of Penetron (0.8%) and Cellulose Nano-Crystal before and after the healing exposure .	111
Figure 0–1. Load-displacement graph H0.....	122
Figure 0–2. Load-strain graph H0 Beam I .....	122
Figure 0–3. Load-strain graph H0 Beam II .....	123
Figure 0–4. Load-displacement graph H1.....	123
Figure 0–5. Load-strain graph H1 Beam III .....	124
Figure 0–6. Load-strain graph H1 Beam IV .....	124
Figure 0–7. Load-displacement graph HB3 .....	125
Figure 0–8. Load-strain graph HB3 Beam V.....	125
Figure 0–9. Load-strain graph HB3 Beam VI.....	126
Figure 0–10. Load-displacement graph HB4 .....	126
Figure 0–11. Load-strain graph HB4 Beam VII.....	127
Figure 0–12. Load-strain graph HB4 Beam VIII.....	127
Figure 0–13. Load-displacement graph HB3 + Penetron (0.8%) .....	128
Figure 0–14. Load-strain graph HB3 + Penetron (0.8%) Beam IX.....	128
Figure 0–15. Load-strain graph HB3 + Penetron (0.8%) Beam X.....	129
Figure 0–16. Load-displacement graph HB3 + NAFEN (0.25%) + Penetron (0.8%) .....	129
Figure 0–17. Load-strain graph HB3 + NAFEN (0.25%) + Penetron (0.8%) Beam XI ....	130
Figure 0–18. Load-strain graph HB3 + NAFEN (0.25%) + Penetron (0.8%) Beam XII ...	130
Figure 0–19. Load-displacement graph HB3 + NAFEN (0.25%) + Penetron (1.6%) .....	131
Figure 0–20. Load-strain graph HB3 + NAFEN (0.25%) + Penetron (1.6%) Beam XIII ..	131
Figure 0–21. Load-strain graph HB3 + NAFEN (0.25%) + Penetron (1.6%) Beam XIV ..	132
Figure 0–22. Load-displacement graph HB3 + CNF/CNC (0.15%) .....	132
Figure 0–23. Load-strain graph HB3 + CNF/CNC (0.15%) Beam XV.....	133
Figure 0–24. Load-strain graph HB3 + CNF/CNC (0.15%) Beam XVI.....	133
Figure 0–25. Load-displacement graph HB3 + CNF/CNC (0,15%) + Penetron (0,8%) ..	134

Figure 0–26. Load-strain graph HB3 + CNF/CNC (0.15%) + Penetron (0.8%) Beam XVII .....	134
Figure 0–27. Load-strain graph HB3 + CNF/CNC (0.15%) + Penetron (0.8%) Beam XVIII .....	135
Figure 0–28. Load-displacement graph HB3 + CNC (0,15%) + Penetron (0,8%) .....	135
Figure 0–29. Load-strain graph HB3 + CNC (0.15%) + Penetron (0.8%) Beam XIX.....	136
Figure 0–30. Load-strain graph HB3 + CNC (0.15%) + Penetron (0.8%) Beam XX.....	136
Figure 0–31. Load-displacement graph HB4 + Penetron (0,8%) .....	137
Figure 0–32. Load-strain graph HB4 + Penetron (0.8%) Beam XXI.....	137
Figure 0–33. Load-strain graph HB4 + Penetron (0.8%) Beam XXII.....	138
Figure 0–34. Load-displacement graph HB4 + NAFEN (0,25%) + Penetron (0,8%) .....	138
Figure 0–35. Load-strain graph HB4 + NAFEN (0,25%) + Penetron (0,8%) Beam XXIII	139
Figure 0–36. Load-strain graph HB4 + NAFEN (0,25%) + Penetron (0,8%) Beam XXIV	139
Figure 0–37. Load-displacement graph HB4 + CNC (0,15%) + Penetron (0,8%) .....	140
Figure 0–38. Load-strain graph HB4 + CNC (0,15%) + Penetron (0,8%) Beam XXV .....	140
Figure 0–39. Load-strain graph HB4 + CNC (0,15%) + Penetron (0,8%) Beam XXVI ....	141
Figure 0–1. Self-healing outcome HB3 .....	142
Figure 0–2. Self-healing outcome HB4 .....	143
Figure 0–3. Self-healing outcome HB3 + Penetron (0.8%) .....	143
Figure 0–4. Self-healing outcome HB3 + NAFEN (0.25) + Penetron (0.8%) .....	144
Figure 0–5. Self-healing outcome HB3 + NAFEN (0.25) + Penetron (1.6%) .....	145
Figure 0–6. Self-healing outcome HB3 + CNF/CNC (0.15%) .....	145
Figure 0–7. Self-healing outcome HB3 + CNF/CNC (0.15%) + Penetron (0.8%) .....	146
Figure 0–8. Self-healing outcome HB3 + CNC (0.15%) + Penetron (0.8%) .....	146
Figure 0–9. Self-healing outcome HB4 + Penetron (0.8%) .....	147
Figure 0–10. Self-healing outcome HB4 + NAFEN (0.25%) + Penetron (0.8%).....	148
Figure 0–11. Self-healing outcome HB4 + CNC (0.15%) + Penetron (0.8%) .....	148

## List of tables

Table 1. Classification of known autonomous healing mechanisms (adapted from M. Roig Flores, 2018) .....	17
Table 2. Summary of advantages and disadvantages of autonomous healing mechanisms (adapted from M. Roig Flores, 2018) .....	22
Table 3. Summary of advantages and disadvantages of methods to evaluate self-healing (adapted from Ferrara et al., 2018) .....	26
Table 4. H0 Conventional Concrete mix design.....	44
Table 5. H1 High Performance Concrete mix design .....	44
Table 6. Base HB3 mix design .....	45
Table 7. Base HB4 mix design .....	45
Table 8. Control group mix design.....	45
Table 9. Comparison between HB3 and HB4 composition .....	46
Table 10. Batches casted with the addition of functionalities .....	47
Table 11. HB3 + 0.8% Penetron .....	48
Table 12. HB3 + 0.8% Penetron + NAFEN 0.25% .....	49
Table 13. HB3 + 1.6% Penetron + NAFEN 0.25% .....	49
Table 14. HB3 + CNF/CNC 0.15% .....	49
Table 15. HB3 + 0.8% Penetron + CNF/CNC 0.15% .....	50
Table 16. HB3 + 0.8% Penetron + CNC 0.15% .....	50
Table 17. HB3 + 2.4% Penetron .....	50
Table 18. HB4 + 0.8% Penetron .....	51
Table 19. HB4 + 0.8% Penetron + NAFEN 0.25% .....	51
Table 20. HB4 + 0.8% Penetron + CNC 0.15% .....	51
Table 21. Inverse analysis formulation for slenderness ratio of 4.5 .....	61
Table 22. High-pressure water permeability preliminary test results .....	74
Table 23. Tensile strength results.....	86
Table 24. Control group crack analysis results .....	94
Table 25. HB3 mixes crack analysis results.....	94
Table 26. HB4 mixes crack analysis results.....	95

Table 27. High-pressure water permeability test results (UHPFRC) .....	97
Table 28. High-pressure water permeability test results (traditional and high-performance concrete).....	98
Table 29. Low-pressure water permeability test results.....	100
Table 30. Low-pressure water permeability test results after 28 days of healing exposure .....	107





# 1. Introduction

This Master of Science thesis, made on behalf of *Politecnico di Milano*, describes the research performed from October 2018 to March 2019, at the *Instituto de Ciencia y Tecnología del Hormigón* (ICITECH, Institute of Concrete Science and Technology) of the *Universitat Politècnica de València* (UPV, Polytechnic University of Valencia).

The investigation carried out is part of a wider project called "ReSHEALience" which involves a community of European researchers, deserving the financial support of the European Commission. The main goal of the project is to develop, by the year 2020, an Ultra High Durability Concrete and a Durability Assessment-based Design methodology for structures, to improve durability and predict their long-term performance under Extremely Aggressive Exposures like chloride induced corrosion and chemical attack. The improvement consists in upgrading Ultra-High-Performance Fibre-Reinforced Concrete with new functionalities. Focus is on marine structures and infrastructures for geothermal/biomass energy plants, whose severe conditions put a strain on the performance, lead to a swift deterioration and shortening of the lifespan, resulting in billions of euro spent every year on maintenance operations and repairs (Ferrara L., ReSHEALience).

This study is part of the work package 4 of the aforementioned project, whose leader is the *Universitat Politècnica de València* (UPV), focused on the use of nano-additions and the improvement of autogenous healing by crystalline admixtures, nano-cellulose, superabsorbent polymers, with evaluation of their effects on durability. A small part of the study is related to the work package 5 as well, which focuses on the factors that affect durability of UHDC, with particular reference to chloride induced corrosion and chemical attack.

## 1.1 Background

The investigation in self-healing capability of concrete is justified by the increasing safety and sustainability requirements of structures. Concrete is very sensitive to crack formation; during its service life, due to its low tensile strength, it frequently suffers small cracks ( $< 0,03$  mm), as a result of external actions like shrinkage, thermal effects or freeze/thaw cycles. These cracks not necessarily represent a risk of collapse for the structure, but surely may jeopardize its performance, causing the entry of aggressive chemical agents which can accelerate the degradation process and decrease its service life. Since cracks impair the service life, a repair may be required. However, these rehabilitation works increase the life-cycle cost of concrete. In this perspective, self-healing may represent a solution able to prevent structures from continuous expensive maintenance operations. As a matter of fact, concrete has a natural self-healing capability, called autogenous healing, which, although limited, is able to seal small cracks by means of continuing hydration and carbonation process.

## 1.2 Objectives

This research is focused on evaluating the enhancement induced in self-healing phenomenon when adding crystalline admixtures and nanoparticles in the reference Ultra-High-Performance Fibre-Reinforced Concrete mix design, by developing a methodology to efficiently quantify permeability.

- Provide a methodology to evaluate self-healing in Ultra-High-Performance Fibre-Reinforced Concrete based on the study of permeability in cracked state;
- Characterize concrete durability by means of water permeability and chloride penetration tests;
- Analyse and compare the cracking pattern, durability and self-healing performance of Ultra-High-Performance Fibre-Reinforced Concretes and ordinary concretes;

- Assess the effectiveness of the addition of functionalities such as crystalline admixtures and nanoparticles in Ultra-High-Performance Fibre-Reinforced Concrete.

## 1.3 Outline of the document

The document consists of five chapters:

- The first introductory chapter includes the background on self-healing concrete and the objectives of the thesis;
- The second chapter reports the state of the art on self-healing and methodologies used to date to evaluate its effects;
- The third chapter provides a description of the whole experimental phase, with focus on the methodology employed for the evaluation of self-healing effectiveness;
- The fourth chapter presents the results obtained from the tests and the analysis of them;
- The fifth and final chapter provides a summary reflection on the outcomes achieved and aims for future investigations.

## 2. State of the art

### 2.1 Introduction to self-healing

Concrete is the most used material in the construction field, due to its high compressive strength and low cost of its constituents. However, because of its low tensile strength, concrete is often coupled with steel reinforcing bars which, thanks to the bond forces, are able to resist tensile loads as well. Nevertheless, rebars are not always designed to totally prevent the formation of cracks. Damage induced by cracks does not threaten the stability of the structure from the mechanical point of view, but can endanger the durability of concrete, allowing the entrance of aggressive chemical agents which initiate the degradation process inside the element. When external agents are able to penetrate inside the matrix, reinforcing bars start to corrode and collapse of the structure may occur (Van Tittelboom and De Belie, 2013). Consequently, it is clear that constant repair operations of cracks are needed. However, since rehabilitation of structures represents half of the costs of the annual construction budget (Cailleux, E., 2009), the interest in studying innovative solutions to extend structures life, and thus diminish maintenance activities, has considerably increased. In this perspective, self-healing concrete would be absolutely helpful.

Self-healing is the natural capability of a material to repair its damage autogenously or with minimal help of an external stimulus, with the recovery of lost properties (De Rooij et al., 2013). This phenomenon has been well known for years, observed in bones and trees (Speck et al., 2013). However, self-healing in concrete is limited to the sealing of small cracks, mainly caused by ongoing hydration of clinker minerals and carbonation process of calcium hydroxide  $\text{Ca(OH)}_2$ . In 1994, C. Dry was the first who suggested the intentional introduction of self-healing properties in concrete. Over the last 25 years, whereas numerous researches were aimed at the creation of concrete compositions to improve the autogenous self-healing, other investigations were aimed at the addition of healing agents in concrete mixture in order to trigger self-healing process. These include mineral additions, crystalline admixtures, superabsorbent polymers, encapsulated agents, and even calcium carbonate-precipitating bacteria. In literature, the two

aforementioned mechanisms are clearly distinguished according to the materials that give rise to self-healing. The first one, called *autogenous healing*, is a natural process, intrinsic to the properties of the cementitious matrix itself, mainly produced by continuing hydration of unhydrated cement grains and precipitation of calcium carbonate crystal (De Belie et al., 2018). The second one, called *autonomous healing*, is an engineered process, implemented through different methods, in order to improve the self-healing capability of a concrete element (M. Roig Flores, 2018).

In RILEM State-of-the-art of Self-Healing Phenomena in Cement-Based Materials (De Rooij et al., 2013) the following definitions are provided:

*Self-healing is any process by the material itself involving the recovery and hence improvement of a performance after an earlier action that had reduced the performance of the material.*

– *Autogenic: the self-healing process is autogenic when the recovery process uses materials components that could otherwise also be present when not specifically designed for self-healing (own generic materials).*

– *Autonomic: the self-healing process is autonomic when the recovery process uses materials components that would otherwise not be found in the material (engineered additions).*

## 2.2 Autogenous healing

Autogenous healing of cementitious materials is the basic phenomenon that determines partial or total self-closure of cracks, with a consequent a partial regaining of the initial durability and mechanical properties (De Belie et al., 2018). It has been known for years without univocal assent on the reasons that trigger it. This phenomenon was considered one of the main causes of the long-life span of ancient structures (Ghosh, 2009), receiving the first attentions from the French Academy of Science in 1836 (Lauer, 1956) when autogenous healing of cracks was noted in water retaining structures

(Johannesson, 2012). Nowadays, in literature there is a substantial consensus that autogenous healing is mainly due to two mechanisms: continuing hydration of unhydrated cement particles and calcium carbonate precipitation. However, further mechanisms take part in the healing process, although in a lesser extent, and while different opinions exist about how much each mechanism actually affects autogenous healing, researchers agree that the presence of water is essential (Van Tittelboom and De Belie, 2013). In 1997 Hearn and Morley drew up a list of the possible mechanisms causing self-healing in concrete (Figure 2–1):

**a) Physical causes:**

- Matrix swelling: increase of volume caused by the saturation of the cement paste due to water absorption by calcium silicate hydrates.

**b) Chemical causes:**

- Continued hydration: unhydrated cement particles in contact with water form by-products that fill cracks.
- Calcium carbonate formation: calcium hydroxide (portlandite) in the concrete matrix reacts with water and, in presence of carbon dioxide, a precipitation of calcium carbonate is formed filling the cracks.

**c) Mechanical causes:**

- Sedimentation of fine concrete particles and debris: crack blocking as a direct result of the cracking process.
- Sedimentation of concrete particles and debris: crack blocking due to impurities contained in external water entering the cracks.

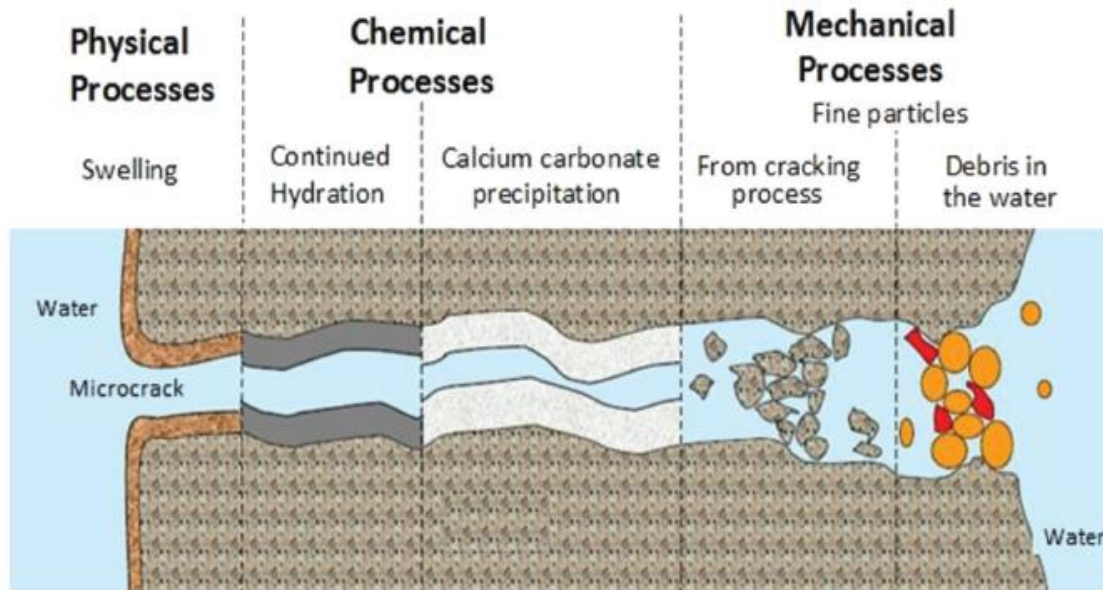


Figure 2–1. Processes causing autogenous healing (De Rooij et al., 2013)

### 2.2.1 Continuing hydration effect on autogenous healing

The effect of ongoing hydration on autogenous healing have been proved to depend both on the water/cement ratio and the availability of external water. Depending on these factors, when unhydrated particles react with water, the newly formed hydration products can produce crack healing. In traditional concrete (water/cement ratio = 0.4) about 30% of the cement particles remain unhydrated, although this ratio should be enough to complete the whole hydration (Van Breugel, 2007). The percentage of unhydrated particles increases with the use of higher quantity of cement and coarser ones. Furthermore, it has been supposed that the hydrated cement particles keep an inner unhydrated nucleus that is subjected to slow hydration over the years (Scrivener, 1984). After cracking of a concrete element, the external water or humidity that get in touch with the unhydrated particles, can give rise to hydration products capable of filling up crack spaces. This phenomenon increases with a low water/cement ratio, as there is a greater amount of available unhydrated particles.

Autogenous healing due to ongoing hydration has also shown remarkable effects in the recovery of mechanical properties (D. Snoeck, 2015), since the hydration products have

been proved to have a greater or equal resistance than, respectively, the calcium carbonate and the calcium silicate hydrate (CSH). However, the processes of formation of hydration products are different inside a crack and inside the cement paste, because of the greater free space in a crack and accordingly more water available for the reaction (higher water/binder ratio) than in a hydrating cement past (De Belie et al., 2018).

In order to evaluate the effects on autogenous healing due exclusively to continuous hydration, it would be appropriate to carry out researches where the possibility of interactions with other processes that may favour self-healing, such as carbonation, are excluded. However, nowadays such investigations are still limited. Huang et al. (2014) have recently analysed and quantified the reaction products formed inside the cracks of a Portland cement paste (water/cement ratio = 0.3) due to ongoing hydration. Samples were in closed containers to avoid contact with carbon dioxide, hence to avoid the carbonation process. From the thermogravimetric analyses, it was observed that the percentage of  $\text{Ca(OH)}_2$  in the reaction products was much higher (78%) compared to the percentage of CSH (17%), strongly in contrast with the hydration products distribution present in the cement paste.

### 2.2.2 Carbonation effect on autogenous healing

Evidently, the most effective mechanism for achieving autogenous healing depends on the age of concrete at the time of cracking. Because of its high content of unhydrated cement particles, continuous hydration seems to be the major healing mechanism in young concrete, while calcium carbonate precipitation the main one at a later age (Neville, 2002).

Carbonation process occurs when water dissolves and conveys portlandite ( $\text{Ca(OH)}_2$ ), the compound of greater solubility in water, and all the other soluble compounds outside the concrete matrix. In particular, carbonation is the result of the chemical reactions between calcium ions  $\text{Ca}^{2+}$  present in the concrete matrix and carbonate ions



$\text{CO}_3^{2-}$  available in water or carbon dioxide  $\text{CO}_2$  available in the air, with the precipitation of calcium carbonate crystals ( $\text{CaCO}_3$ ) (De Belie et al., 2018). The

Figure 2–2 shows an example of carbonation phenomenon in a cracked concrete wall of a water tank (Edvardsen, 1996).

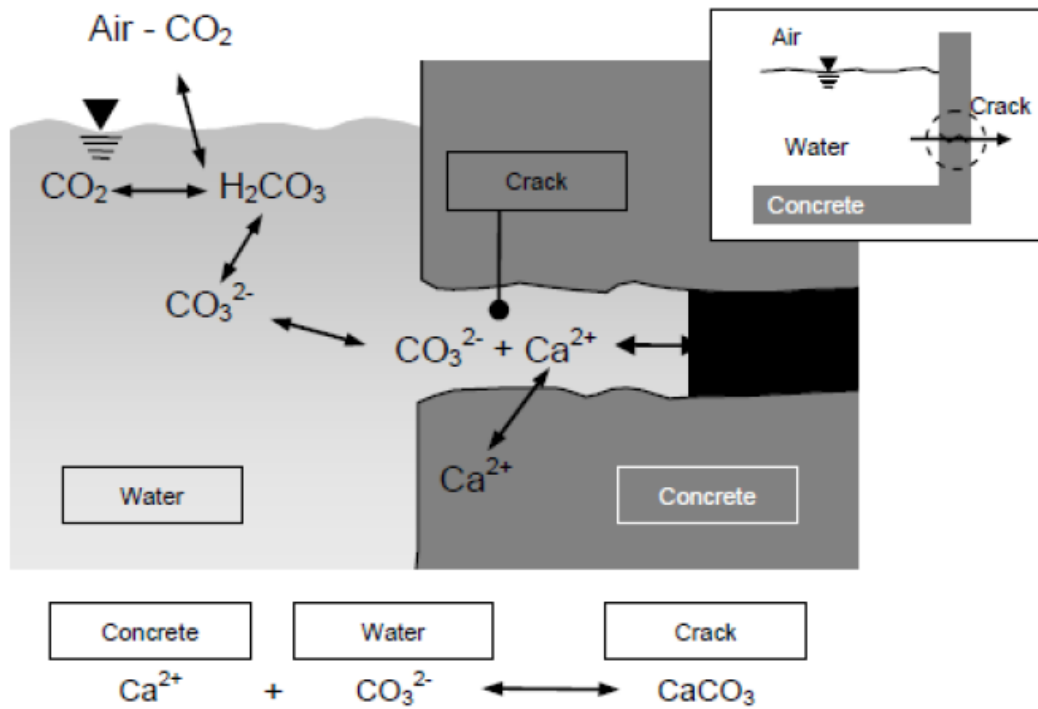
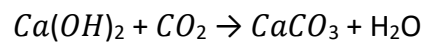


Figure 2–2. Carbonation process in a crack produced in a water tank (Edvardsen, 1999)

However, being calcium hydroxide the most water-soluble compound, most of the studies are referred to its carbonation, according to the following reaction:



Edvardsen studied the crack healing of concrete by means of water permeability tests, concluding that calcium carbonate precipitation was the main cause for autogenous healing, as the major crack filling fraction was calcite. As analysed by Edvardsen, if calcium ions ( $\text{Ca}^{2+}$ ) are available in proximity of a crack, the precipitation of calcium carbonate may occur. When water enters the crack, its pH will locally raise owing to the contact with the alkaline concrete matrix. Thus, conditions are suitable for calcium carbonate precipitation. At the moment of cracking, calcium ions are directly available

from crack walls, favouring the deposit of crystals, during the so-called phase "surface-controlled crystal growth". However, once an initial film of calcite has formed on the crack faces, the concrete matrix nearby has remained poor in calcium ions. Here the second phase called "diffusion-controlled crystal growth" takes place, which implies a slow diffusion of  $\text{Ca}^{2+}$  ions which have to cross the cement and the  $\text{CaCO}_3$  layer to ensure a crack width reduction (Figure 2–3) (De Belie et al., 2018).

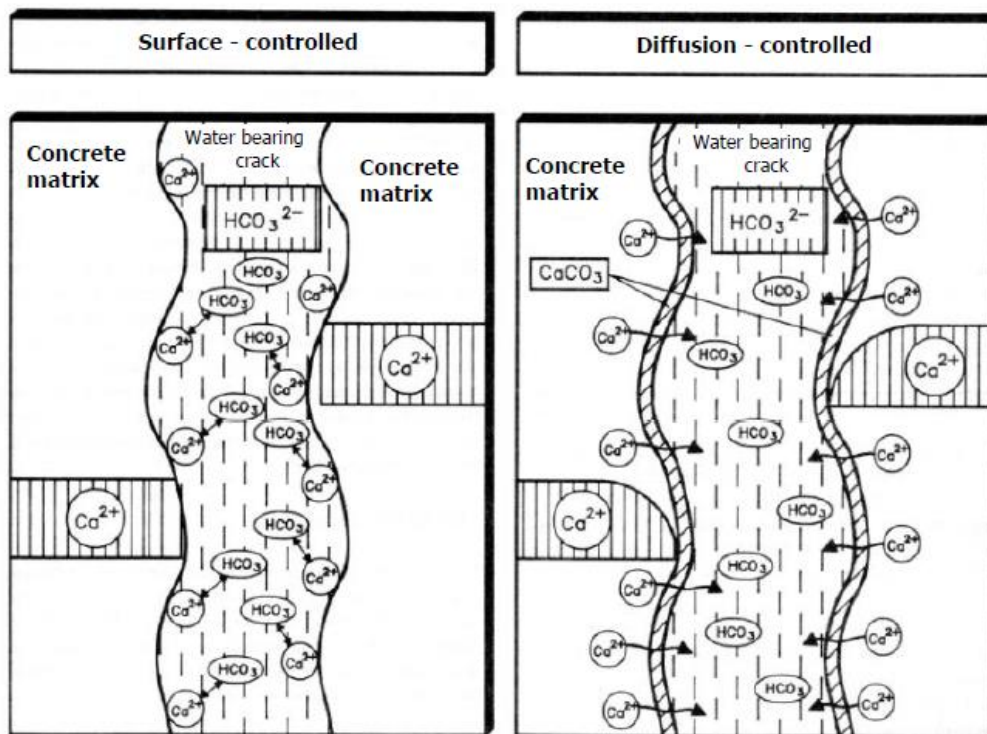


Figure 2–3. Surface and diffusion healing process by carbonation (Edvardsen, 1999)

This decrease in time of the autogenous healing effect achieved by carbonation denotes that a limit exists to its effectiveness. Once this limit is reached, it is likely that only lesser healings will occur (M. Roig Flores, 2018).

### 2.2.3 Effect of various parameters on autogenous healing

In the past, many experiments have been carried out to study and evaluate the effectiveness of autogenous healing, and the factors and parameters that affect this intrinsic performance of the material. Each author provides the experimental criterion

adopted in carrying out the tests and the results obtained in terms of crack sealing and recovery of the mechanical and durability properties. In general, it is possible to affirm that autogenous healing is possible but limited to small cracks. The range of crack width where the healing process seems to be more efficient is between 10 and 100  $\mu\text{m}$ , sometimes up to 200  $\mu\text{m}$  but less than 300  $\mu\text{m}$ , always in the presence of water (De Belie et al., 2018). The large proposed range of healable cracks depends on the influence of many parameters on this phenomenon, which will be discussed below based on their origin: concrete composition, water availability and crack width.

#### 2.2.3.1 Effect of the age and concrete composition

The concrete age at the moment of pre-cracking proves to be essential with respect to the healing phenomena. Two main mechanisms result to be dominant at different concrete ages. In young concrete there is still a substantial amount of un-hydrated cement particles which makes the ongoing hydration the dominant mechanism. The continuous hydration of the cement paste, in fact, produces the hydration of cement particles that have not yet reacted due to the unavailability of water. The presence of such unhydrated particles is especially plentiful in case of a concrete with a low water-cement ratio. Carbonation is the dominating mechanism for autogenous healing at later ages instead, mainly characterized by calcium carbonate precipitation ( $\text{CaCO}_3$ ) for crack closing (Neville, 2002).

The use of mineral additions like Blast Furnace Slag or pozzolanic materials such as Fly Ash and Silica Fume, was suggested to enhance autogenous healing owing to their delayed reaction respectively with water and calcium hydroxide (M. Roig Flores, 2018). In latent hydraulic or pozzolanic binder materials, which have slower hydration than cement, hydration may be delayed further at later ages, ensuring a longer period in which the unreacted material is available, thus promoting the autogenous healing due to ongoing hydration. According to various authors, autogenous healing is actually improved when cement is partially replaced by Blast Furnace Slag and Fly Ash (Olivier et al., 2016).

Ter Heide (2005) analysed autogenous healing in early age cracked concretes concluding that the degree of crack healing decreases when crack is produced at a later time. Results are coherent if healing is caused by continuous hydration, but not if it is caused by carbonation instead. Besides, Gagné and Argouges (2012) compared autogenous healing of cracks produced at different ages (28 days and 6 months) showing that the former healed only lightly better than the latter, probably due to the almost complete hydration of the cement particles at 28 days and the almost total healing due to carbonation.

While the type of cement is considered to be less important, the clinker content determines the  $\text{Ca}^{2+}$  ions supply and consequently the ability of the matrix to generate calcium carbonate precipitation products. A lot of studies were also carried out on the effect of the water/cement ratio and cement content itself. High performance concretes, being characterized by higher quantity of binding components and low water/cement ratio, could contain important resources of unhydrated cement particles which can give rise to significant amounts of calcium silicate hydrate (C-S-H) products as a result of continuous hydration (De Belie et al., 2018). Some studies performed comparing different mixes increasing water to binder ratio (Van Tittelboom et al., 2012) showed that a lower w/c ratio is able to promote autogenous healing due to continuous hydration, however other experiments with ratios between the standard values 0.40 and 0.60 did not show clear differences (Gagné and Argouges, 2012).

Aggregate type may also indirectly affect the healing process because of the specific cracking pattern which can produce. Nevertheless, the influence on autogenous healing due to the type and composition of the aggregates is proved to be of lesser influence (Edvardsen, 1996, 1999; Ferrara et al. 2016, 2017).

#### 2.2.3.2 Effect of water availability

Water is an essential factor for autogenous healing, since, as explained above, its availability is necessary for the chemical reactions to occur. Furthermore, it represents

the transport medium for fine particles and can also influence the efficiency of the process according to its temperature and the type of water used. In general, water immersion has been reported as the best exposure for self-healing, while autogenous healing capability is very limited in air exposure, as confirmed by the experiments of many authors (Kim, et al., 2014; Jiang, et al., 2015). Only few authors detected better healing in cycling wet-dry conditions compared to complete water immersion conditions (Ma, et al., 2014). Those authors assume that this is due to easier  $\text{CaCO}_3$  formation because of the plentiful availability of  $\text{CO}_2$  in the air during the dry cycle (De Belie et al., 2018). The water usually employed is tap water or distilled water, but it can also contain beneficial or aggressive substances, for example dissolved chloride to simulate sea water (Ferrara et al., 2018). Tests carried out with different water concentration of  $\text{CaCO}_3$  showed that the hardness of water has only a minimal influence on autogenous healing (Edvardsen, 1996, 1999).

#### 2.2.3.3 Effect of crack width

The geometry of cracks, namely, crack width, length, depth, and cracking pattern (branched crack or accumulated crack) may determine their autogenous healing degree. Edvardsen (1996, 1999) reported that crack width is the parameter that most affects the healing process, since the narrower the cracks, the more efficient the autogenous healing. Therefore, by limiting and controlling the crack width, the potential autogenous healing can be substantially improved. The addition of fibres to the cementitious matrix, which resulted into the development of fibre-reinforced concrete (FRC) and high-performance fibre reinforced cementitious composites (HPFRCCs), has been proposed for the first time by Li and co-workers in order to promote autogenous healing, due to due to fibres ability in restrict crack width (Van Tittelboom and De Belie, 2013).

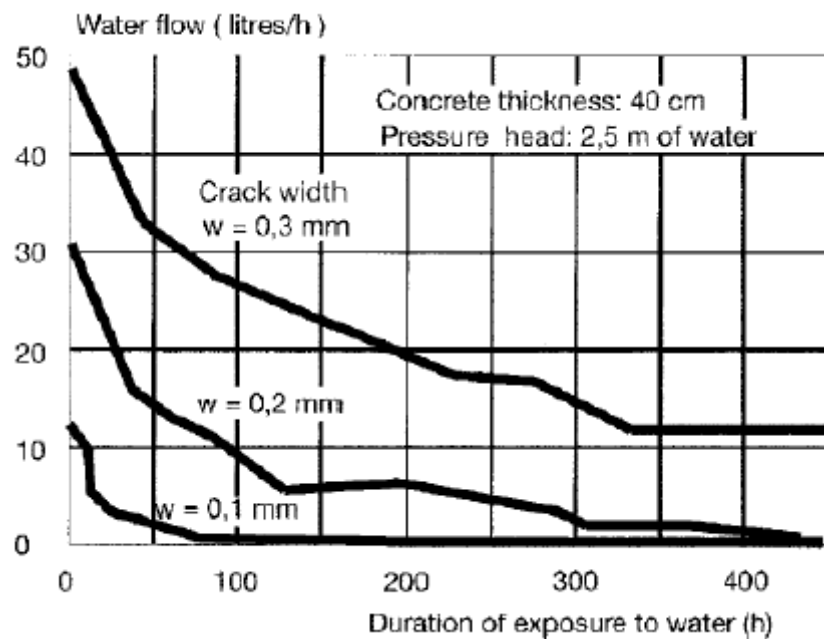


Figure 2-4. Correlation between water flow and time for different crack widths (Edvardsen, 1999)

Figure 2-4 shows how the water flow varies as a function of time through different crack widths, and it is evident that the wider the crack is, the higher the water flow through the sample (Edvardsen, 1999). Because of the predominance of studies demonstrating that wider cracks require longer healing times, it is generally assumed that the reduction in crack size is beneficial for self-healing. Therefore, limiting the level of damage or the crack width can be used as a method to improve the self-healing concrete behaviour. Two methods are usually used to limit crack width and improve self-healing: the use of fibre-reinforced concrete and the application of compressive strength in order to bring crack faces closer (M. Roig Flores, 2018).

The use of high volume of fibres in Strain-Hardening Cementitious Composites (SHCC), also called Engineered Cementitious Composites (ECC), allows a better stress redistribution and a ductile concrete behaviour, which gives rise to a specific cracking pattern characterized by multiple narrow cracks, with maximum cracks width below 0.06 mm (Van Tittelboom and De Belie, 2013). Desmettre and Charron (2012) compared the behaviour of fibre-reinforced concrete (with silica fume,  $w/b = 0.43$ ) with normal strength concrete ( $w/c$  ratio = 0.6). Results proved the benefits of a combination of using

fibres and lower water/cement ratio, as it is shown in the Figure 2–5 with the different healing evolutions of the two concrete types.

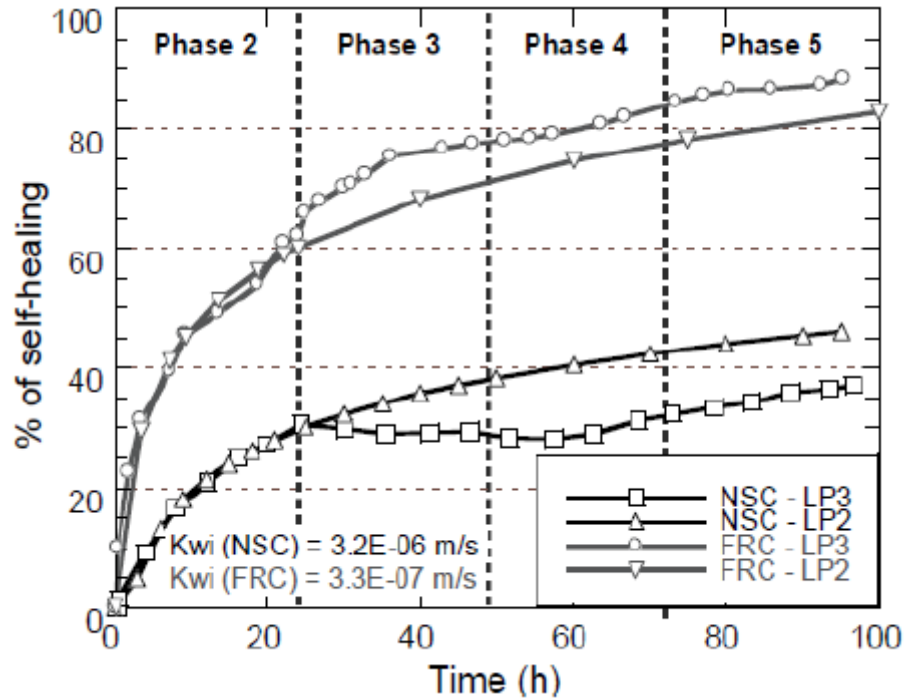


Figure 2–5. Self-healing evolution for NSC and FRC samples (Desmettre & Charron, 2012)

Yang et al. (2009; 2011) conducted experiments with ECC demonstrating that after the healing process, the healed material retained a ductile behaviour and the healed cracks were sufficiently resistant to produce new cracks in the adjacent areas when a reload was applied (Figure 2–6).

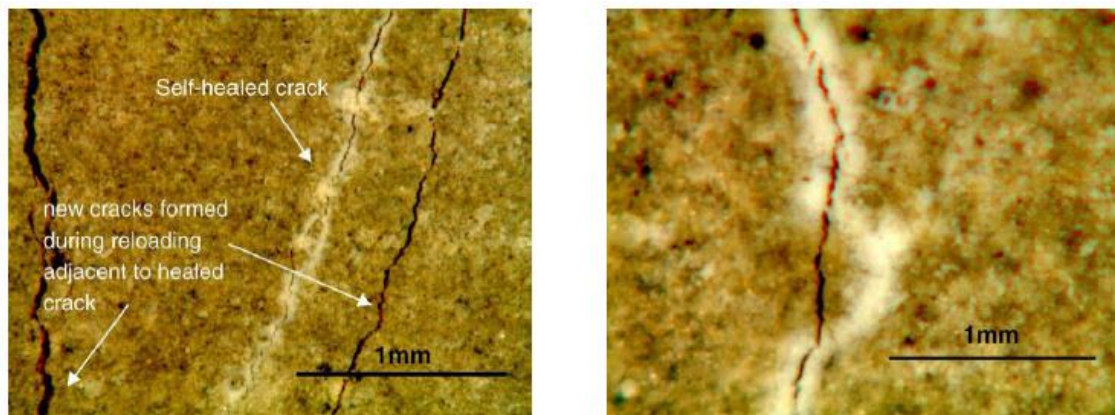
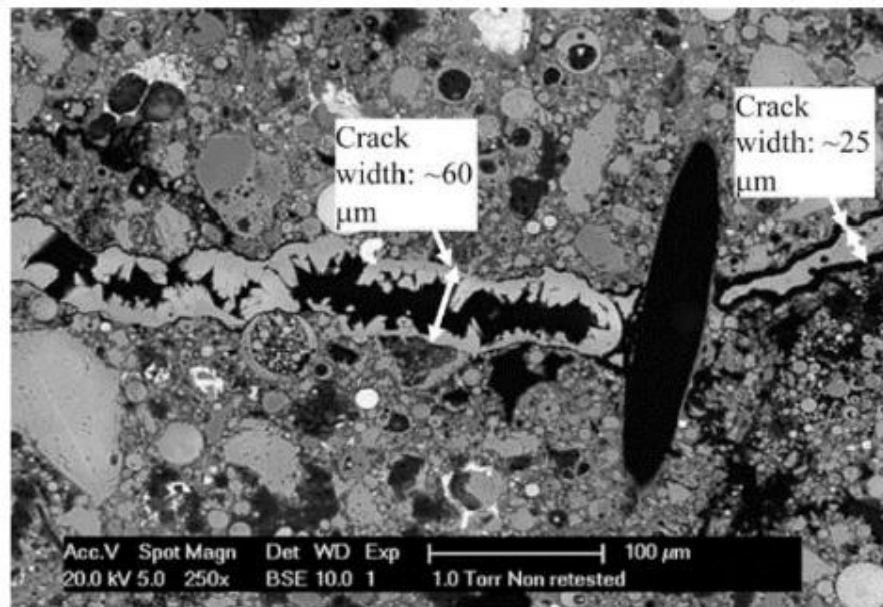


Figure 2–6. Old healed crack and new cracks produced (Yang et al., 2009)

In literature, a wide range of possibilities of healable cracks can be found, ranging from a few tens  $\mu\text{m}$  (Jacobsen et al., 1995) to 100  $\mu\text{m}$  (Reinhardt and Jooss, 2003) and even 300  $\mu\text{m}$  (Edvardsen, 1999). This healing naturally depends on the duration of the healing time and its conditions as well, for this reason it is necessary to look at these data with the right degree of criticality. Generally, it is accepted that only narrower cracks are likely to be totally healed and that only partial healing is feasible in wider cracks. When using crystalline admixtures even larger cracks up to 300–500  $\mu\text{m}$  can be closed (Roig Flores et al., 2015, 2016; Ferrara et al., 2016). However, visual healing by means of microscopy or naked eye does not always mean that the specimen is completely healed. The extent of healing in the interior of the specimen has to be analysed in order to assess whether the closure only affects the surface or is also extended within the sample, where the cracks may still be not totally healed. Recent studies such as these by Nishiwaki et al. (2012) state that cracks up to 300  $\mu\text{m}$  are healable by carbonation, whereas more recent studies performed by Kim, et al. (2014) state that autogenous healing capability is limited to cracks of about 50  $\mu\text{m}$  (Figure 2–7).



*Figure 2–7. Partial crack healing after water exposure (Qian et al., 2009)*



## 2.3 Autonomous healing

Because of the limitations of autogenous healing, several methods were designed to achieve an engineered self-healing, generally referred to as "autonomous healing". In general, this process is characterized by the introduction, with or without encapsulation, of a healing agent that reacts with a catalyst. The catalyst can be part of the concrete matrix or an additional product (M. Roig Flores, 2018).

The autonomous healing mechanisms present in literature are listed in the following Table 1:

<b>Healing agent</b>	<b>Catalyst</b>	<b>Mechanism</b>
Cement	Water	Without encapsulation
		Water encapsulation (e.g. superabsorbent polymers, porous natural fibres)
Chemical agent (crystalline admixtures, expansive admixtures, epoxy resins, sodium silicate, etc.)	2 <sup>nd</sup> component	Without encapsulation
		Dispersed encapsulation (e.g. microcapsules, porous aggregates or fibres)
		Located encapsulation (e.g. glass tubes)
Biological agent (bacteria)		Without encapsulation
		Dispersed encapsulation
		Located encapsulation

*Table 1. Classification of known autonomous healing mechanisms (adapted from M. Roig Flores, 2018)*

All the autonomous healing methods listed above have the purpose to locate the crack when it appears and trigger the healing mechanisms, transporting the filling materials to the damaged area. As anticipated, the healing agent may be introduced into the mixture without an external protection, namely without encapsulation, or it may remain inside a capsule until it is activated by a physical breakage or an increase of porosity. The main disadvantage of not encapsulating is the potential loss of part of the healing product during mixing or hydration, which will no longer be available in future healing processes. The encapsulation like introduction method can be achieved with the use of two types of capsules. The first type consists of dispersed capsules, mainly

microcapsules, used as additional product in the mix for widespread and unpredictable cracks. The use of microcapsules as carriers of the self-healing agent was proposed by White, et al. (2001). According to White et al., when a crack appears and crosses a microcapsule, the latter releasing the healing agent and activating the reaction with a catalyst that will fill the crack by capillary action (Figure 2–8). The second type consists of localized capsules, mainly glass tubes, filled with healing agents and embedded in the structural element in fixed positions, where cracks are supposed to be formed (M. Roig Flores, 2018).

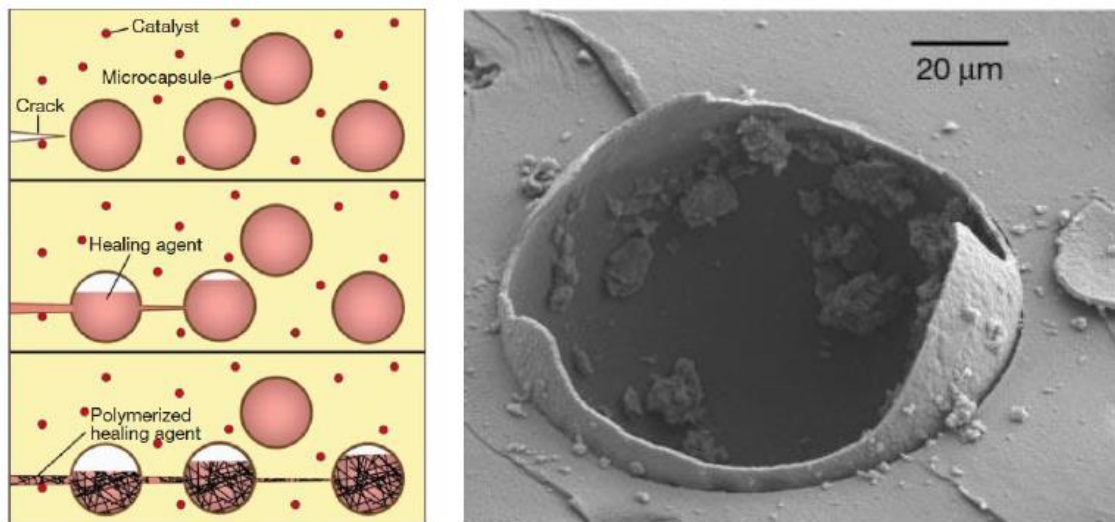


Figure 2–8. Process of release of the healing agent (left) and a broken microcapsule (right) (White et al., 2001)

### 2.3.1 Crystalline admixtures as healing agent

The term "crystalline admixtures" is generally used to indicate a wide range of products present on the market capable to reduce permeability. Thus, this term does not necessarily reflect the molecular structure or functionality of the product in question, since being a commercial product with proprietary constituents its formulation is kept confidential. Crystalline admixtures are classified as a special type of permeability-reducing admixtures (PRAs) (ACI Committee 212, 2010). ACI-212 distinguishes between PRAs that reduce permeability under non-hydrostatic conditions (PRAN), and PRAs also

able to reduce permeability under hydrostatic pressures (PRAH). Crystalline admixtures are included in the latter, whereas water-repellent or hydrophobic products fall into the former category. Generally, crystalline admixtures are products formed by "active chemicals" with a high hydrophilic behaviour, usually mixed with cement and sand. They react in the presence of water, giving rise to insoluble precipitates capable of closing cracks and pores, which increase calcium silicate hydrate (C-S-H) density and resistance to water penetration.

Experiments reported by the ACI Committee 212 (2010) have showed a major permeability reduction with the addition of crystalline admixtures, by comparing the results achieved with other types of PRA, as the following Figure 2–9 shows.

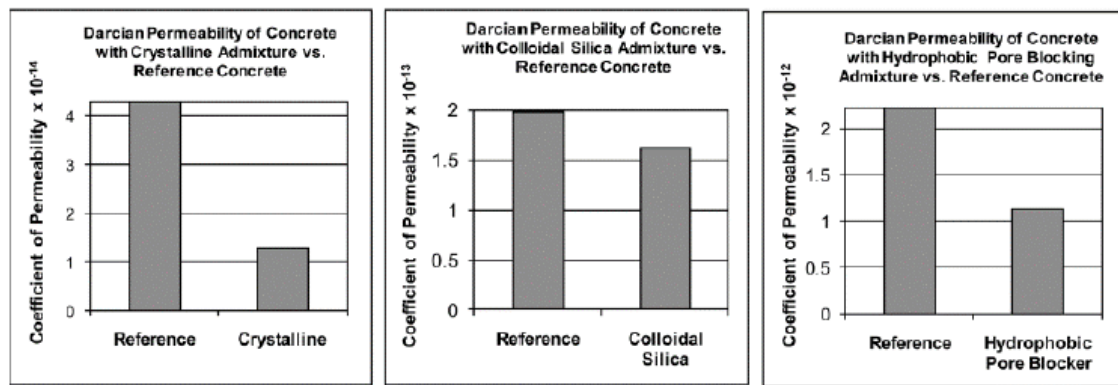


Figure 2–9. Comparison of permeability reduction achieved by different PRA (ACI Committee 212, 2010)

The typical dosage for crystalline admixtures is about 1% by the weight of the cement, however it has also been shown an improvement of concrete mechanical properties with contents of 3%, 5%, and 7% in presence of moisture. At the time of the reaction crystalline admixtures react with the tricalcium silicate of the cement matrix to form a modified CSH, according to the crystalline promoter, and a precipitate formed by calcium and water molecules, although other researches indicate that crystalline admixtures react with portlandite (Ferrara et al., 2016). The chemical reaction is the following:



*Tricalcium silicate + crystalline promoter + water → modified CSH + pore-blocking precipitate*

Several studies have been carried out on the benefits provided by crystalline admixtures on self-healing.

Sisomphon, et al. (2012), reported as maximum self-repair capacity with crystalline admixtures crack widths of 0.15 mm, after 30 days of immersion in water. Besides, they obtained a rapid reduction in water permeability during the first 5 days for mortars with crystalline admixtures addition, whereas only a faint reduction for control mortars. Regarding the recovery of mechanical properties in SHCC containing crystalline admixtures (1.5% by the weight of the cement content), additives produced no benefit compared to the control samples (Sisomphon et al., 2013), even though their results proved good effects when added in combination with an expansive agent.

Ferrara et al. (2014) studied the effect of crystalline admixtures, at a dosage of 1% by the cement weight, on strength recovery in normal strength concrete samples, obtaining an improvement of 14% in properties recovery. Samples, healed underwater, had an initial crack width of 0.13 and 0.27 mm. The results showed that samples containing crystalline admixtures recovered about 80% of the crack width whereas reference samples only healed up to 70%. Afterwards, Ferrara et al. (2016) reported that the improvement can be considerably greater in High Performance Fibre-Reinforced Concretes. De Nardi et al. (2016), using crystalline admixtures in lime mortars, obtained similar results in terms of recovery of compressive strength.

Borg et al. (2017) reported the enhancement provided by the addition of crystalline admixtures in concrete specimens exposed both in immersion and wet/dry cycles to artificially replicated seawater. Cuenca et al. (2018) also hypothesized the contribution of crystalline admixtures in chloride penetration hindrance. Moreover, Cuenca et al. (2018) studied concrete self-healing capability with and without crystalline admixtures under repeated cracking and healing cycles up to 1 year. Concrete specimens with

crystalline admixtures have shown 20% higher and less dispersive performance than the reference ones.

Roig-Flores et al. (2015, 2016) analysed the healing efficiency of crystalline admixtures by means of high-pressure water permeability tests (2 bar) and visually examined cracks closure, in early-age cracked samples (2/3 days). Crystalline admixtures were added in place of the fine material (limestone) in order to isolate the admixture effect from the filler one. Results showed that crystalline admixtures were not able to heal cracks when stored at 95-100% of relative humidity. However, when samples healed in water immersion, crystalline admixtures gave rise to a steadier behaviour than pure autogenous healing. Nevertheless, the results obtained were not resolutely different from the reference group, and no melioration was detected in the visual closure of cracks (De Belie et al., 2018).

### 2.3.2 Comparison of autonomous healing methods

Table 2 summarizes the advantages and disadvantages related to each autonomous healing mechanism present in literature.

<i>Family</i>	<i>Method</i>	<i>Advantages</i>	<i>Disadvantages</i>
<b>Cement healing agent</b>	Autogenous healing	- Natural process	- Low efficacy - Low reliability
	Encapsulation of water	- Good compatibility of healing products such as SAP and porous fibres	- Low reliability of the activation - Shrinkage of the SAPs after drying
<b>Chemical healing agents</b>	None encapsulation (crystalline and expansive admixtures)	- Easy to add - Good compatibility with concrete - Products commercially available	- Low reliability of the activation - Low knowledge of their effectiveness - Inconclusive capability
	Dispersed microencapsulation	- Selection of designed healing agents - Effective for widespread cracks	- Difficulty for microcapsules of resisting the mixing and casting process - Difficulty of activation when cracking

<b>Biological healing agents</b>			- With high amounts of microcapsule other properties such as strength may be negative affected
	Located encapsulation	<ul style="list-style-type: none"> <li>- Selection of designed healing agents</li> <li>- Higher healing capability due to the larger volume</li> <li>- Short reaction time</li> </ul>	<ul style="list-style-type: none"> <li>- Difficulty in resisting the impact of concrete at the time of casting</li> <li>- Viscosity of the healing agents</li> <li>- Prediction of cracks</li> <li>- Incompatibility with cement matrix</li> </ul>
	None encapsulation (bacterial solution)	<ul style="list-style-type: none"> <li>- Easy to add</li> <li>- Compatible by-products</li> </ul>	<ul style="list-style-type: none"> <li>- Low life expectancy and difficulty of survivability of bacteria in concrete matrix</li> </ul>
	Dispersed microencapsulation	<ul style="list-style-type: none"> <li>- Compatible by-products</li> <li>- Protection of bacteria</li> </ul>	<ul style="list-style-type: none"> <li>- Difficulty for microcapsules of resisting the mixing and casting process</li> <li>- Difficulty of activation when cracking</li> <li>- Still in development</li> </ul>
	Located encapsulation	<ul style="list-style-type: none"> <li>- Compatible by-products</li> <li>- Protection of bacteria</li> </ul>	<ul style="list-style-type: none"> <li>- Difficulty in resisting the impact of concrete at the time of casting and activation when cracking</li> </ul>

Table 2. Summary of advantages and disadvantages of autonomous healing mechanisms (adapted from M. Roig Flores, 2018)

## 2.4 Experimental tests to evaluate self-healing

This section reports the experimental tests commonly used to quantify self-healing capability and the related properties recovery phenomena in concrete, with special attention to the literature concerning the permeability tests. In general, the methodology used to assess the effectiveness of self-healing consists of five main stages.

1. Production of concrete samples;
2. Generation of a controlled damage (e.g. pre-cracking);
3. Quantification of certain properties (e.g. crack closure, durability or mechanical properties);
4. Healing period under exposure conditions;
5. Evaluation of the healing effects, quantifying the recovery of the properties previously measured.

These five stages are clearly shown in the following diagram:

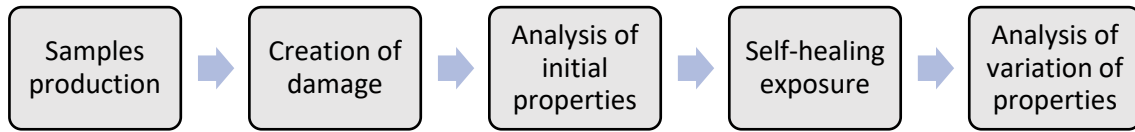


Figure 2–10. Methodology procedure for self-healing evaluation (adapted from M. Roig Flores, 2018)

Regarding the analysis of variation of properties, it has been proved that concrete permeability is closely related to the rates at which liquids and gases diffuse through it (Ferrara et al., 2018). In literature, methods based on the study of water permeability have been used by Edvardsen (1999) and Homma et al. (2009), who exposed concrete specimens to water pressure to evaluate the water flow passing through the cracks. Roig-Flores et al. (2015, 2016) proposed a version to study permeability, easier to be implemented, which is based on the standard test described in the UNI-EN 12390-8 (Testing hardened concrete - Part 8: Depth of penetration of water under pressure) but measuring the water flow instead of the water depth penetration. For the evaluation of self-healing, two main formulas have been proposed. The equation proposed in HealCON (2.1) uses data of a twin unhealed specimen as reference, while the equation proposed by Roig-Flores et al. (2.2) uses the same specimen and compares the water flow before and after healing. While the first method can prevent influences generated by aging in concrete, the second method can prevent the different crack width in two different specimens, since crack width has the greatest influence on the water flow compared to the concrete age (Ferrara et al., 2018).

$$SH_1 = \frac{W_{unhealed,t} - W_{healed,t}}{W_{unhealed,t}} \quad \text{Eq. 2.1}$$

$$SH_2 = \frac{W_{initial} - W_{final}}{W_{initial}} \quad \text{Eq. 2.2}$$

- SH = Self-Healing index;
- $W_{unhealed,t}$  = amount of water passed through the unhealed specimen at time t;
- $W_{healed,t}$  = amount of water passed through the healed specimen at time t;

- $W_{\text{initial}}$  = amount of water passed through the specimen before healing;
- $W_{\text{final}}$  = amount of water passed through the specimen after healing.

In the Figure 2–11 is shown the relation obtained by Roig-Flores et al. (2015) between water flow ratio and crack area ( $\text{mm}^2$ ) ratio (a) and average crack width  $w_{\text{avg}}$  ratio (b) for a control concrete and a concrete with the addition of crystalline admixtures.

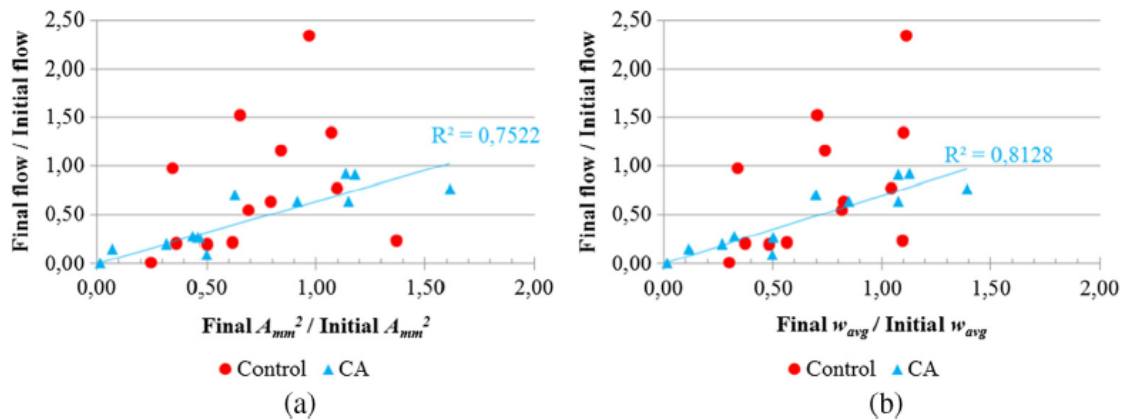


Figure 2–11. Correlation between water flow and crack area (a) and average crack width (b) for control concrete and concrete with crystalline admixtures (Roig-Flores et al., 2015)

Another version of the permeability test present in literature consists in the measurement of the decrease in pressure (water-height) after a certain period (Ferrara et al., 2018). The methodology of this type of test to measure concrete water permeability is based on the proposal by Aldea et al. (1997) and Wang et al. (1999).

Chloride penetration is another transport property which has been analysed in order to evaluate self-healing effects. It allows to characterize the durability of concrete with reference to its ability of providing adequate protection to reinforcing bars against chloride-induced corrosion. As a matter of fact, although very few studies have been done on normal chloride penetration in concrete, the rapid chloride-ion permeability tests demonstrate that there is a correlation between crack width and chloride migration, able to detect a reduction in cracks width after the healing process. Win et al. (2004) reported that the chloride diffusion in both cracked and uncracked specimens increases with the w/c ratio. Akhavan et al. (2013) showed that the chloride diffusion coefficient is high dependent on the crack volume fraction. Sahmaran et al. (2007),



Ismail et al. (2008) and Maes et al. (2016) confirmed the effectiveness of crack closing in reducing chloride penetration as a function of initial crack opening and mortar pre-cracking age. Moreover, Ismail et al. reported that no chloride diffusion occurs in cracks up to 30  $\mu\text{m}$  while Sahmaran found a slight effect of crack width on chloride diffusion for cracks up to 135  $\mu\text{m}$ . Ferrara et al. (2018) correlated the surface crack sealing with the chloride penetration depth. The authors reported that specimens with crack sealing larger than 90% showed higher values of chloride penetration than the values measured for twin un-cracked specimens.

Table 3 summarizes the advantages and disadvantages related to the experimental methodologies used in the literature for the evaluation of self-healing in concrete, classified according to the type of property of interest.

<i>Family</i>	<i>Method</i>	<i>Advantages</i>	<i>Disadvantages</i>
<b>Crack closure</b>	Study of surface cracks through photography cameras, light microscopy, electron microscopy	<ul style="list-style-type: none"> <li>- Straightforward method</li> <li>- Economic equipment</li> </ul>	<ul style="list-style-type: none"> <li>- Limited only to surface cracks</li> </ul>
	Study of internal cracks through X-ray tomography, Neutron tomography, Computerized Tomography scan	<ul style="list-style-type: none"> <li>- Complete analysis of the internal phenomenon in the damage and healing stage</li> <li>- Allow differentiation by densities of the materials</li> </ul>	<ul style="list-style-type: none"> <li>- Expensive and low availability of equipment</li> </ul>
<b>Transport properties</b>	Water permeability	<ul style="list-style-type: none"> <li>- Practicable with high or low water pressure, discrete or continuous measures, etc.</li> <li>- Useful when watertightness is required</li> </ul>	<ul style="list-style-type: none"> <li>- Effectiveness is dependent on how the cracks were produced</li> <li>- Water flow reduction because of the presence of air bubbles that affect the measures</li> </ul>
	Chloride diffusion and penetration	<ul style="list-style-type: none"> <li>- Feasible and useful to study chloride permeability of structures situated in marine environments</li> </ul>	<ul style="list-style-type: none"> <li>- Correlation between the water permeability and rapid chloride ion permeability so far demonstrated only for concrete sample with <math>w/c &gt; 0.40</math></li> </ul>

<b>Mechanical tests</b>	Air permeability	<ul style="list-style-type: none"> <li>- Different types of gases</li> <li>- Useful for applications with high security requirements</li> </ul>	<ul style="list-style-type: none"> <li>- Very sensitive to the sample composition: methanol can dissolve organic polymers used as healing agents.</li> <li>- More complex setup than the water permeability test</li> </ul>
	Water absorption and sorptivity	<ul style="list-style-type: none"> <li>- Setup easy to implement</li> </ul>	<ul style="list-style-type: none"> <li>- Needs a reference specimen as water uptake happens also from the undamaged matrix</li> <li>- Complex interpretation if cracks are too small or too large due to the lack of suction</li> </ul>
	Flexural tests (Three Points Bending Test, Four Points Bending Test)	<ul style="list-style-type: none"> <li>- Cracking process easy to control</li> </ul>	<ul style="list-style-type: none"> <li>- Quantification of the recoveries hard to interpret due to the presence of the reinforcement</li> </ul>
	Tensile tests (Direct tensile test, Tensile splitting test)	<ul style="list-style-type: none"> <li>- Direct evaluation of crack mechanical properties</li> </ul>	<ul style="list-style-type: none"> <li>- Hard to implement and difficulty in controlling the cracking process</li> </ul>
	Compressive tests	<ul style="list-style-type: none"> <li>- Easy to implement</li> </ul>	<ul style="list-style-type: none"> <li>- Complicated interpretation concerning the healing of a single crack</li> </ul>
<b>Non-destructive testing</b>	Resonant frequency, Acoustic emissions, Electrical impedance	<ul style="list-style-type: none"> <li>- Allow taking measures of internal properties at multiple times and during testing</li> </ul>	<ul style="list-style-type: none"> <li>- Provide an indirect measure of properties that indicate the presence of the crack, hardly interpretable</li> </ul>

Table 3. Summary of advantages and disadvantages of methods to evaluate self-healing (adapted from Ferrara et al., 2018)

## 2.5 Nanomaterials in concrete technology

The study of nanomaterials within the concrete matrix has recently emerged in the field of Civil Engineering as innovative tool for the design of engineering cement composites with improved performance and sustainability in order to increase their durability and service life.

### 2.5.1 Nano-cellulose

Nanocellulose, as is extracted from trees and is able to provide considerable properties such as the increasing of the elastic modulus and the hydrophilicity, represents the most generous and renewable natural raw material on the planet, turning out to be an excellent candidate to be used as enhancer of concrete properties. Its sustainability

derives from intrinsic characteristics such as biodegradability, low toxicity, low environmental and health risks associated with the production process as well as low production costs (Ousmane et al., 2018).

Different type of nanocellulose are emerging for their use as concrete additive, like cellulose nano-fibres (CNF), cellulose nano-crystals (CNC), bacterial nanocellulose (BC) and cellulose filaments (CF). The addition of nano-products in concrete technology may result in a significant improvement of concrete macro-properties, such as strength and durability, due to their hydrophilicity, high surface area and their particular size and molecular structure described below.

- CNF consists of crystalline and amorphous domains made of bundles of stretched cellulose chain molecules with long, flexible, and entangled cellulose nanofibers of approximately 1–100-nm diameter and 500–2,000-nm length (Moon et al. 2011); Figure 2–12 below shows the production process of cellulose nano-fibres.

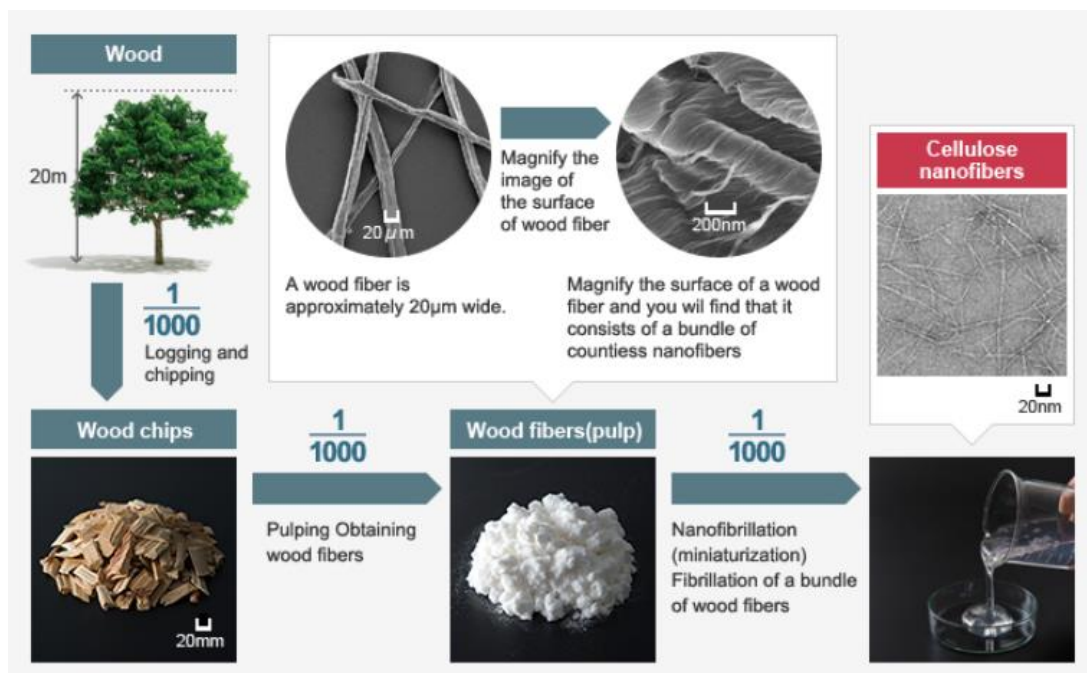


Figure 2–12. CNF production process (Nippon Paper Group)

- CNC consists of highly crystalline cellulose particles of 2–20-nm diameter and 50–500-nm length, thereby exhibiting a lower aspect ratio compared to NFC and a

limited flexibility due to the absence of amorphous domains (Brinchi et al. 2013); Figure 2–13 below shows the production process of cellulose nano-crystals.

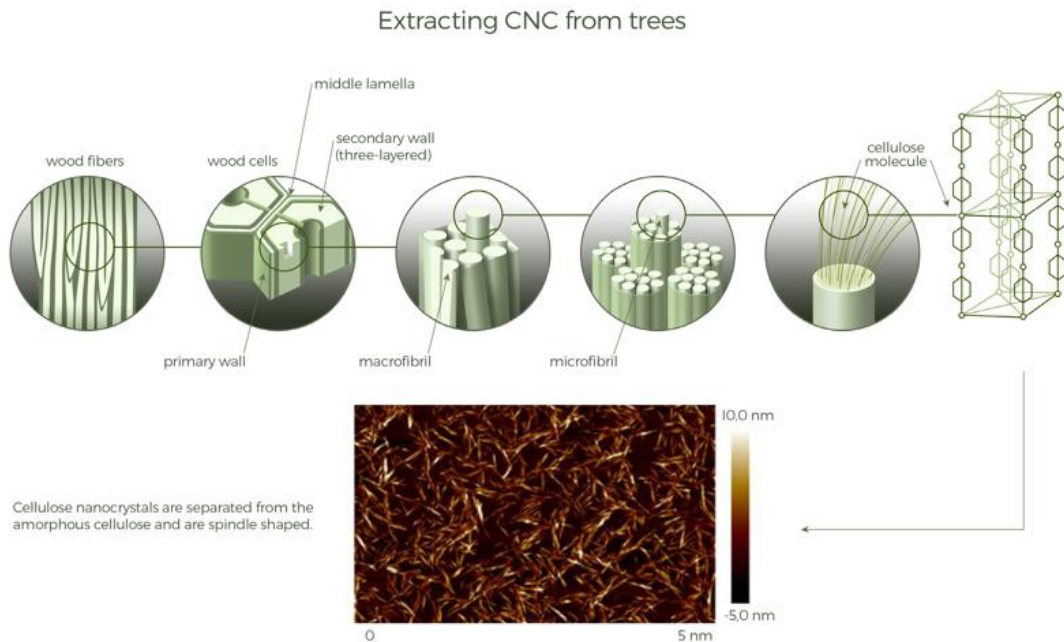


Figure 2–13. CNC production process (CelluForce)

- BC particles are microfibrils secreted by different bacteria and have different morphologies, but their shape is usually rectangular like, 6–10 nm wide and 30–50 nm long (Eichhorn et al. 2010);
- CFs are cellulose fibrils mechanically processed with 100–2,000  $\mu\text{m}$  length and a 30–400 nm diameter, thereby resulting in a higher aspect ratio of 100–1,000 (Ousmane et al., 2018).

To date, very few investigations have been reported in literature regarding the incorporation of nanocellulose particles in cement and concrete composites, however the literature available reports effects on mechanical performance, kinetics of hydration and rheological properties. Concerning the mechanical properties, Peters et al. (2010) observed that a 0.5% CNF addition by the cement content was optimal for improving the cracking properties of ultra-high-performance concrete. Onuaguluchi et al. (2014) noticed approximately a 106% increase in flexural strength of cement pastes containing 0.1% of CNF by the cement content. Cao et al. (2015) reported an improvement in flexural strength of 20–30% at an optimal CNC dosage of 0.2% by the cement content

owing to a better degree of hydration. Regarding the kinetics of hydration, the influences reported comprise a reduction in the degree of hydration in the first concrete age and an acceleration of the hydration process at later ages (Jongvisuttisun et al., 2013). The effects on rheological properties consist in an increase in viscosity and yield stress (Cao et al., 2015), a decrease in workability and consequently a greater demand in water and superplasticizer (Peters et al., 2010; Ferrara et al., 2015).

### 2.5.2 Nano-alumina

It has long been known that mineral additives can significantly improve concrete durability related to permeability, however the performance of cement-based materials strongly depends on nano-sized particles ( $10^{-9}$  m) that can affect properties such as strength, durability, shrinkage and steel-bond (Behfarnia and Salemi, 2018). All the studies reported in this state of the art are about nano-alumina in powder form; from that material, depending on the method of synthesis, several nanostructures can be produced, such as nano-fibres of aluminium oxide ( $\text{Al}_2\text{O}_3$ ), or aerogel from oxyhydroxide aluminium.

While a lot of studies have been performed on the effect of the addition of nano-silica ( $\text{SiO}_2$ ) at nano-scale, only few investigations have been reported on the use of nano-alumina ( $\text{Al}_2\text{O}_3$ ). It has been stated that the use of nano-alumina as a partial replacement by cement reacts with calcium hydroxide produced by the hydration of calcium aluminates, leading to the formation of C-A-S (calcium aluminium silicate) gel in concrete (Behfarnia and Salemi, 2018). Nano-alumina is reported to improve the mechanical properties of concrete such as compressive and tensile strength, reduces water absorption and chloride penetration, improving concrete durability (Shekari and Razzaghi, 2011). Studies have shown that the cement could be replaced with nano-alumina particles up to a maximum limit of 2% with an average particle size of 15 nm (Nazari et al., 2010). Results reported that nano-alumina particles mixed with concrete are able to improve its characteristics; a significantly higher compressive strength was observed in the samples with addition of nano-alumina particles compared to the

samples without additions. Furthermore, it has been proved that nano-alumina is able to considerably increase the modulus of elasticity up to 143% at a dosage of 5% by the weight of the cement (Li et al., 2006).

Behfarnia and Salemi (2013) analysed frost resistance and mechanical properties of concrete containing nano-silica and nano-alumina as a partial substitute of the cement. Results showed that concrete frost resistance containing nanoparticles was significantly improved, as a result of a more compact and denser microstructure capable of absorbing less water. Moreover, frost resistance of concrete containing nano- $\text{Al}_2\text{O}_3$  was better than that containing the same amount of nano- $\text{SiO}_2$ . Compressive strength increased by using nano- $\text{Al}_2\text{O}_3$ , however the compressive strength of traditional concrete specimens containing nano- $\text{SiO}_2$  was higher than that containing the same amount of nano- $\text{Al}_2\text{O}_3$ .

Gowda et al. (2016) investigated the effects of nano-alumina on mechanical properties of cement mortar as a partial cement replacement. Using different concentrations (1%, 3% and 5%), they evaluated the effects on compressive strength at 7 and 28 days and changes in workability. Results showed that the addition of nano-alumina led to a slight increase in compressive strength. The maximum compressive strength was noticed at 7 days with a 1% replacement whereas at 28 days with a 5% replacement. A decrease in workability in cement mortar due to higher rate of water absorption was also noted. A 5% replacement was found to be the least workable mix.

Jaishankar and Karthikeyan (2017) studied the effect of nano-alumina on compressive strength of cement composites, with different volume percentages (0%, 0.5%, 0.75% and 1%). Test results showed that the addition of nano-alumina increased the compressive strength at 28 days. In particular, with a concentration of 1% by the cement weight, the compressive strength of cement composites increased by 33.14%. Furthermore, a microanalysis was carried out by Scanning Electron Microscope (SEM) and Energy Dispersive Spectroscopy (EDS) which confirmed the greater uniformity of concrete microstructure.

## 3. Experimental phase

### 3.1 Introduction

The main objective of the experimental phase is to define a methodology to evaluate self-healing capability of *Ultra-High-Performance Fibre-Reinforced Concrete* (UHPFRC) with the addition of Crystalline Admixtures and Nanoparticles, comparing it with reference concretes for similar structural deformation values. For this purpose, pre-cracking methods and permeability tests previously implemented have been modified to adapt to the needs of this experimental campaign. The performance improvements analysed in these concretes have been compared with the control group made of *Conventional Concrete* (C25/30, named H0 in this document), *High-Performance Concrete* (C80/95, named H1 in this document) and the two base *Ultra-High-Performance Fibre-Reinforced Concrete* (HB3 and HB4), which will be later discussed.

It was decided to study the self-healing efficiency of *Ultra-High-Performance Fibre-Reinforced Concrete* since it proved to be the best candidate owing to its intrinsic properties. It incorporates the advantages of the Self-Compacting Concrete (SCC), Fibre-Reinforced Concrete (FRC) and Ultra High Strength Concrete (UHSC). Among its properties it is worth mentioning:

- The higher durability provided by a high cement content and a very low water/binder ratio (between 0.15 and 0.25) which minimize the number of capillary pores avoiding the penetration of external agents inside the concrete matrix; this also make available a large amount of unhydrated particles able to stimulate autogenous healing;
- The presence in the mix of high-density mineral materials such as Silica Fume which aims to improve self-healing because of its pozzolanic features;
- The reduced diameter of the aggregates;
- The use of steel fibres both to control the micro and the macro crack evolution, increasing ductility, flexural, shear and tensile strength;
- Its characteristic cracking pattern with narrow widespread cracks;

- Its remarkable mechanical properties, namely a compressive strength of about 150 MPa, a flexural strength up to 45 MPa, and tensile strength over 8 MPa;
- Its optimal rheological properties.

The functionalities added to the base UHPFRC mixes are: Crystalline Admixtures (Penetron Admix), Cellulose Nano-Crystal (CNC) and Cellulose Nano-Fibres (CNF). These additions aim to improve concrete durability and consequently self-healing effectiveness, however, while some studies have already been performed on the use of crystalline admixtures to enhance self-healing phenomenon, no experiments have ever been made on the possible improvement induced by the addition of nanomaterials. Penetron is a crystalline waterproofing admixture used for its ability of sealing capillary cracks, while Cellulose Nano-Crystal and Cellulose Nano-Fibres for their property of storing and releasing water progressively. Moreover, Alumina Nano-Fibres (ANF) were added to the base UHPFRC mixes to study their effect in a better crack control, especially about the early crack opening, and accordingly, in sealing of cracks produced.

## 3.2 Experimental program

The whole experimental phase is substantially divided into two basic parts, the first one about the manufacture of the different concrete mixes and the second one about pre-cracking and permeability tests related to the study of self-healing. At first, concrete was produced with a small cement mixer with a maximum capacity of 10 litres, and later, with a larger one, equipped with a capacity of more than 100 litres. In the entire experimental campaign an amount of about 1 cubic meter of concrete was casted. Each concrete batch had a volume of 70 litres, to produce the following samples:

- 4 beams 100x150x750 mm<sup>3</sup>
- 2 prisms 100x100x500 mm<sup>3</sup>
- 4 cubes 100x100x100 mm<sup>3</sup>

The experimental program (see Figure 3–2) consisted first of all in producing the base concrete mixes which have been used as a reference (HB3, HB4, H0, H1) and afterwards



in producing functionalized UHPFRCs, based on the HB3 and HB4 mix design, with the addition of different concentrations of crystalline admixtures and nanomaterials just mentioned. Beams used for the study of durability properties were provided with 2 $\phi$ 8 lower reinforcing bars and 6 $\phi$ 6 stirrups which afterwards have been pre-cracked at different cracking levels. Subsequently, beams have been sawed to obtain smaller specimens and perform permeability tests before healing (BH) and after healing (AH). Dimension, number and layout of the reinforcing bars and stirrups with the relative distances and points of support for performing the four-point bending test are shown in Figure 3–1.

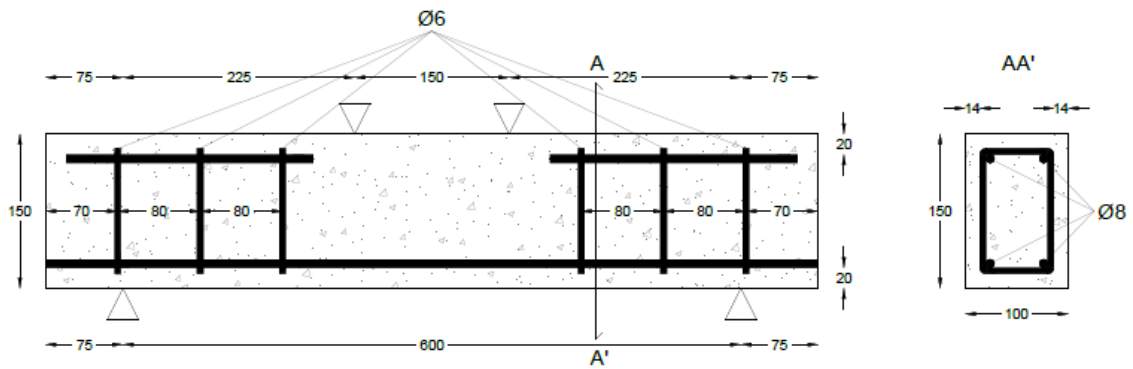


Figure 3–1. Reinforced beam model

With the aim of characterizing the casted concrete, every batch also consisted in four cubes to test compressive strength at 28 days and two prisms to test flexural strength at 28 days. The final goal of the whole production was to identify, among all the batches casted, the concrete mixes with the best behaviour in terms of durability (water and chloride permeability) and accordingly in terms of properties recovery capability after 1 month of self-healing exposure; furthermore, the degree of improvement induced by the additional products has been assessed.

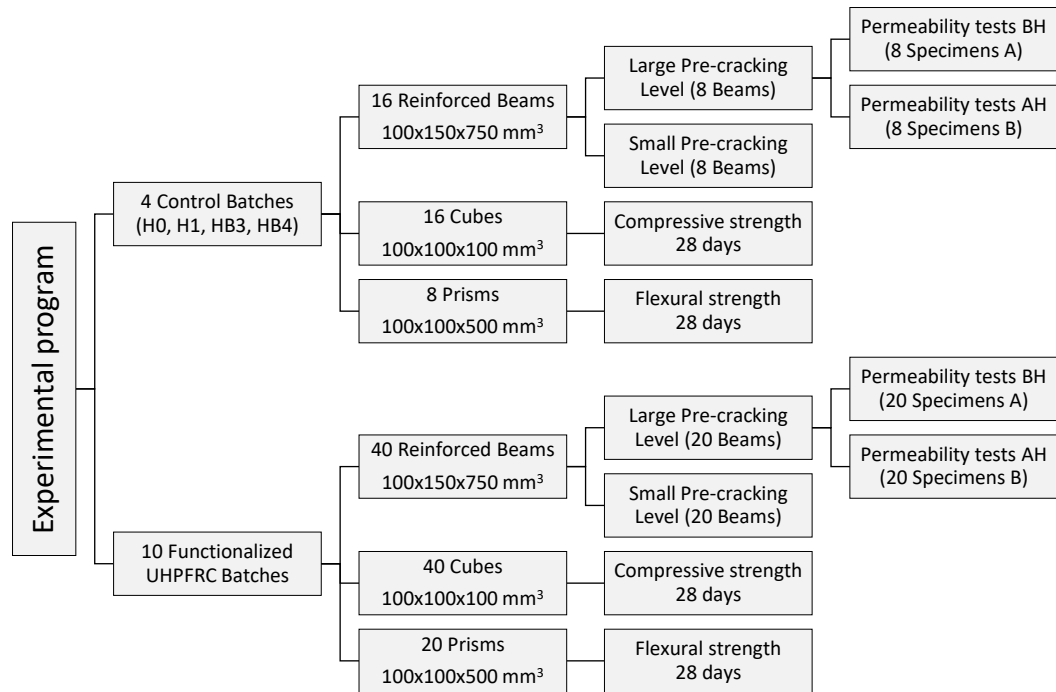


Figure 3–2. Experimental program

### 3.3 Materials

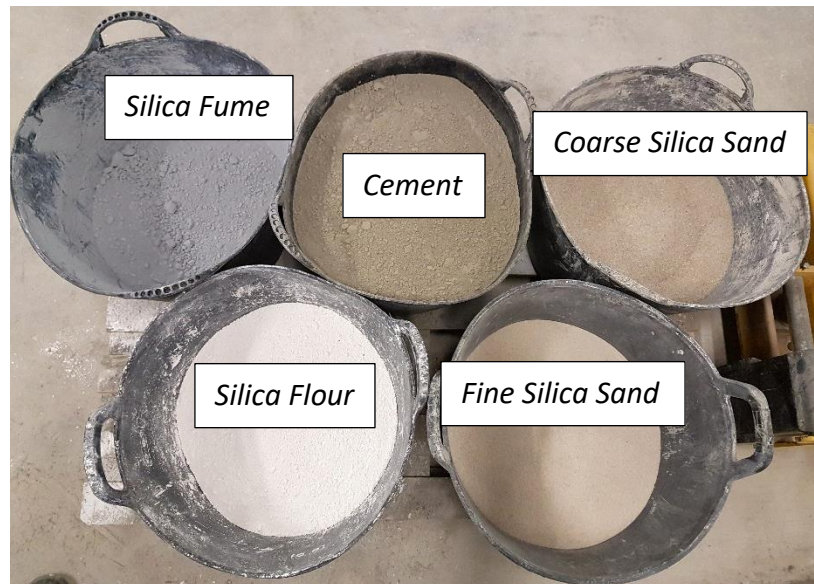


Figure 3–3. Binder materials and aggregates used in the UHPFRC mix

### 3.3.1 Cement

The cement used for the production of all types of concrete was *CEM I 42,5 R-SR5* from Lafarge (Figure 3–4). It is a sulphate resistance cement containing Portland cement clinker, ideal for high strength and protection in marine environment. The surface of the particles of this type of cement is smaller than the type I-52,5, accordingly the water demand is reduced, and the water/binder ratio can be decreased with respect to a cement type I-52,5 with the same workability, hence higher strength can result (Camacho Torregrosa, 2013).



Figure 3–4. Cement used in concrete mix

### 3.3.2 Silica Fume

Undensified Microsilica from Elkem (Figure 3–5) was used as part of the binder in the concrete paste mix in producing UHPFRC for its pozzolanic beneficial properties in hardened state. Silica Fume particles are much smaller than the cement ones, thus allowing to reach the highest degree of compactness of the microstructure of the matrix. It is also able to improve the interfacial transition zone between paste and aggregates. However, in fresh state, the addition of silica fume leads to a reduction in workability (Camacho Torregrosa, 2013).



Figure 3-5. Silica Fume used in UHPFRC mix

### 3.3.3 Water

The water used during the entire experimental research was tap water. The type of water used can lead to different results depending on its chemical composition since it is an essential component for the reaction. However, it has been considered more practical and useful to use tap water instead of distilled water, as considered the most used in civil construction sites, with a neutral pH measured around seven.

Regarding the water/cement ratio, the effective water has been used, not the total water considered by the EHE-08 (*Instrucción de hormigón estructural*); the only difference being that the latter does not consider the water absorbed by the aggregates, which therefore is not chemically available to react. Effective water is the one that really is useful for the reaction with binder. As a matter of fact, to achieve high strength concrete the water not used for cement hydration has to be as less as possible. When capillary porosity is minimal, strength and durability increase.

In the following expressions these different terms are explained:

- *Water/cement ratio (W/C)*: it is the main characteristic of concrete. Knowing the value of the weight of the cement C, through this relation it's possible to obtain the defined amount of water;
- *Effective water*: it is the amount of water (W) obtained from the required W/C ratio.
- *Total water*: it is the sum of the water to be added to the concrete mix, the water in the aggregates and the water that the additive provides. It is equivalent to the effective water without considering the water absorbed by the aggregates;
- *Water in the aggregates*: it is the water that the aggregates have naturally because of their humidity. It is a parameter that varies according to the environmental conditions;
- *Water absorbed by aggregates*: it is the water absorbed by aggregates. It depends on the moisture state of the aggregates and on their absorption capacity, intrinsic parameter of the material. This water does not react because it is situated in the pores of the aggregates, so it is not part of the "W" of the W/C ratio;
- *Water to be added/weighted*: it is the water that needs to be added in the mix according to the W/C ratio. It is the sum of the effective water and the water absorbed by the aggregates, without considering the water already contained in the aggregates.

If the amount of additive is considerable, the liquid fraction of the additive must be taken into account, since it is also adding water. In this case, it must be subtracted by the water to be added. Therefore, summing up:

$$\text{Total water} = \text{Water to be added} + \text{Water in the aggregates} + \text{Liquid fraction additive}$$

$$\text{Effective water} = \text{Total water} - \text{Water absorbed by aggregates}$$

$$\text{Water to be added} = \text{Effective water} + \text{Water absorbed by aggregates} - \text{Water in the aggregates} - \text{Liquid fraction additive}$$

### 3.3.4 Aggregates

In this study different aggregates were used according to the type of concrete produced. For traditional and high-performance concretes (respectively C25/30 and C80/95) gravel of the categories 4/6 and 6/10 ( $d_{min}/D_{max}$ ) and a mix of pebbles and sand were used in the mix. In the traditional concrete mix limestone filler was also added. The aggregates are of considerable importance in the dosage of a concrete. In UHPFRC fine silica sand (0/0.6 mm) and coarse silica sand (0/2 mm) were used (Figure 3–6), characterized by high compressive strength, zero water content and maximum diameter between 0.6 and 2 mm, as microcracks strongly depend on their size.

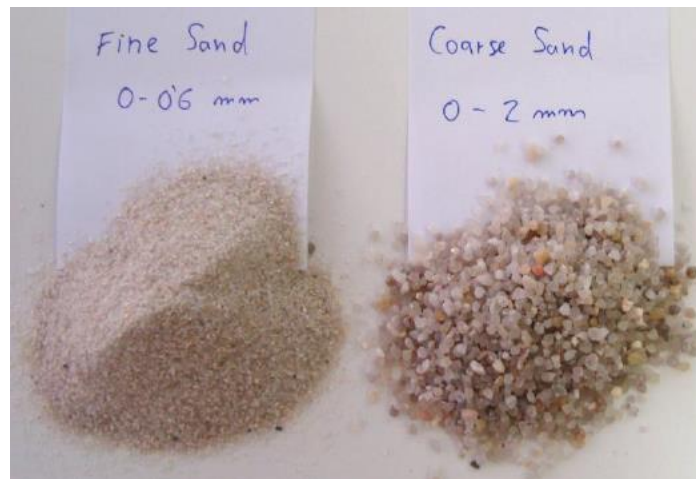


Figure 3–6. Fine and coarse silica sand used in UHPFRC mix

### 3.3.5 Silica Flour

The silica flour Quarzfin U-S 500 from Sibelco (Figure 3–7) was used in the concrete paste mix to produce UHPFRC. This product has the same composition of silica sand but with smaller diameter, more similar to the one of the cement particles.



Figure 3–7. Silica Flour used in UHPFRC mix

### 3.3.6 Superplasticizer

The high-performance Superplasticizer ViscoCrete-20 HE from Sika (Figure 3–8) was used to achieve the desired workability and consistency. This admixture is able to reduce the water content and modify the rheological properties of concrete making it more fluid.



Figure 3–8. Superplasticizer used in concrete mix



### 3.3.7 Fibres

In UHPFRC mix high tensile strength micro steel fibres 0,22x13 mm were used. This type of fibres provides a better control of the first microcracks that appear in the concrete, thus increasing the pseudo-elastic phase and avoiding brittle fractures; furthermore, fibres allow to keep crack width fixed after the pre-cracking has been performed. In traditional and high-performance concrete, no fibres were added.



*Figure 3–9. Fibres used in concrete mix*

### 3.3.8 Penetron Admix

Penetron is a Crystalline Waterproofing Admixture that is claimed to produce self-healing of capillary cracks and is expected to improve transport properties. In its technical sheet Penetron is defined a permeability-reducing admixture for hydrostatic conditions, which provides comprehensive protection against concrete deterioration caused by chemical attack, freeze-thaw cycles, and corrosion, while withstanding high hydrostatic pressure. Added during batching, it should significantly increase concrete durability and service life. Overall it should provide the following performances:

- Resists high hydrostatic pressure;
- Provides self-healing capabilities for cracks up to 0.5 mm;



- Enhances the compressive strength of concrete;
- Non-toxic and contains no VOCs;
- Resists chemical attacks (pH 3-11);
- Significantly reduces chloride penetration and carbonation;
- Effectively counters alkali silica reaction;
- Prevents corrosion of reinforcement steel;
- Not a vapor barrier, allows concrete to breathe;
- Protects against sulphate attack;
- Exceeds requirements of ASTM C494-S (Specific Performance Admixtures);
- Provides a fully waterproof and permanently dry concrete structure;
- No incompatibility issues with workability admixtures, such as superplasticizers;
- Does not require specific W/C or cement content to perform.

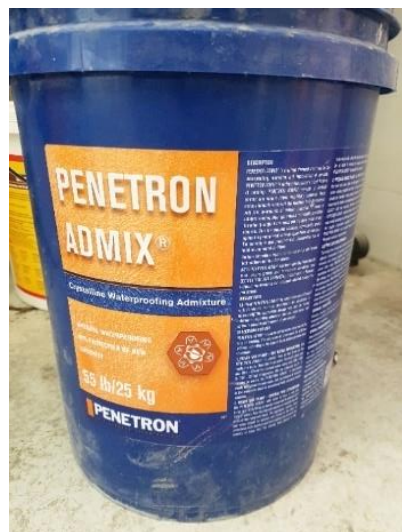


*Figure 3–10. Crystalline Admixtures from Penetron used as addition in UHPFRC mix*

Penetron Admix (Figure 3–10) is made of Portland cement and various active chemical formulations which produce a catalytic reaction when in contact with moisture in fresh concrete and by-products of cement hydration. This chemical reaction generates a non-soluble crystalline formation throughout the pores and capillary tracts of the concrete that permanently seals micro-cracks against the penetration of water or liquids. It is supplied in powder form, so it is easily mixed into the concrete during batching. From

technical sheet is recommended a 0.8-1.0% of dosage rate by the weight of the binder. In this research experiments were done with 0.8%, 1.6% and 2.4% dosage rate, to evaluate how different concentrations affect workability, strength, durability and self-healing in concrete.

Parallel investigations at ICITECH have confirmed that the inclusion of Penetron has almost no impact in workability at low concentrations (0.8%, 1.6%) but a considerable effect with higher concentrations (2.4%), also reducing the time of workability change. Moreover, added to HB3 mix, it has proved to reduce compressive strength at the age of 7 days but to maintain the same value as the base concrete at the age of 28 days.

### 3.3.9 Cellulose Nano-Crystals and Cellulose Nano-Fibres

Cellulose Nano-Crystals (CNC) and Cellulose Nano-Fibres (CNF) from API Europe are expected to promote internal self-curing. CNC have a diameter between 4 and 5 nm and a length between 50 and 500 nm. CNF have a diameter between 5 and 200 nm and a length between 500 and a few micrometres. They are supplied in a solution with the appearance of a paste in which the solid content is diluted in water at a 10% concentration (10% solid / 90% water). This has been considered during the addition of water in the mixture, subtracting from the water to be added the water already present in the diluted product. At the moment of pouring, since both were not enough dissolved, they have been diluted with further water (Figure 3–11) to ensure an adequate and better dispersion, maintaining fixed the total amount to be added in the concrete mix. In this research experiments have done with the recommended 0.15% of the weight of the binder. Parallel investigations have confirmed that for dosages ranging between 0.1% and 0.15% by the weight of cement the inclusion of nanocellulose has almost no impact in workability, but both the products reduce the time of workability change. The reduction of the time for the workability change is greater for higher contents in nanocellulose. It has proved to considerably reduce compressive strength at the age of 7 days.



*Figure 3–11. Dilution of Nanocellulose in tap water*

### 3.3.10 Alumina Nano-Fibres

Alumina Nano-Fibres (ANF) from Nafen (Figure 3–12) are expected to improve the cracking behaviour. These nanoparticles have a diameter between 4 and 11 nm and a length between 100 and 900 nm. They are supplied in a white opaque liquid solution in which the solid content is diluted in deionized water for a 10% concentration (10% solid / 90% water). This was considered when adding the product into the concrete mix to maintain the same final amount of water. In this research experiments have done with the recommended 0.25% of the weight of the binder. Parallel investigations have confirmed that the addition of ANF for dosages up to 0.25% by the weight of cement produces reductions in compressive strength in the base mixes HB3 and HB4 and a loss of workability for the only concrete HB3, which has been compensated by adding 5 litres/m<sup>3</sup> of water without impairing significantly the final compressive strength.



*Figure 3–12. Alumina Nano-Fibres from Nafen used as addition in concrete mix*

### 3.4 Methodology

#### 3.4.1 Mix design

Thanks to previous investigations performed at ICITECH of the *Universitat Politècnica de València*, standard dosages have been developed for different types of concretes, which have been used as a reference to carry out the experimental phase of the project. The composition of the mixes is displayed in the following tables (Table 4, Table 5, Table 6, Table 7). Water contents displayed in the tables are "Total water" values, which in the case of HB3 and HB4 families is equal to the "Effective water".

<b>H0 Conventional Concrete</b>	<b>kg / m<sup>3</sup></b>
Cement 42.5 R-SR	350
Water	207
Gravel 4/6	300
Gravel 6/10	600
Natural Sand	950
Filler	60

*Table 4. H0 Conventional Concrete mix design*

<b>H1 High Performance Concrete</b>	<b>kg / m<sup>3</sup></b>
Cement 42.5 R-SR	450
Silica Fume	50
Water	160
Gravel 4/6	600
Gravel 6/10	200
Natural Sand	950
Superplasticizer Sika 20 HE	3.5

*Table 5. H1 High Performance Concrete mix design*

<b>Base HB3</b>	<b>kg / m<sup>3</sup></b>
Cement 42.5 R-SR	800
Silica Fume	175
Water	160
Medium siliceous sand	565
Fine siliceous sand	302
Siliceous flour	225
Short fibres	160
Superplasticizer Sika 20 HE	30

Table 6. Base HB3 mix design

<b>Base HB4</b>	<b>kg / m<sup>3</sup></b>
Cement 42.5 R-SR	800
Silica Fume	175
Water	160
Fine siliceous sand	1092
Short fibres	130
Superplasticizer Sika 20 HE	30

Table 7. Base HB4 mix design

Table 8 below compares the four base concretes used as a reference:

<b>kg / m<sup>3</sup></b>	<b>Traditional H0</b>	<b>HPC H1</b>	<b>UHPFRC HB3</b>	<b>UHPFRC HB4</b>
Cement I 42.5 R-SR	350	450	800	800
Silica Fume		50	175	175
Water	207	160	160	160
w/c	<b>0.591</b>	<b>0.356</b>	<b>0.200</b>	<b>0.200</b>
w/b	<b>0.591</b>	<b>0.320</b>	<b>0.164</b>	<b>0.164</b>
Aggregate 6/10	600	200		
Aggregate 4/6	300	600		
Natural sand	950	950		
Limestone filler	60			
Siliceous medium sand			565	
Siliceous fine sand			302	1092
Silica Flour			225	
Short fibres			160	130
Superplasticizer Sika 20 HE		3.5	30	30

Table 8. Control group mix design

As it is possible to observe from the tables, by convention, an acronym has been assigned to each type of concrete:

- H0 is the *Conventional Concrete*, which corresponds to a compressive strength concrete C25/30, with water/cement ratio of 0.60 and a low workability, it must be vibrated when cast into the moulds;
- H1 is a *High-Performance Concrete*, which corresponds to a compressive strength concrete C80/95, with water/cement ratio of 0.40 and a modest workability, it may need to be vibrated when cast into the moulds;
- HB3 is the one that best represents the *Ultra High-Performance Fibre-Reinforced Concrete*, with compressive strength up to 150 MP, water/cement ratio of 0.20, a fluid consistency and a great workability so that it does not need any vibration;
- HB4 is an *Ultra High-Performance Fibre Reinforced Concrete*; it consists of only aggregates of fine sand, free of medium sand and silica flour, and of a lesser amount of fibres (130 kg/m<sup>3</sup>), focusing on the reduction of the cost of materials. It has compressive strength up to 135 MPa, water/cement ratio of 0.20, a fluid consistency and a great workability so that it does not need any vibration.

The two selected base UHPFRCs that have been improved with crystalline admixtures and nanomaterials are compared in the following Table 9, where the differences between the two compositions are highlighted.

<i>kg / m<sup>3</sup></i>	<b>HB3</b>	<b>HB4</b>
<b>Cement 42.5 R-SR</b>	800	800
<b>Silica Fume</b>	175	175
<b>Water</b>	160	160
<i>w/c</i>	<i>0.200</i>	<i>0.200</i>
<i>w/b</i>	<i>0.164</i>	<i>0.164</i>
<b>Siliceous sand - medium</b>	565	
<b>Siliceous sand - fine</b>	302	1092
<b>Siliceous sand - flour</b>	225	
<b>Short fibres</b>	160	130
<b>Superplasticizer Sika 20 HE</b>	30	30

Table 9. Comparison between HB3 and HB4 composition

In total, 14 concrete batches have been casted for a total quantity of 56 beams, 28 prisms and 56 cubes. Firstly, the reference concrete batches were casted (H0, H1, HB3, HB4) and subsequently, two series of functionalized UHPFRCs have been prepared, based on the HB3 and HB4 concrete mixes. These UHPFRCs have some similarities due to their use in reinforced elements under Mediterranean XS conditions, but while HB3 concrete targets an optimal durability performance, HB4 concrete targets to maintain excellent durability at a reduced cost. Table 10 presents the functionalized batches produced with the addition of specific concentrations of Crystalline Admixtures and Nanoparticles, while Figure 3–13 shows the preparation phase of the raw materials for HB3 and HB4 before mixing.

<b><i>HB3 series</i></b>	<b><i>HB4 series</i></b>
HB3 + 0.8% Penetron	HB4 + 0.8% Penetron
HB3 + 0.8% Penetron + 0.25% NAFEN	HB4 + 0.8% Penetron + 0.25% NAFEN
HB3 + 1.6% Penetron + 0.25% NAFEN	HB4 + 0.8% Penetron + 0.15% CNC
HB3 + 0.15% CNF/CNC (50%)	
HB3 + 0.8% Penetron + 0.15% CNF/CNC (50%)	
HB3 + 0.8% Penetron + 0.15% CNC	
HB3 + 2.4% Penetron	

Table 10. Batches casted with the addition of functionalities



Figure 3-13. Preparation of the materials for UHPFRC mixes

The tables below show the functionalized UHPFRCs produced, with the specific amount of the materials which take part in the mix. However, it is worth specifying that, despite the nanomaterials are diluted in water, (10% solid content and 90% water), the dosages in the tables only present the weight of the dry part, which is the active part that actually reacts in the process, namely, without the weight of the water present in the solution. Consequently, the value of the water shown is made of the sum of the weight of the water added plus the liquid fraction present in the additive, thus the effective water.

<b>HB3 + 0.8% Penetron</b>	<b>kg / m<sup>3</sup></b>
Cement 42.5 R-SR	800
Silica Fume	175
<b>Water</b>	<b>160</b>
Medium siliceous sand	565
Fine siliceous sand	302
Siliceous flour	225
Short fibres	160
Superplasticizer Sika 20 HE	30
<b>Penetron</b>	<b>7,80</b>

Table 11. HB3 + 0.8% Penetron



<b>HB3 + 0.8% Penetron + NAFEN 0.25%</b>	<i>kg / m<sup>3</sup></i>
Cement 42.5 R-SR	800
Silica Fume	175
Water	165
Medium siliceous sand	565
Fine siliceous sand	302
Siliceous flour	225
Short fibres	160
Superplasticizer Sika 20 HE	30
Penetron	7,80
NAFEN	2,44

Table 12. HB3 + 0.8% Penetron + NAFEN 0.25%

<b>HB3 + 1.6% Penetron + NAFEN 0.25%</b>	<i>kg / m<sup>3</sup></i>
Cement 42.5 R-SR	800
Silica Fume	175
Water	165
Medium siliceous sand	565
Fine siliceous sand	302
Siliceous flour	225
Short fibres	160
Superplasticizer Sika 20 HE	30
Penetron	15,60
NAFEN	2,44

Table 13. HB3 + 1.6% Penetron + NAFEN 0.25%

<b>HB3 + CNF/CNC 0.15% (50% each one)</b>	<i>kg / m<sup>3</sup></i>
Cement 42.5 R-SR	800
Silica Fume	175
Water	180
Medium siliceous sand	565
Fine siliceous sand	302
Siliceous flour	225
Short fibres	160
Superplasticizer Sika 20 HE	30
CNF	0,73
CNC	0,73

Table 14. HB3 + CNF/CNC 0.15%

<b>HB3 + 0.8% Penetron + CNF/CNC 0.15% (50% each one)</b>	<b>kg / m<sup>3</sup></b>
Cement 42.5 R-SR	800
Silica Fume	175
Water	180
Medium siliceous sand	565
Fine siliceous sand	302
Siliceous flour	225
Short fibres	160
Superplasticizer Sika 20 HE	30
Penetron	7,80
CNF	0,73
CNC	0,73

Table 15. HB3 + 0.8% Penetron + CNF/CNC 0.15%

<b>HB3 + 0.8% Penetron + CNC 0.15%</b>	<b>kg / m<sup>3</sup></b>
Cement 42.5 R-SR	800
Silica Fume	175
Water	180
Medium siliceous sand	565
Fine siliceous sand	302
Siliceous flour	225
Short fibres	160
Superplasticizer Sika 20 HE	30
Penetron	7,80
CNC	1,46

Table 16. HB3 + 0.8% Penetron + CNC 0.15%

<b>HB3 + 2.4% Penetron</b>	<b>kg / m<sup>3</sup></b>
Cement 42.5 R-SR	800
Silica Fume	175
Water	160
Medium siliceous sand	565
Fine siliceous sand	302
Siliceous flour	225
Short fibres	160
Superplasticizer Sika 20 HE	30
Penetron	23,40

Table 17. HB3 + 2.4% Penetron

<b>HB4 + 0.8% Penetron</b>	<b>kg / m<sup>3</sup></b>
Cement 42.5 R-SR	800
Silica Fume	175
Water	165
Fine siliceous sand	1092
Short fibres	130
Superplasticizer Sika 20 HE	30
Penetron	7,80

Table 18. HB4 + 0.8% Penetron

<b>HB4 + 0.8% Penetron + NAFEN 0.25%</b>	<b>kg / m<sup>3</sup></b>
Cement 42.5 R-SR	800
Silica Fume	175
Water	170
Fine siliceous sand	1092
Short fibres	130
Superplasticizer Sika 20 HE	30
Penetron	7,80
NAFEN	2,44

Table 19. HB4 + 0.8% Penetron + NAFEN 0.25%

<b>HB4 + 0.8% Penetron + CNC 0.15%</b>	<b>kg / m<sup>3</sup></b>
Cement 42.5 R-SR	800
Silica Fume	175
Water	190
Fine siliceous sand	1092
Short fibres	130
Superplasticizer Sika 20 HE	30
Penetron	7,80
CNC	1,46

Table 20. HB4 + 0.8% Penetron + CNC 0.15%

The batches listed above at the moment of casting presented good workability with a fluid consistency very similar to that of HB3 (Figure 3–14), characterized by a diameter in the mini-slump test between 23 and 27 cm (Figure 3–15).



*Figure 3-14. Casting into the moulds of base concrete HB3 with self-compacting property*

**Target in the mini-slump test: 230-270 mm**



*Figure 3-15. Mini-cone workability test in UHPFRC base mixes*

The only concrete batch that within the casting program presented the total lack of workability was the HB3 with 2.4% of Penetron. As is shown from the Figure 3-16, below it was almost impossible pouring it into the moulds.



*Figure 3–16. Lack of workability when using HB3 + 2.4% of Penetron Admix*

As it is possible to observe from the tables above, Crystalline Admixtures and Nanoparticles only have been added to the two base UHPFRC mixes (HB3 and HB4), that turn out to be the most suitable concretes to evaluate self-healing. Additives concentration are always expressed in percentage (%) of the weight of the binder, which in this type of concrete is composed of cement and silica fume. Besides, it is possible to observe that from the base mixes, with the addition of the products, the amount of water which takes part in the reaction changes. While the addition of Penetron Admix does not affect this amount of water, nanomaterials such as Cellulose Nano-Crystals (CNC), Cellulose Nano-Fibres (CNF) and Alumina Nano-Fibres (ANF) affect it, because of the geometry of their dry particles that are included in the dissolution. These nanoparticles have a greater specific surface, and their hydrophilic properties increase the demand for water in order to reach a certain workability.

### 3.4.2 Mixing process

Concrete mixing is the initial and fundamental part of the whole investigation, since all the subsequent tests depend on the quality and care wherewith this phase is carried out. The same procedure has always been followed. Generally, concrete manufacturing is made of the following steps: preparation of the moulds with a demoulding agent from

Sika, weighing of the materials which take part in the mix, concrete mixing and, the day after, unmoulding.

Concrete mixing is made of four main phases:

1. Mixing of dry aggregates and binder materials at least for 1 minute;
2. Adding of water, superplasticizer and eventually nanomaterials;
3. Measuring of the time of workability change ( $T_c$ );
4. Adding of steel fibres to the mix after 3 minutes from the workability change.

The mixing process starts pouring dry materials in the cement mixer (not yet in motion) from the highest density material to the lower one. It's very important to keep over time the same process in this phase, because a different order or a different method of pouring could change the results. When those materials are in the cement mixer, the latter can be switch on. It is necessary to wait at least 1 minute that is generated a uniform mixture and, at that point, it is possible to pour water, superplasticizer and eventually add nanomaterials. Superplasticizer and water were poured simultaneously. These additions in about 3 minutes (this time is very variable depending on the type of mix design) change the consistency of concrete, making it more fluid and workable. After other 3 minutes when concrete has reached a fluid consistency, has come the moment to pour fibres, and waiting again a few minutes (from 4 to 5 minutes in general) to achieve a uniform dispersion of the fibres in the mixture, it is possible to switch off the mixer and pouring out fresh concrete into containers. It was customary to leave a bit of water to be poured into the mix during the last 4/5 minutes. Fresh concrete, from containers, was poured in moulds where rests for 24 hours (Figure 3–17).

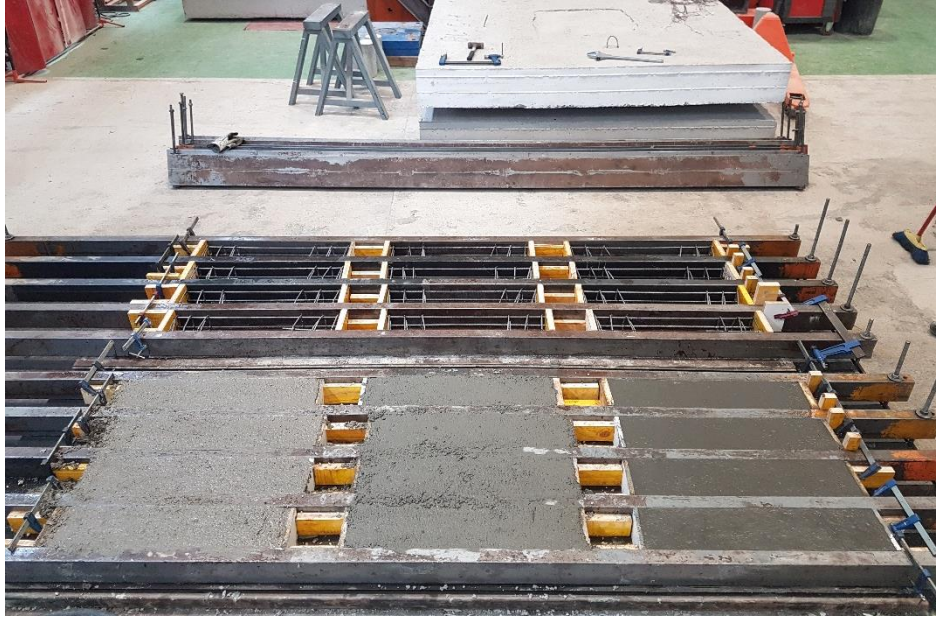


*Figure 3-17. Concrete cast into the moulds*

After 24 hours concrete has achieved an adequate hardness that allows it to be removed from the moulds. Thus, cubes and prisms used for characterization were ready to be moved in a humid chamber with temperature and relative humidity conditions respectively of 20°C and 100%. Beams stayed in "laboratory conditions" until the 28th day instead, when concrete, according to the standard way of designating it, has practically reached its maximum resistance.

### 3.4.3 Compressive strength tests

Control tests were performed on cubes and prisms with the purpose of evaluating how the addition of Crystalline Admixtures and Nanoparticles in the base mix of UHPFRCs affects their compressive and flexural strength, comparing the values obtained with the reference ones (H0, H1, HB3 and HB4). Control tests were also performed with the object of verifying the homogeneity of the results among specimens belonging to the same batch. For each concrete batch four 100x100x100 mm<sup>3</sup> cubic specimens have been casted to determine the compressive strength at 7 and 28 days, according to the provisions of the European Standard UNI EN 12390-3 of the year 2009 "*Testing hardened concrete - Part 3: Compressive strength of test specimens*". At the time of testing the



specimen is placed in a compression testing machine (Figure 3–18). It is very important that the specimen is free from asperities, so in advance, it is necessary to scrape the corners of the specimen to ensure a homogeneous contact with the machine's platens; furthermore, the dimensions of the specimen have to be measured to allow, starting from the attained maximum load, the correct determination of the compressive strength. Load has been applied at a constant rate of stress, 8 kN/s and 0,8 MPa/s. The specimen takes only a few minutes to break, and when the test ends, the program gives back the attained maximum load (kN), the duration of the test (s), the load-displacement graph (kN-mm) and the compressive strength value (MPa).



*Figure 3–18. Compressive strength test*

### 3.4.4 Inverse analysis

For each concrete batch also two 100x100x500 mm<sup>3</sup> prismatic specimens have been casted to study the tensile properties of Ultra-High-Performance Fibre-Reinforced Concrete through a four-point bending test (FPBT). This analysis was not carried out in



first person; however, the methodology is presented in order to be able to characterize the UHPFRCs produced.

The following distances have been used (see Figure 3–19):

- Length of the span  $L = 450$  mm
- Distance between rollers  $a = L/3 = 150$  mm

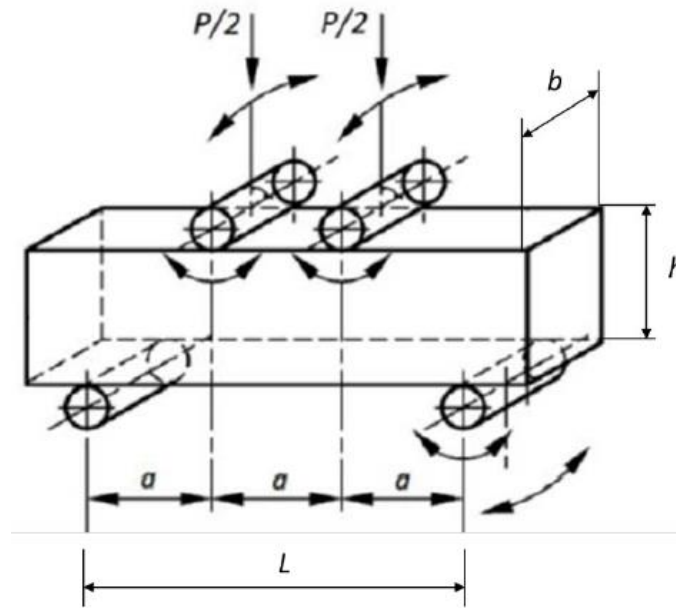


Figure 3–19. Specimen size and degrees of freedom FPBT

The support and bearing rollers must allow the degrees of freedom shown in Figure 3–19. This is a necessary condition that has to be guaranteed to avoid overestimating the tensile performance of UHPFRC. Tests have been performed at a constant frame displacement of 0.05 mm/min up to maximum load. From this point onwards, it has been increased up to 0.2 mm/min. Test finished when a load equal to 70% of the maximum was reached in the unloading phase. Rollers position was ensured with a precision of 2 mm. Two Linear Variable Displacement Transducers (LVDT) with a minimum precision of 0.01 mm were placed at each side of the sample to record the displacement at mid-span (Figure 3–20). The distance of the crack from the mid-span was also measured (Figure 3–21). Tests in which the crack appeared out of the central

one-third were discarded. After the test, specimen's depth and width were measured at failure section with a ruler that guarantees a precision of 0.1 mm.

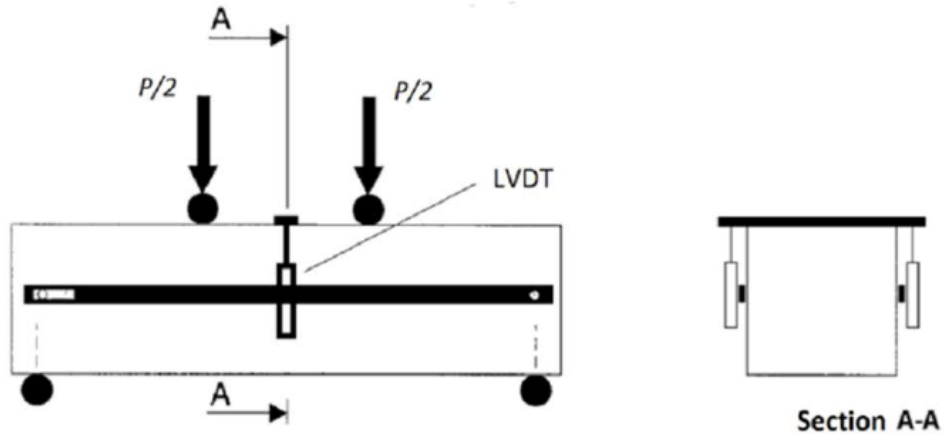


Figure 3-20. Displacement measurement at mid-span by means of two LVDTs

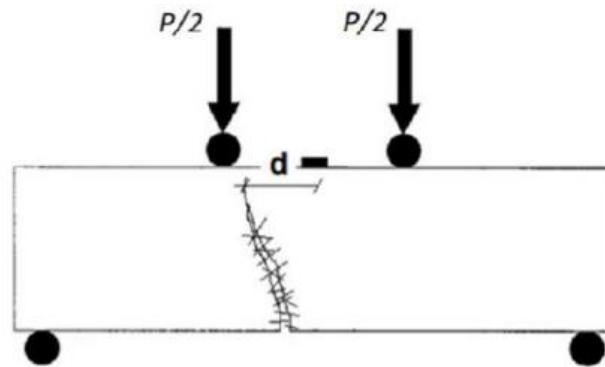


Figure 3-21. Measurement of the distance of the crack from the mid-span ( $d$ )

After the test was performed, load is converted into equivalent flexural strength:

$$\sigma_{fl} = \frac{PL}{bh^2} \quad \text{Eq. 3.1}$$

In case that extension of linear elastic slope of the  $\sigma_{fl} - \delta$  curve intersects the  $\delta$  axis in a point  $\delta_c$  different to 0, every  $\delta$  value measured was corrected according to the equation:

$$\delta_{corr} = \delta - \delta_c \quad \text{Eq. 3.2}$$

After this correction, the new  $\sigma_{fl} - \delta$  is obtained. Three steps are needed to determine  $f_t$ ,  $\gamma$ ,  $\epsilon_{t,u}$  and  $w_0$ :

- I. A point in the linear elastic part of the curve has to be chosen  $P_I (\delta_I, \sigma_I)$ . The slope of the line  $OP_I$  defines the initial stiffness of the curve ( $S_0$ ), being O the point with coordinates (0,0). Its slope ( $m$ ) can be derived using the equation:

$$m = \frac{\sigma_I}{\delta_I} \quad \text{Eq. 3.3}$$

- II. On the experimental corrected curve two lines are drawn up:
  - $S_{75}$ : line passing through the origin with slope equal to 0.75m;
  - $S_{40}$ : line passing through the origin with slope equal to 0.40m.
- III. Key points 1, 2, 3 and 4 are defined as follows. Their graphical definition is shown in Figure 3–22.

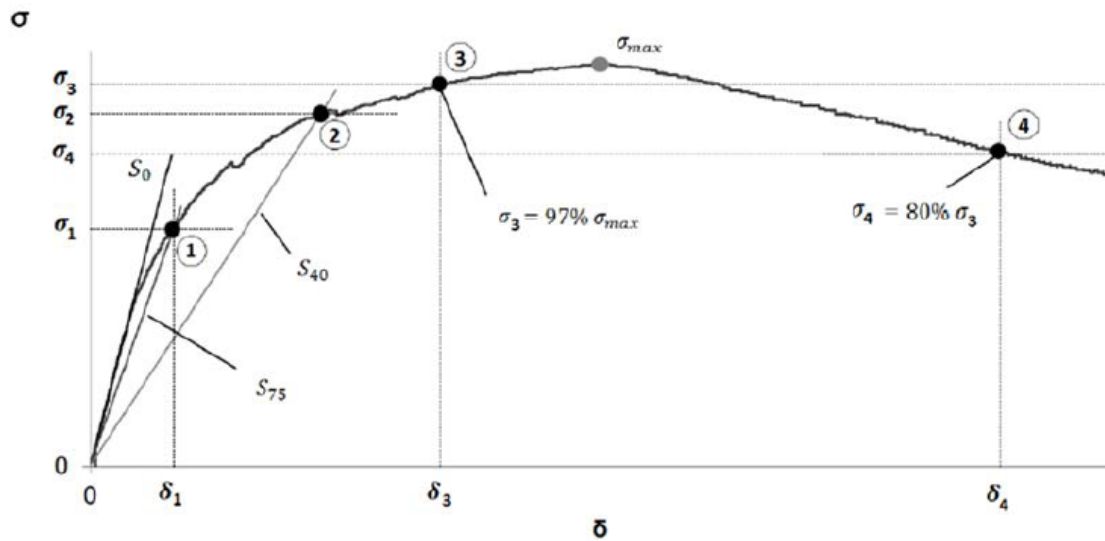


Figure 3–22. Definition of the 4 key points on the experimental  $\sigma_{fl} - \delta$  curve

- $P_1 (\delta_1, \sigma_1)$  is defined as the intersection between line  $S_{75}$  and the experimental curve;
- $P_2 (\delta_2, \sigma_2)$  is defined as the intersection between line  $S_{40}$  and the experimental curve;

- P3 ( $\delta_3, \sigma_3$ ) is defined as 97% of the flexural strength in the loading experimental curve;
  - P4 ( $\delta_4^*, \sigma_4$ ) is defined as 80% of  $\sigma_3$  in the unloading experimental curve.
- Displacement at this point is defined as  $\delta_4$ , however in order to take into account the crack location effect, the following equation has been used:

$$\delta_4^* = \delta_4 \left( 1 + \frac{9d}{20(L - 2d)} \right) \quad \text{Eq. 3.4}$$

Constitutive model for UHPFRC proposed is illustrated in Figure 3–23 which is defined as a function of six parameters: elastic modulus ( $E$ ), cracking strength ( $f_t$ ), ultimate cracking strength ( $f_{tu}$ ) and its associated strain ( $\epsilon_{t,u}$ ), crack opening at the intersection of the line that defines the initial slope to the  $w$  axis ( $w_0$ ) and the characteristic crack opening ( $l_f/4$ ), being  $l_f$  the fibre length.

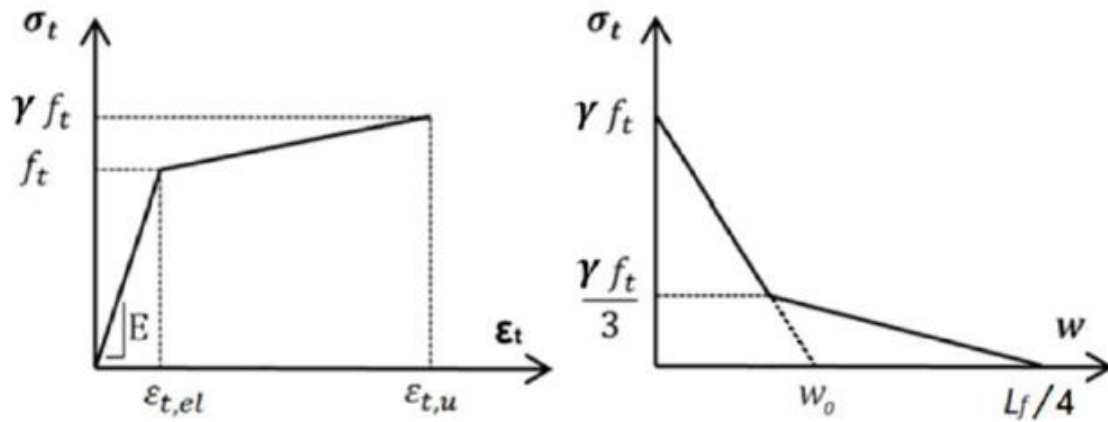


Figure 3–23. Constitutive model for UHPFRC proposed

Inverse analysis formulation to determine these parameters are summarised in Table 21 for a 4.5 slenderness ratio considered.

	$\frac{L}{h} = 4.5$	Normalised parameters
$E$	$4.79 h m$	
$f_t$	$\frac{\sigma_1}{1.59} \left( \frac{\sigma_1}{\sigma_2} \right)^{0.21}$	
$\varepsilon_{t,u}$	$\frac{f_t}{E} \left( 6.65 \frac{\delta_3}{\delta_1} - 9.40 \right)$	
$\gamma$	$\alpha^{-0.17} \left( 2.24 \frac{\sigma_3}{\sigma_1} - 1.55 \right)$	$\alpha = \varepsilon_{t,u} \frac{E}{f_t}$
$\varepsilon_{t,d}$	$\gamma^{-0.38} \alpha^{0.89} \left( 2.82 \frac{\delta_4^*}{\delta_3} - 1.68 \right) \frac{f_t}{E}$	
$w_0$	$\left( \varepsilon_{t,d} - \varepsilon_{t,u} + \frac{10\gamma f_t}{3E} \right) \frac{9h}{4}$	

Table 21. Inverse analysis formulation for slenderness ratio of 4.5

### 3.5 Self-healing methodology

The methodology used in this research to evaluate self-healing effects is based on the study of durability by means of permeability tests. Reinforced concrete beams, previously shown, made of traditional, high-performance and ultra-high-performance fibre-reinforced concrete with a size of 150×100×750 mm<sup>3</sup> have been casted. These beams were pre-cracked through controlled four-point bending tests up to fixed strain levels in the tension area to allow the analysis of the different cracking patterns in terms of crack width and number of cracks. Afterwards, the investigation was focused on the study of the durability. For traditional and high-performance concretes water permeability tests were performed before and after healing exposure under 28 days of water immersion. For UHPFRCs a modification of the water permeability test was explored, using chloride penetration tests to evaluate the protection guaranteed by the healing in chloride-rich environments. Overall, the methodology can be summarized in seven main steps as follows (Figure 3–24).

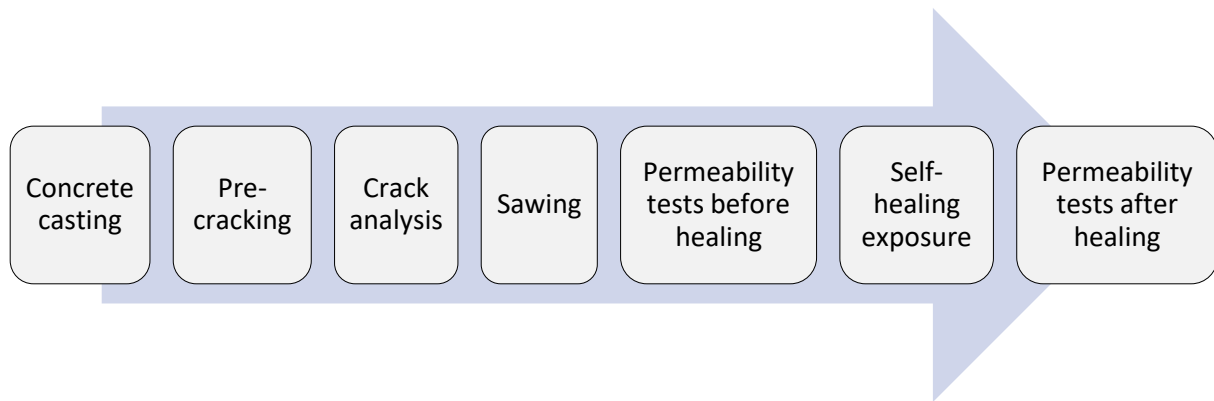


Figure 3–24. Methodology procedure

Initially, the idea was to evaluate concrete durability by using high-pressure water permeability tests. However, both the tests in traditional concretes and UHPFRCs provided remarkable but not quantifiable results. On the one hand, in the case of traditional concretes tests were ineffective because of the breakage of the specimens. On the other hand, in the case of UHPFRCs no water passed, demonstrating its superior durability for a similar deformation level. Accordingly, for UHPFRCs the study has been carried out by means of chloride penetration tests while for traditional and high-performance concrete it has been decided to perform a modified water permeability test in low-pressure conditions, more suitable for the particular cracking pattern with few large cracks. What has been explained is summarized in the following diagram (Figure 3–25).

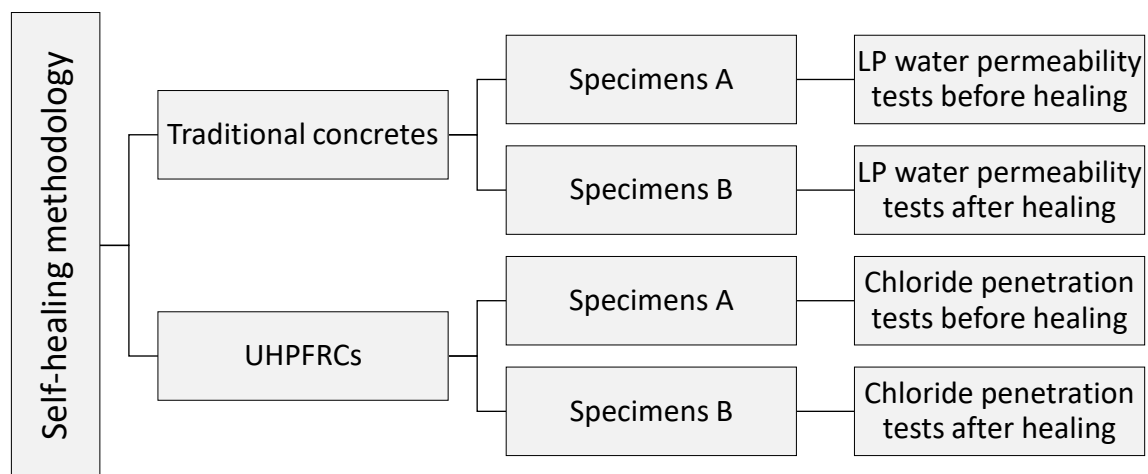


Figure 3–25. Scheme of self-healing methodology

### 3.5.1 Preliminary tests

To evaluate the self-healing efficiency, a preliminary level of damage, preferably a controlled pre-cracking, has to be induced on the samples. In self-healing investigation, cracks were most commonly induced in a mechanical way (Ferrara et al., 2018). In this thesis the well-known four-point bending test was used, which allows to achieve multiple cracks in the central constant bending moment area of the UHPFRC samples.

Before the beginning of the experimental phase, several pre-cracking attempts were carried out, with beams previously cast which had far exceeded 28 days. These samples, with the same size used subsequently in the real experimental phase (100x150x750 mm<sup>3</sup>), were provided only with 2ø8 or 2ø10 lower reinforcing bars, no stirrups.

Tests were performed to standardize the executive methodology, since these experiments were designed at ICITECH for the first time. Moreover, these tests were carried out in order to evaluate the capability of actually being able to control the pre-cracking procedure in detail, hence, of being able to reach the desired cracking level in different types of concrete. This phase was essential to learn the appropriate control methodology to be employed for the four-point bending test, since each type of concrete is characterized by its own cracking behaviour, depending on its basic composition. Tests were performed with four different kind of concretes: Conventional Concrete (C25/30), High-Performance Concrete (C80/95), Ultra High-Performance Concrete (without fibres) and Ultra High-Performance Fibre-Reinforced Concrete.

At the beginning, it was difficult to control the crack opening during the whole test; in particular, at high levels of strain, diagonal shear cracks (Figure 3–26) appeared before reaching the desired cracking level in the tension area (flexural cracks) where fibres are stretched.



*Figure 3–26. Shear crack appeared during pre-cracking*

These preliminary tests have basically led to the conclusion that the most appropriate reinforcement for a better execution of the four-point bending test and a better control of the crack opening are  $\varnothing 8$  steel bars. Furthermore, to perform the tests preventing the premature appearance of the shear cracks with respect to the flexural ones, the use of stirrups is needed.

Further preliminary tests related to the permeability were performed; they will be presented further on in the respective methodology sections.

### 3.5.2 Pre-cracking

Two beams for each batch have been pre-cracked using a four-point bending machine with a span of 600 mm and a distance of 150 mm between the loading points. It was decided to carry out the experimental tests on samples provided with  $\varnothing 6$  stirrups as shear reinforcement, making sure to be able to control the test. As a result, beams (Figure 3–27) were provided with:

- 2 $\varnothing 8$  inferior reinforcing bars throughout the length;
- 6 $\varnothing 6$  stirrups, 3 for each side, with central section free;
- 2 $\varnothing 8$  superior bars, with central section free, with the only aim of supporting stirrups.





*Figure 3–27. Reinforced beams with rebars and stirrups*

Using this reinforcement, it was possible to perform a controlled test and achieve the desired cracking level in the central area subject to bending (Figure 3–28)

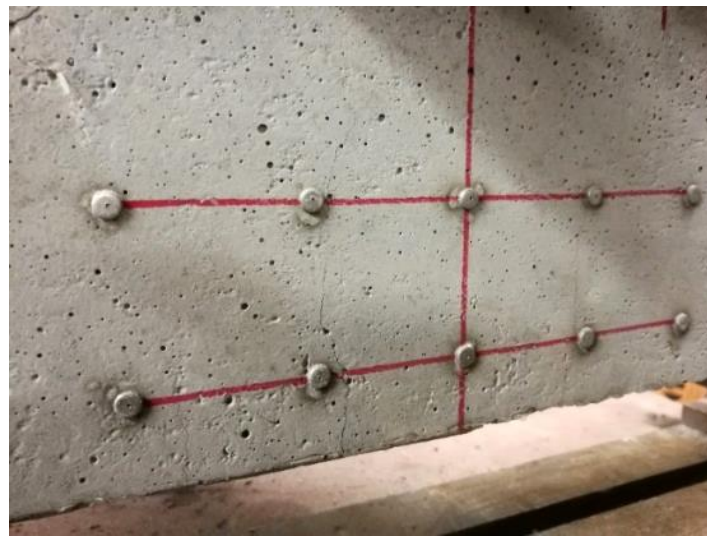


*Figure 3–28. Visible crack in the bending area*

Before starting the test, it was necessary to prepare the samples. These were polished from asperities to ensure a homogeneous contact with the supports and the loading device. In addition, two rows of small discs were glued to the side of each sample, setting up an upper row and a lower row, to be able to measure the strain variation at two different levels with a Demountable Mechanical Strain Gauge (DEMEC) before, during and after every loading-unloading cycle. The device has two positioning points, one fixed

and one mobile; it allows to measure lengths with the precision of thousandth of a millimetre, being previously calibrated on the length of a reference bar. However, it is important to specify that the device is only indicative of a certain level of overall damage but is not representative of the opening of each single crack. Finally, a displacement sensor (Figure 3–29) has been installed on the other side of the sample which, connected with a personal computer, provides in real time the load-displacement graph related to the test. Once the sample is ready and placed symmetrically respect to the points of support, the test can start. Since a press with manual loading has been used, it was necessary to pay close attention in increasing and decreasing load slowly, with a rate of stress as constant as possible.



Figure 3–29. Displacement sensor used in the pre-cracking stage

The procedure for controlling crack width was based on calculating the strain at six intervals separated by initial distance of 100 mm (Figure 3–30). First, the change in length between the points with the DEMEC was detected and then strain ( $\epsilon$ ) was calculated through the following formula:

$$\epsilon = \frac{\Delta L_0 - \Delta L_x}{l_0} 1000 \quad \text{Eq. 3.5}$$

- $\varepsilon$  = strain [‰]
- $\Delta L_0$  = length between 2 DEMEC points at zero load [mm];
- $\Delta L_x$  = length between 2 DEMEC points at x load [mm];
- $l_0$  = original length of 100 mm

This method allows to control crack width at two different heights: at the lower row (points 1-5) and at the upper row (points 6-10). The first one is located at middle depth of the beam and the second at the reinforcement level. The latter suffers the highest deformation and has been used in this study as reference for reaching the "large cracking level".

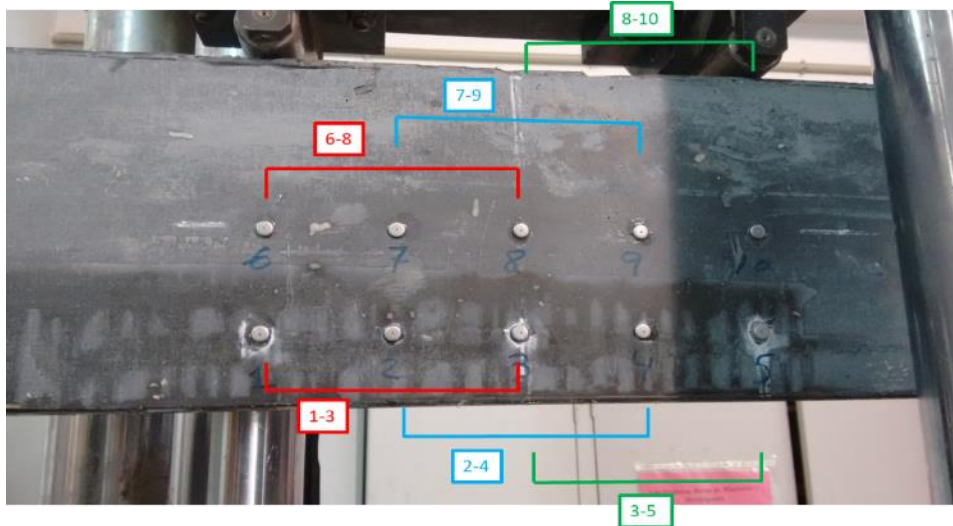


Figure 3-30. DEMEC points glued to the beam to measure strain

The goal of the pre-cracking stage was to create a damage with basically 2 different levels of cracking, summarized below:

- *Small crack / crack closed*: achieved with a strain equal to 0,5‰ (0,05 mm / 100 mm) during loading at the upper DEMEC row;
- *Large crack*: achieved with a residual strain between 1‰ and 2‰ after unloading at the lower DEMEC row (reinforcement level).

The first level of cracking represents a situation that can occur in service conditions, while the second one represents a condition that goes beyond the service limit state,

since during loading the strain value of 2‰ is abundantly exceeded, value for which rebars start to yield. In this study beams have been pre-cracked reaching the "large cracking level", while the "small cracking level" will be performed in future investigations as a continuation of this study.

The load-displacement curves obtained with this method show the expected different trends for the two rows (Figure 3–31), demonstrating that the levels proposed are possible to be reached and measured.

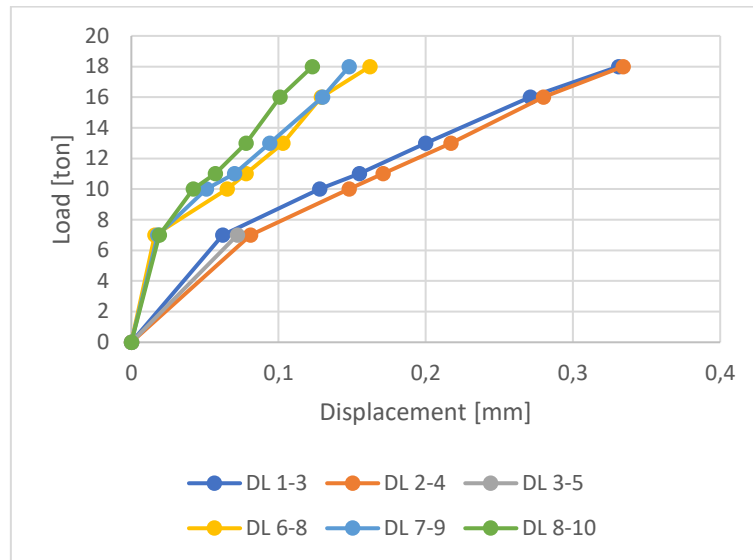


Figure 3–31. DEMEC intervals displacement as a function of the load

Regarding the different proposed crack levels, "small crack" or "crack closed", defined as the set of cracks obtained during loading when measuring an average strain of 0,5‰ at the upper row, is translated after unloading into strains close to 0,25‰. "Large crack", defined as the set of residual cracks obtained after loading when measuring an average strain between 1‰ and 2‰ at the lower row, is achieved after strains of 4‰ - 5‰ under load.

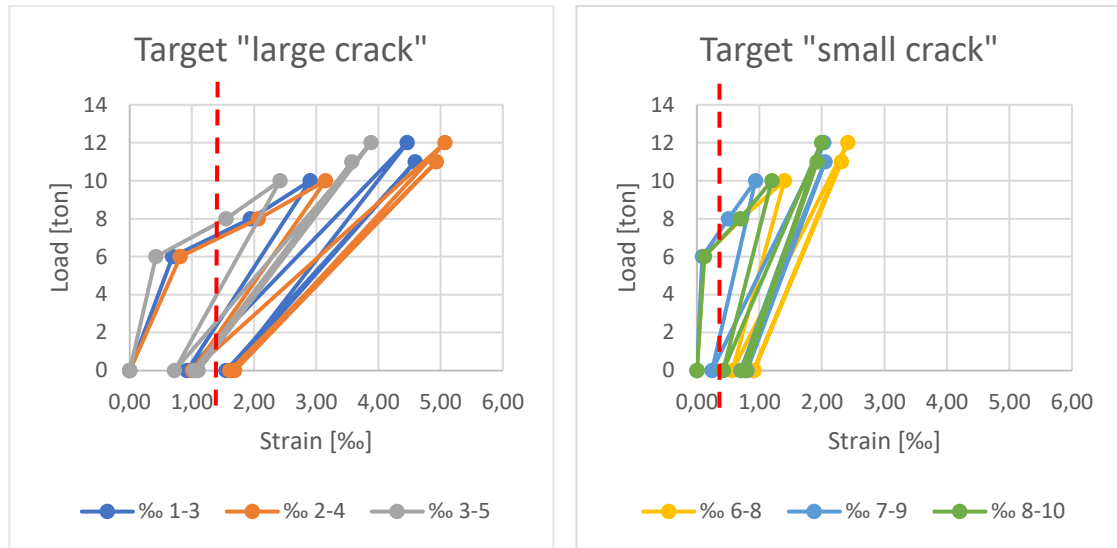


Figure 3-32. Strain target for "large crack" and "small crack"

The strain values obtained with DEMEC points have been then complemented with measures with optical microscope at either at upper or lower row levels to correlate strain rates and crack widths, a critical relation for the evaluation of the durability parameters.

### 3.5.3 Cracks analysis

The analysis of the cracks has been done on the cracked beams to inquire in the MEDEC's area: the number of cracks, their exact position and in particular their size.

The method followed was as follows:

- 1) The total number of cracks is counted on each of the two DEMEC rows;
- 2) The position of every crack is determined in the intervals of the DEMEC area (1-3, 2-4...);
- 3) Cracks width is measured. Two tools have been used:

- A *Crack Width Meter*, used to easily measure visible cracks, with graduations from 0,05 mm to 0,9 mm (Figure 3-33);





*Figure 3-33. Crack Width Meter*

- A *PCE-MM200 Microscope*, used to observe and measure every crack  $< 0,05$  mm, which cannot be seen with naked eye; besides, this tool has the possibility to make photos, videos and measure widths, so it was also used to map every kind of crack.



*Figure 3-34. PCE-MM200 Microscope*

Dealing with visible cracks, the measurement performed with the Crack Width Meter have been compared with the crack opening previously measured with the DEMEC, dividing this value by the numbers of cracks present in the specific DEMEC interval (1-3, 2-4...). Dealing with not visible cracks, an optical microscope has been used to analyse them. In this case the measurement with DEMEC has been compared with the measurement done at the computer on the picture taken under the microscope, to verify that the results coincide. The crack width has been measured with AutoCAD comparing cracks to a reference measure of 0,1 mm at the same scale. The microscope

has the possibility to take photos at two magnification ratios, 60X and 200X; the first one was used for large cracks ( $>0,1$  mm) in traditional concretes, whereas the second one was used for small cracks ( $<0,1$  mm) in UHPFRC. The pictures were taken before and after healing, to be able to evaluate the effects of self-healing on cracks closing.

### 3.5.4 Sawing

Cracks, after the pre-cracking stage, are located in the central section of the beam (zones A to D in the picture) while the lateral portions of the beam remain un-cracked. For this reason, beams have been sawn to obtain four smaller specimens of the size of  $150 \times 150 \times 50$  mm<sup>3</sup> to perform the subsequent permeability tests, according to the following scheme (Figure 3–35):

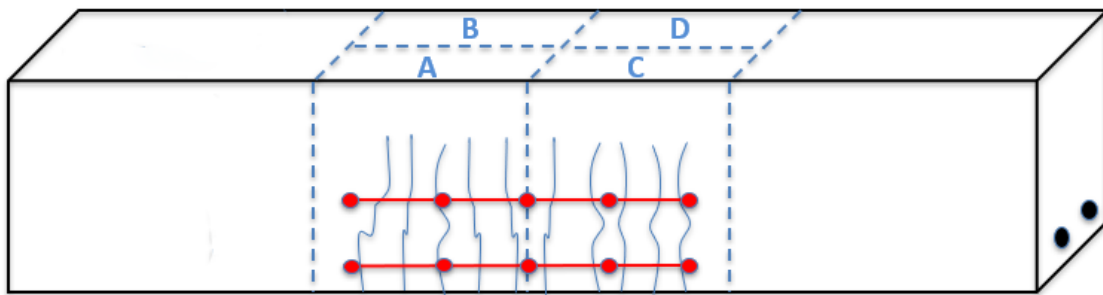


*Figure 3–35. Sawing scheme*

In this study, only the specimens A and B of each beam have been tested, while the specimens C and D will be temporarily preserved for future investigations as a continuation of this work. In total 52 specimens have been taken, four for each concrete batch, to ascertain homogeneity and consistency in the results, and then decrease the degree of uncertainty. The result obtained after sawing is shown in the picture below (Figure 3–36).



Figure 3-36. Specimens A and B obtained after sawing

### 3.5.5 High-pressure water permeability test

In this investigation for the evaluation of permeability of cracked and healed concrete specimens was employed a method called "Water Permeability Test" (WPT) which allows measuring the water flow passing through the specimen during a certain period. Water flow was measured by weighting the amount of water passed through the cracked specimen in a fixed time (gH<sub>2</sub>O). Tests were performed for a testing time of 5 minutes, collecting water with an ordinary bucket.

This study was implemented in order to analyse the durability of UHPFRCs with a determined cracking level, related to their capacity in preventing the entry of liquids, then comparing their performance with the traditional concretes one. The objective is to demonstrate that the behaviour in terms of permeability of a UHPFRC is better than the behaviour of a traditional concrete, thanks to its features such as its cracking pattern with multiple micro-cracks.





*Figure 3–37. Permeabilimeter used for performing high-pressure water permeability tests*

Tests were carried out using an equipment called "Permeabilimeter" (Figure 3–37) capable of exerting 2 bar water pressure, always kept under control thanks to a pressure gauge. To guarantee the success of the test it was also necessary to use four rubber gaskets with ring shape to allow a homogeneous contact of the device with the sample and consequently avoid pressure losses due to the premature leakage of water. Four gaskets were necessary because of the 50 mm specimens' thickness. The best layout was achieved after some attempts placing two gaskets at the top and two at the bottom of the specimen, making sure that all the water pressure was directed to the cracked area, forcing water to find a possible escape route only through cracks. An example of the test with a UHPFRC specimen is shown in the picture below (Figure 3–38).



Figure 3–38. High-pressure water permeability test methodology

Preliminary tests performed with different type of concretes characterized by different cracking level and the subsequent tests strictly related to the study of self-healing, confirmed the correlation between average crack width and water flow, allowing to develop a standardized methodology to study the durability properties connected to self-healing. The results in the following Table 22 show the degree of permeability proved by the samples in the preliminary tests.

<i>Concrete</i>	<i>Average Crack Width [mm]</i>	<i>High-pressure WPT results [g H<sub>2</sub>O]</i>
<b>UHPFRC</b>	< 0,05	0
<b>UHPC</b>	0,05	60
<b>HPC</b>	0,30	8300

Table 22. High-pressure water permeability preliminary test results

As it is possible to notice from the photo taken from below during one of the preliminary tests (Figure 3–39), drops of water exactly comes out from the crack. This was the case of 0,05 mm crack (the UHPC in the Table 22).



*Figure 3–39. Drops of water from a 0.05 mm crack during high-pressure water permeability test*

However, traditional concretes showed a totally opposite behaviour in water permeability tests. It was not possible performing the whole 5 minutes test, since specimens, as soon as the water valve was opened, immediately allowed the water flow to pass through the cracks. Most of times water did not escape from the bottom of the specimens as expected, but from side cracks (Figure 3–40), flooding the laboratory and making the measurements impossible. Besides, during tests, because of the water pressure and the compression applies from the device, two specimens broke.



*Figure 3–40. Leakage of water from a side crack during the high-pressure water permeability test in a traditional concrete*

The reason of this event lies in the fact that the cracking level reached with this type of concrete was too high to allow performing this test under water pressure achieving measurable results. Traditional concrete, in fact, since is made of bigger aggregates, lower cement content and total absence of fibres makes cracks easier to open (compared to a UHPFRC) when subjected to further external stresses. For this reason, to evaluate self-healing capability in traditional and high-performance concrete, it has been decided to perform a water permeability test in low-pressure conditions, which will be discussed in the next section.

### 3.5.6 Low-pressure water permeability test

Using a PVC tube ( $\varnothing_e = 75$  mm) glued to the specimens, the purpose of the test was to calculate the time taken by a 50 cm column of water to empty, passing through the cracked specimen (Figure 3–41). When cracks were too small to allow the column to empty within a few hours, it was decided to calculate the decrease in water-height of the water column in a given time frame (3 hours).

These further tests, as previously mentioned, have been performed only for traditional and high-performance concrete samples, as a result of the outcomes of the water permeability tests. In fact, since no quantifiable result was achieved, the high-pressure water permeability test was modified into the low-pressure one. Thanks to this test, it was possible to have reference values related to the degree of permeability provided by the specimens. These have been then tested a second time after the healing period in water and, according to the new results, assessments have been made on self-healing effects in recovery of durability properties.



*Figure 3-41. Low-pressure water permeability test methodology*

### 3.5.7 Chloride penetration test

This test was designed to reproduce the aggressive conditions that characterize the chloride-rich environments (exposure class XS), where steel bars present in concrete are exposed to the chemical attack of salts, which can provoke their corrosion and compromise the efficiency. The test can be applicable for marine structures as well as to structures exposed to de-icing salts.



*Figure 3-42. Chloride penetration test methodology*



Test consists in calculating the sodium chloride penetration into a cracked specimen, caused by a salt water column of 50 cm, after 3 days of testing time. To actualize the test, PVC tubes with outer diameter of 75 mm were used. Tubes were glued to the specimens with a high-performance sealant from Sika (Sikaflex), that prevents the water to come out from the bottom of the tube owing to the non-perfect flatness of the two surfaces. Every tube was filled with salt water with a concentration of 35 g NaCl/litre, in such a way as to reproduce the conditions to which concrete is exposed in marine environment. Attention was paid that the water was every day on the marked line of 50 cm and, in case of evaporation, distilled water was added to maintain the same pressure level. The day before the beginning of the test, the specimens were put in oven at the temperature of 100°C for 24 hours, to eliminate any present residue of water or humidity due to the previous water permeability test. Once three days of testing have passed, the tube was removed, and the specimen was dissected transversely to the direction of the cracks with a circular saw (Figure 3–43).



*Figure 3–43. Specimen transversely sawn after chloride penetration test*

In order to measure the chloride penetration depth a specific procedure was carried out. Firstly, specimens were left to dry, afterwards a Silver Nitrate ( $\text{AgNO}_3$ ) solution with a concentration of 0,1 mol/l was sprayed on the both cracked surface where the cut was made. The solution induces a chemical reaction whereby two different brown and white areas form on the surface of the specimen. The white precipitate, the area of interest, is formed because of the reaction between the silver ions and the chloride ions, while the brown one is formed when the silver ions react with the hydroxyl ones. Before being

able to clearly see the different areas, specimens were put again in oven (Figure 3–44). After 24 hours, the reaction has ended, and colours are more discernible obtaining a diffusion like the one in the picture below (Figure 3–45).



*Figure 3–44. Sawn specimens in oven to dry*



*Figure 3–45. Chloride penetration through the specimen thickness (HB4)*

Preliminary tests performed on different types of concrete with different cracking levels demonstrated the efficiency of this test in the evaluation of chloride penetration in concrete, allowing to develop a standardized methodology which has been used in the study of self-healing. Preliminary tests confirmed that this type of test can easily be performed with superficially measured crack widths  $< 0.1$  mm but appears to be totally ineffective for crack widths  $> 0.1$  mm. In fact, as the Figure 3–46 shows, performing the

test with a high-performance concrete specimen with 0.3 mm of crack width, water immediately passed through the crack, flooding the table.



*Figure 3–46. Attempt of chloride penetration test with a HPC with 0.3 mm of crack width*

### 3.5.8 Self-healing

To study the effects due to the self-healing, specimens have been left in a tank full of water for 28 days (Figure 3–47). The water used for the self-healing process comes from demineralizers with ion-exchange resins; it is about water treatment plants used for the removal of ions to obtain water with low salt content. The purification is ensured by an ion exchange action in the filters containing the exchange resins. In this case the filtration system uses mixed-bed resins, i.e., cationic and anionic resins mixed in the same plant, with approximately a proportion of 60% anionic of strong base and 40% cationic of strong acid. Thanks to this ionic exchange it is possible to produce ultra-pure demineralized water with values  $< 0,1 \mu\text{S}/\text{cm}$ . It was decided to use demineralized water not to condition the results of the chloride penetration tests after healing. As previously explained, the twin specimens (B sides) have been immersed in water to heal, since the procedure for detecting chloride penetration does not allow the same sample to be tested twice. After one month in water, it is expected that cracks in the specimens have



closed or partially closed on the surface, thus being able to assess whether the visual crack closure could actually correspond to a recovery of the durability properties.



*Figure 3-47. Specimens in a tank of water during healing exposure*

## 4. Test results and discussion

This chapter reports and discusses the results of the experimental campaign. It shows the results of the compressive strength tests, the results of the pre-cracking phase, the results of the permeability tests and finally the outcomes on self-healing.

### 4.1 Compressive strength results

In this section the results concerning the compressive strength tests are presented. The methodology followed is described in the section "*Mixing process and control tests*". This test is widely employed to identify the strength class of concrete and poorly used to evaluate the healing performance of cement-based materials (Ferrara et al., 2018), however in this study compressive strength tests have not been performed as a method to evaluate self-healing but only to characterize the different mix compositions, namely, to evaluate the influence of the addition of crystalline admixtures and nanomaterials on compressive strength, compared to the control group. Four 100x100x100 mm<sup>3</sup> cubes for each concrete batch have been casted. Only for the batch "HB3 + Penetron (2,4%)", the one with poor workability, eight cubes were produced. Initially, the intention was to test cubes both at the ages of 7 and 28 days, however, because of logistic problems, most of the cubes were only tested at 28 days (Figure 4–1).



Figure 4–1. Broken sample after a compressive strength test

Graphs below report the averaged compressive strength values obtained with their own standard deviation at the age of 28 days for the different mixes. Figure 4–2 shows the compressive strength results (MPa) obtained for the control group made of the two types of commonly used concrete H0 (traditional concrete) and H1 (high-performance concrete), and the two base mixes of Ultra-High-Performance Fibre-Reinforced Concretes HB3 and HB4. Figure 4–3 shows a comparison among all the functionalized batches based on the HB3 mix design. Figure 4–4 shows a comparison among all the functionalized batches based on the HB4 mix design.

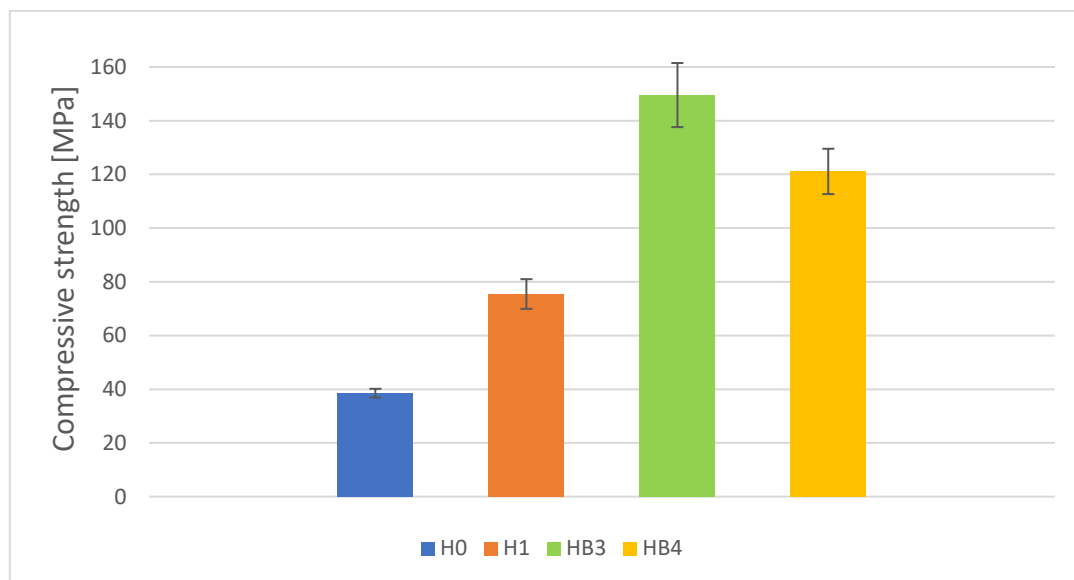


Figure 4–2. Average compressive strength H0, H1, HB3 and HB4

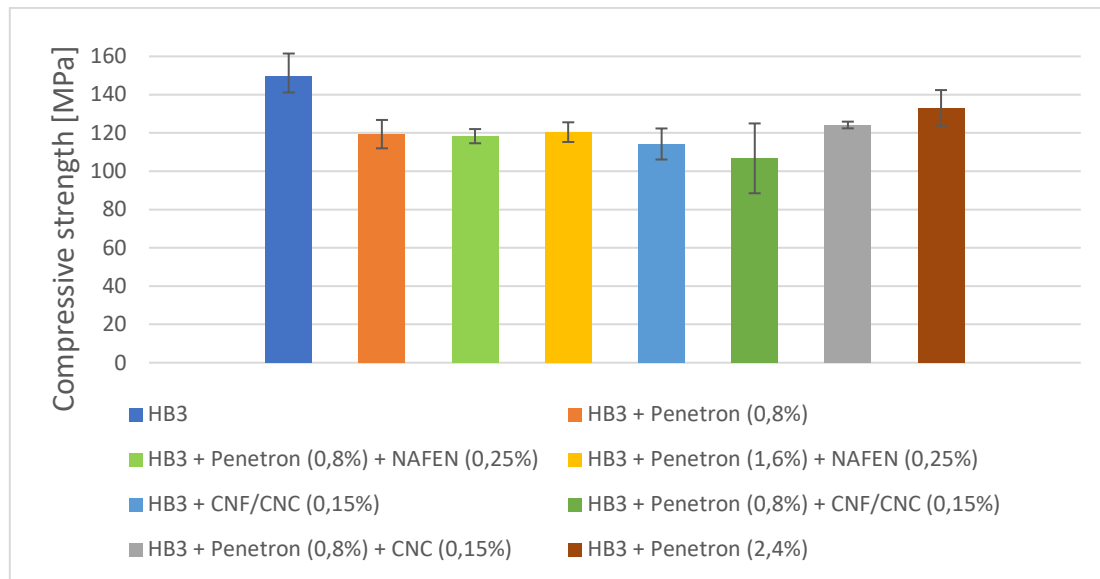


Figure 4-3. Average compressive strength HB3 functionalized batches

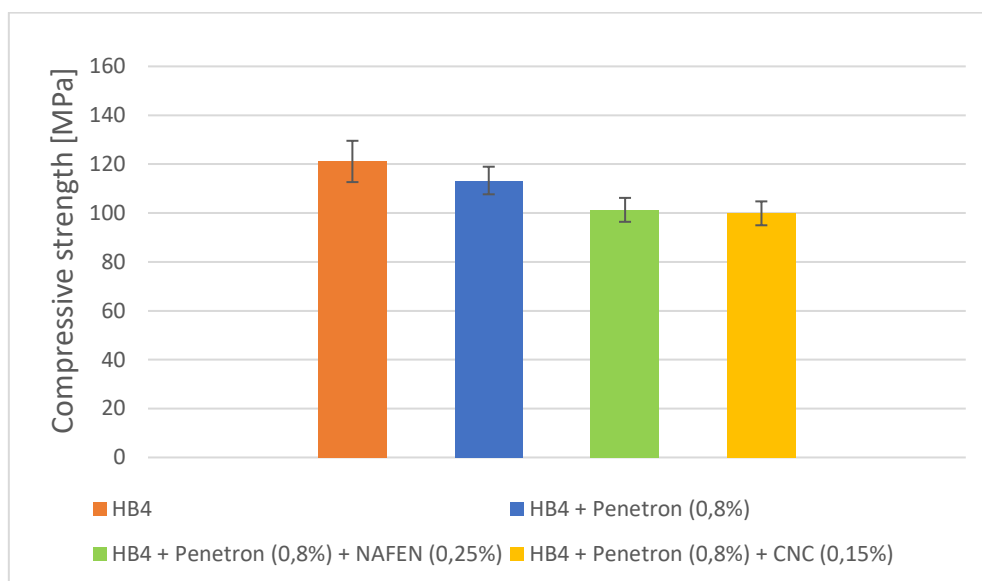


Figure 4-4. Average compressive strength HB4 functionalized batches

As it is possible to observe from the graphs, the addition of crystalline admixtures and nanomaterials negatively affects the compressive strength of UHPFRCs. The only addition of Penetron at low concentrations (0.8% - 1.6%) of the binder materials caused a decrease in compressive strength of 20% in the HB3 mix while a decrease of 6% in the HB4 mix, preserving a good workability. The highest value was obtained with a

concentration of 2.4%, but overly influencing workability. The only addition of Nanocellulose in the HB3 mix, for a 50% of CNC and 50% of CNF, at a concentration of 0.15% of the binder materials caused a decrease in compressive strength of 14%. Regarding the combined addition of Penetron and nano-cellulose or nano-alumina (NAFEN) in the same mix, results show that in the HB4 mix compressive strength is even more negatively affected, while in the HB3 mix results do not present a clear distribution, but a decrease of about 20% is noted though. The higher standard deviation of the mix "HB3 + Penetron (0.8%) + CNF/CNC (0.15%)" with respect to the other mixes could be due to an insufficient dispersion of the nanoparticles in the mixture, however more studies are needed to verify it.

The reason of the decrease in compressive strength with the addition of nanomaterials and crystalline admixtures could be produced by the high water demand of these additions. This point is clear in the case of nanocellulose, since they are potent adsorbents of water (Ousmane et al., 2018), but in the case of alumina nanofibers and crystalline admixture further studies are needed to discern the reasons, since in other studies with different base concretes, strength at the age of 28 days was not reduced but increased (Roig-Flores et al., 2015; Roig-Flores et al., 2016).

## 4.2 Tensile strength results

This section presents the results related to the "Inverse Analysis" carried out in parallel with this work in order to characterize UHPFRC tensile strength. Tests were performed through a Four-Point Bending Test on the 500x100x100 mm<sup>3</sup> prisms casted. Results are reported in the Table 23 to have a complete characterization of the compressive and tensile behaviour of all the concrete mixes produced.

Concrete Mix	Sample	$f_t$
<b>HB3</b>	1	9,17
	2	9,81
<b>HB3 + 0.8% Penetron</b>	1	7,98
	2	7,24
<b>HB3 + 0.8% Penetron + 0.25% NAFEN</b>	1	Bad results
	2	
<b>HB3 + 1.6% Penetron + 0.25% NAFEN</b>	1	9,51
	2	9,67
<b>HB3 + 0.15% CNF/CNC</b>	1	7,12
	2	7,52
<b>HB3 + 0.8% Penetron + 0.15% CNF/CNC</b>	1	7,27
	2	7,51
<b>HB3 + 0.8% Penetron + 0.15% CNC</b>	1	6,88
	2	7,62
<b>HB3 + 2.4% Penetron</b>	Too dry to be poured in the moulds	
<b>HB4</b>	1	7,64
	2	7,87
<b>HB4 + 0.8% Penetron</b>	1	7,19
	2	7,40
<b>HB4 + 0.8% Penetron + 0.25% NAFEN</b>	1	6,48
	2	6,61
<b>HB4 + 0.8% Penetron + 0.15% CNC</b>	1	Bad result
	2	6,49

Table 23. Tensile strength results

As expected, the HB3 base mix, due to its higher fibres content, reported a tensile strength value of about 22% higher than the HB4 base mix. Moreover, as can be observed from Figure 4–5 and Figure 4–6, the addition of crystalline admixtures and nanomaterials caused a general decrease in tensile strength, more emphasized in the mixes with nano-additions than those with only Penetron. The only mix "HB3 + 1.6% Penetron + 0.25% NAFEN" has reported a slight increment with respect to the base mix HB3, however the obtained values turn out to be in contrast with the similar mix "HB3 + 0.8% Penetron + 0.25% NAFEN" whose results were not taken into consideration due to the poor outcome of both the samples tested. From these results it can be deduced that further studies on the influence of these additions on tensile strength of UHPFRC are needed.

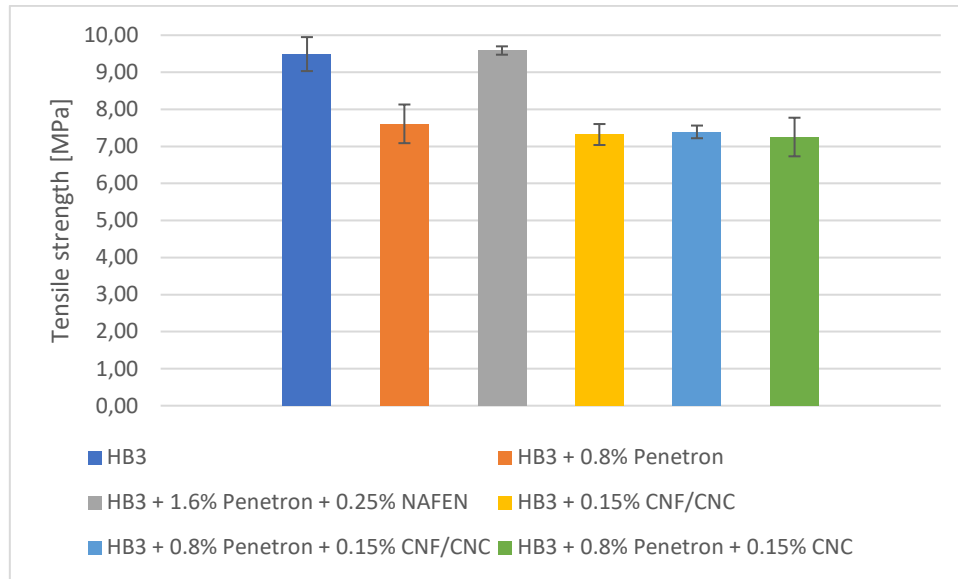


Figure 4-5. Average tensile strength HB3 functionalized batches

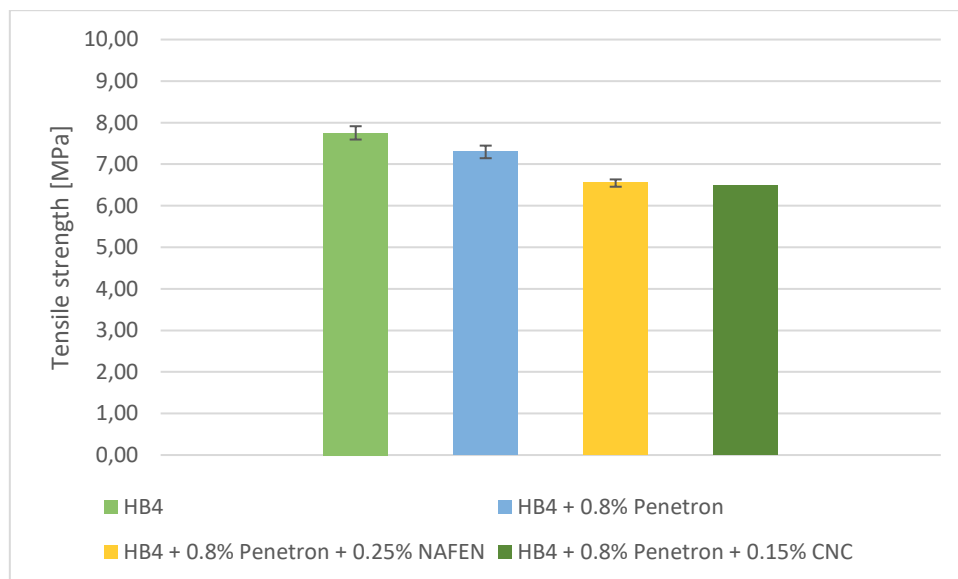


Figure 4-6. Average tensile strength HB4 functionalized batches

### 4.3 Pre-cracking results

The pre-cracking methodology followed is described in the section "Pre-cracking". In this research, using the well-known four-point bending test, two beams for each concrete

batch have been cracked, while the other beams casted will be provisionally preserved for the future investigations with "small cracking level". As previously mentioned, the cracking target was based on achieving a "large crack", or rather, a residual average strain  $\epsilon_{avg}$  between 1‰ and 2‰ after unloading at the lower DEMEC row (reinforcement level). Considering the different values of strain obtained in the intervals (1-3, 2-4, 3-5) between the DEMEC points due to the aleatory appearance of the cracks and to give homogeneity to the results, the condition of "large crack" was considered reached when the averaged strain of the three intervals of the lower DEMEC row exceeded the value of 1.5‰.

The procedure followed with the UHPFRCs (HB3 and HB4) during the controlled cracking was always the same. From zero, load was gradually increased, stopping at certain loading values. Upon reaching loads, the change in length between the DEMEC points was measured and consequently, through a spreadsheet, strain (‰) was obtained in each interval (1-3, 2-4...). Strain was usually measured at zero tons, reference condition whereby strain is equal to zero, 6 tons, 8 tons and 10 tons; arrived at 10 tons, loading-unloading cycles were performed, increasing after each cycle of a ton or medium ton until to get as close as possible to the target ( $\epsilon_{avg} \geq 1.5‰$ ). An example of the load-displacement graph obtained from the test is shown in the Figure 4–7 below.

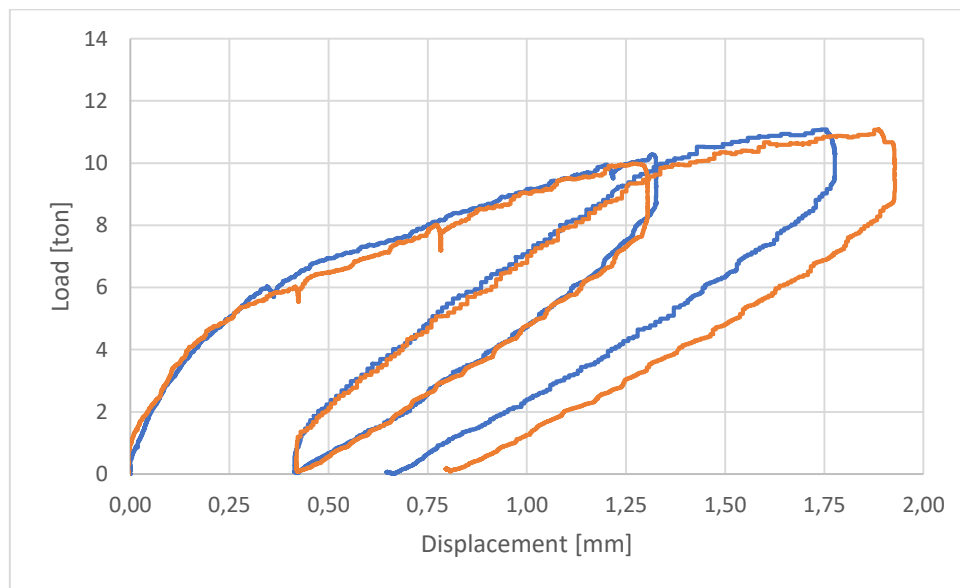


Figure 4–7. UHPFRC Load-Displacement graph



The load-displacement graph compares the trend of the curves related to the beams of the same batch. As it's possible to observe, the curves can be substantially divided in two phases: a first elastic phase and a second plastic one. The first one is referred to when the behaviour of the material is still elastic and reversible, thus the graph roughly resembles a straight line with a constant elastic modulus (Young's modulus). When the line starts curving and changing in slope, plastic deformation begins (Yielding point).

The measurement done is presented in the load-strain graphs below, where is shown how strain in every DEMEC section varies depending on the load. As it's possible to notice from the graphs, the maximum load was reached at 11 tons with strain in concrete around 4‰, far exceeding the service limit. At this strain value reinforcing bars are in full plastic deformation. Upon unloading, the material recovers a great part of its deformation, thus allowing to reach the desired target with an average residual strain value close to 1,5‰ at the lower row and < 1‰ at the upper row.

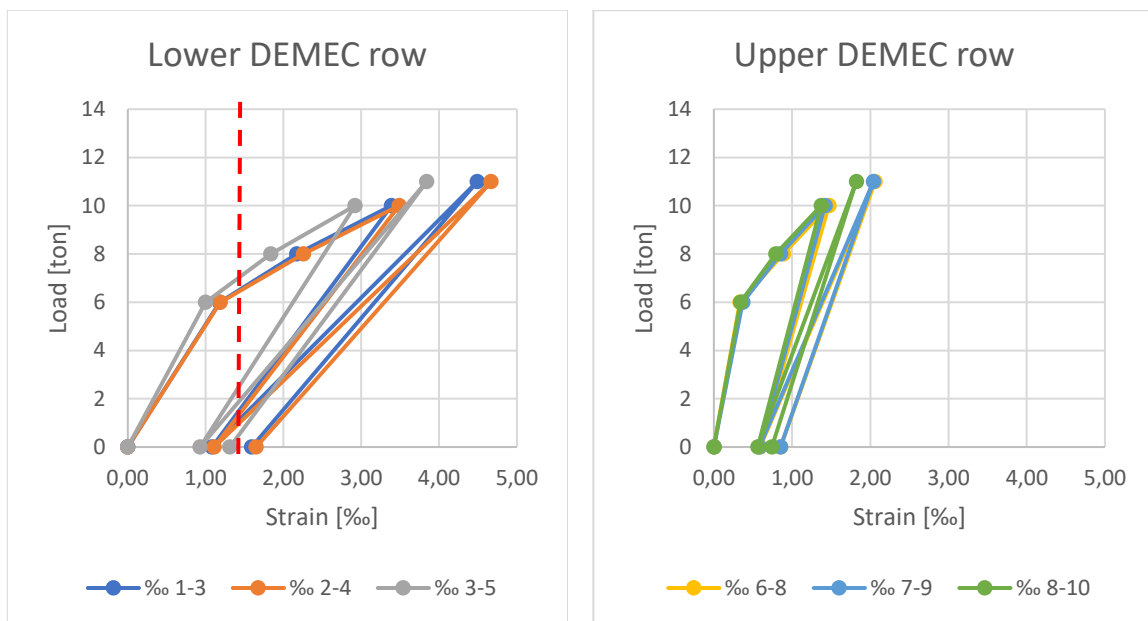


Figure 4–8. UHPFRC Load-Strain graphs

For traditional and high-performance concretes (H0 and H1) the procedure followed was the same but reaching lower loads because of their lower flexural strength. A maximum load of 6 tons has been reached, but due to the greater difficulty in controlling the crack opening with this type of concrete, very high residual strains have been achieved, in the order of 3‰ - 4‰ (Figure 4–9).

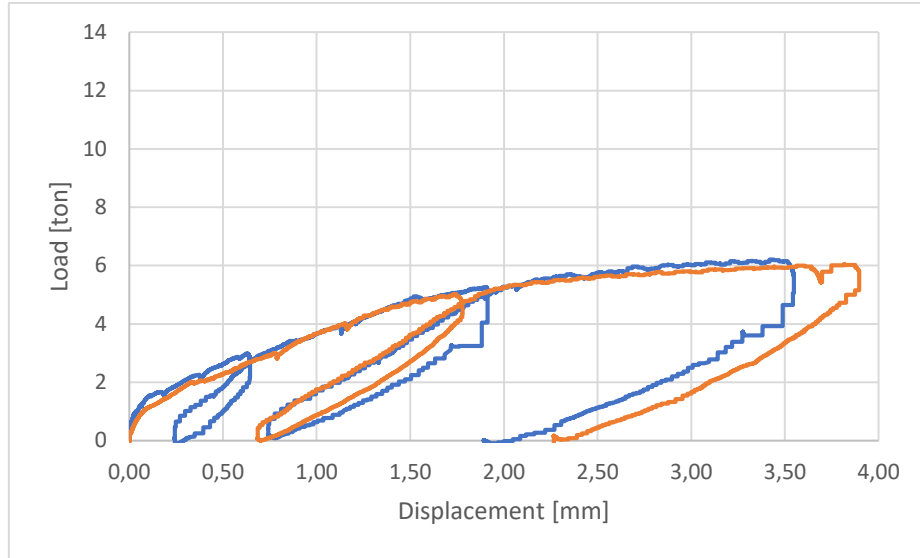


Figure 4-9. Traditional concrete Load-Displacement graph

Analysing the load-strain graphs (Figure 4-10) it is possible to spot the cracking behaviour of a traditional concrete. In fact, under the same load, unlike UHPFRC which has similar strains, in traditional concrete the strain value turns out to be very different in the intervals belonging to the same DEMEC line. This fact is explainable considering the cracking pattern of a traditional concrete, characterized by only few cracks. When cracks appear, they are unpredictable, so they can appear in a position rather than another one. Accordingly, where strain values are higher, this is where crack appeared.

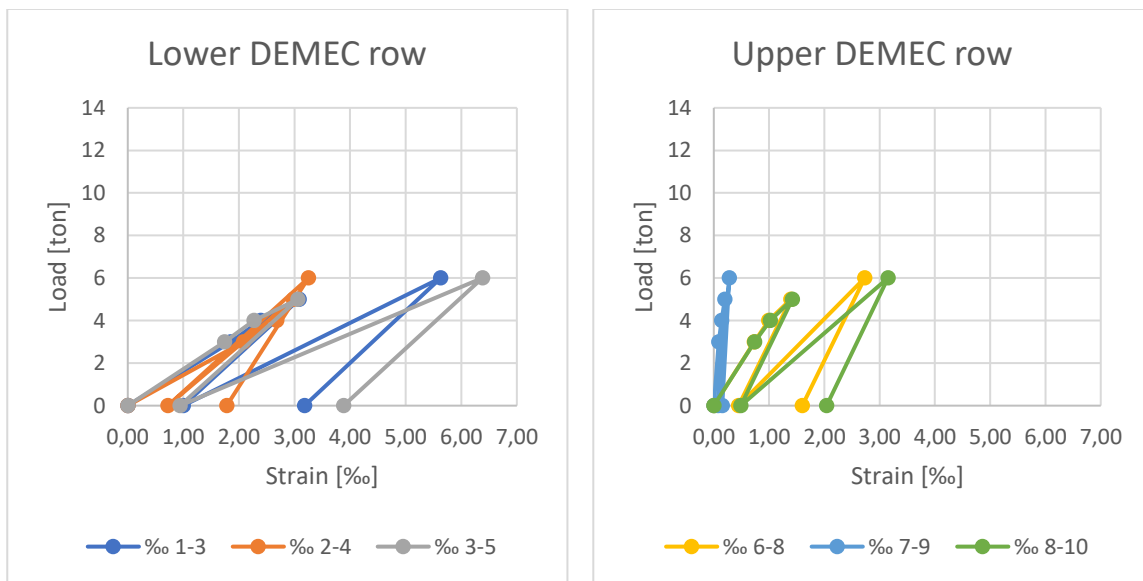


Figure 4-10. Traditional concrete Load-Strain graphs

UHPFRCs during tests showed higher mechanical performance. As expected, after unloading, due to their cracking pattern with multiple micro-cracks, UHPFRCs did not show visible localized cracks, whereas traditional concretes did. In fact, while on the one hand traditional concrete presented only few visible cracks, measurable through the use of a crack width meter (Figure 4–11), UHPFRC on the other hand featured a large number of widespread cracks, not visible to the naked eye. It is possible to notice in the Figure 4–12 how the positions of the cracks analysed with the use of the microscope were marked on the sample, for a total of 12 micro-cracks detected.



*Figure 4–11. Traditional concrete cracking pattern with few localized cracks*



*Figure 4–12. UHPFRC cracking pattern with multiple micro-cracks*

Moreover, by comparing the appearance of the first visible crack under load between traditional concrete and UHPFRC, it has been observed that in the former the first crack appeared at about 2 tons whereas in the latter at about 8 tons. This cracking behaviour of UHPFRC is achieved thanks to its particular mix design consisting of small size of the constituents, high cement content and steel fibres capable of limiting crack opening. The amount of fibres in the mix turned out to be of great importance in the control of crack opening. In fact, the HB4 mix, having a lower amount of fibres (130 kg/m<sup>3</sup> instead of 160 kg/m<sup>3</sup> of the HB3 mix) showed lower flexural strength and lower performance in terms of control of the crack opening. Nevertheless, while the remarkable mechanical properties of this type of concrete are well-known, this thesis mainly focuses on the study of the consequences of this cracking pattern in ensuring a better degree of durability and improving self-healing efficiency.

All the graphs related to pre-cracking stage can be consulted in Appendix 1. Pre-cracking results.

## 4.4 Cracks analysis results

The analysis of surface cracks has been performed to study the different cracking behaviour of the two classes of concrete and afterwards to set a correlation between crack width and the permeability degree provided by the samples, measured in the water permeability and chloride penetration tests.

The reference parameter used to study concrete permeability is the average crack width  $\omega_{avg}$ . For each sample, two average crack widths at two different level have been calculated, one for the upper DEMEC row at the height of 7.5 cm and one for the lower DEMEC row at the height of 2.5 cm from the base. With the optical microscope every kind of crack in the DEMEC area was detected as described in the section "Crack analysis". The number of cracks and their size in each DEMEC interval has been identified, thus being able to estimate an average crack width at the level of the two lines. At the end of the analysis, it was observed that UHPFRCs presented an average

number of 14 micro-cracks in the DEMEC area, with an average width of 0.03 mm at the lower row; cracks width naturally decreases towards the mid depth of the beam. This confirms their peculiar cracking pattern. Traditional concretes, after the analysis, presented only 2 ÷ 3 visible localized cracks instead, each one with an average width of 0.2 mm (see Table 24). The following Figure 4–13 shows a comparison between the different crack width generated by the different cracking pattern of a UHPFRC and a traditional concrete.

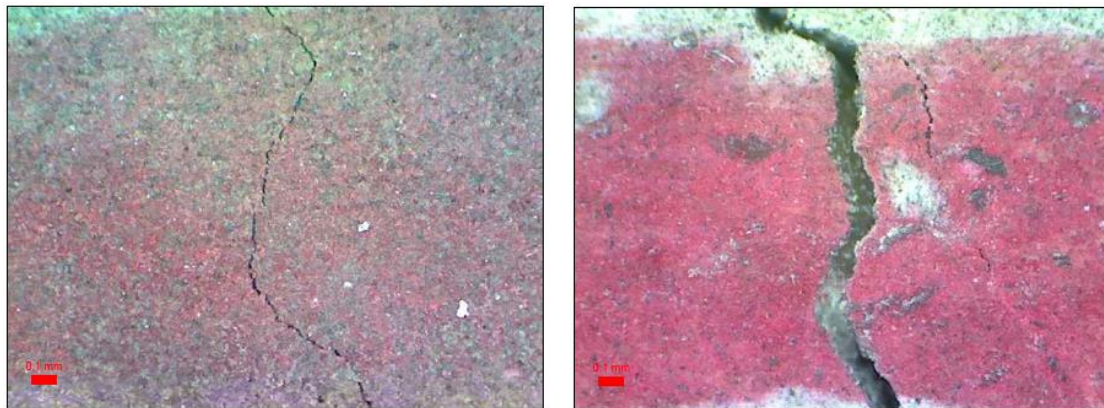


*Figure 4–13. Comparison between a crack of 0.01 mm in a UHPFRC and a crack of 0.1 mm in a traditional concrete at the same magnification (200X)*

Most of the cracks found in the DEMEC area has been photographed and measured to be able to compare cracks before and after healing. Some cracks have also been mapped combining multiple photos. The following Figure 4–14 is an example of a panorama of a 0,01 mm crack in a UHPFRC.

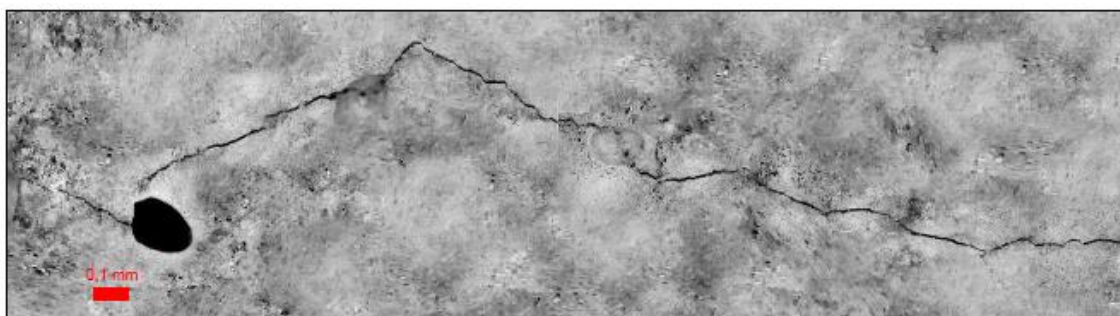


*Figure 4–14. Panorama of a 0.01 mm UHPFRC crack*

Tables below show the results of the crack analysis for all the pre-cracked beams. Each beam has its own number (from I to XXVI) so that it can always be identified. Table 24

show the data obtained in relation to the control group (H0, H1, HB3 and HB4), while Table 25 and Table 26 show the data related to the functionalized batches, with reference to their base mix (HB3 - HB4). The following parameters have been calculated:

- Maximum load reached before unloading at the end of the test;
- $\epsilon_{avg}$  = residual average strain;
- N° cracks = number of cracks detected on the specific DEMEC row (1-5 or 6-10);
- $\omega_{avg}$  = average crack width.

Concrete	Beam	Max. Load [ton]	DEMEC 1-5			DEMEC 6-10		
			$\epsilon_{avg}$ [‰]	N° Cracks	$\omega_{avg}$ [mm]	$\epsilon_{avg}$ [‰]	N° Cracks	$\omega_{avg}$ [mm]
<b>H0</b>	I	6,2	3,7	2	0,2	1,66	2	0,1
	II	6	2,95	2	0,2	1,26	2	0,1
<b>H1</b>	III	6,6	4,33	3	0,15	2,56	3	0,1
	IV	6,5	4,35	2	0,25	2,78	2	0,15
<b>HB3</b>	V	12	1,4	12	0,025	0,81	12	0,015
	VI	13	1,55	11	0,025	0,9	11	0,015
<b>HB4</b>	VII	11	2,26	20	0,025	1,21	11	0,015
	VIII	11	2,19	14	0,05	1,56	10	0,03

Table 24. Control group crack analysis results

Concrete	Beam	Max. Load [ton]	DEMEC 1-5			DEMEC 6-10		
			$\epsilon_{avg}$ [‰]	N° Cracks	$\omega_{avg}$ [mm]	$\epsilon_{avg}$ [‰]	N° Cracks	$\omega_{avg}$ [mm]
<b>HB3</b>	V	12	1,4	12	0,025	0,81	12	0,015
	VI	13	1,55	11	0,025	0,9	11	0,015
<b>HB3 + 0.8% Penetron</b>	IX	11	1,71	12	0,025	0,84	7	0,015
	X	10	1,71	7	0,03	0,8	5	0,02
<b>HB3 + 0.8% Penetron + NAFEN 0.25%</b>	XI	13	1,73	16	0,015	0,92	9	0,015
	XII	12	1,67	10	0,05	0,88	14	0,015
<b>HB3 + 1.6% Penetron + NAFEN 0.25%</b>	XIII	11	1,69	9	0,03	0,88	8	0,015
	XIV	12	2,68	12	0,03	1,32	8	0,015
<b>HB3 + CNF/CNC 0.15%</b>	XV	10	1,79	11	0,025	0,87	3	0,015
	XVI	11	1,52	11	0,025	0,81	7	0,015
<b>HB3 + 0.8% Penetron + CNF/CNC 0.15%</b>	XVII	12	2,37	13	0,025	1,25	15	0,015
	XVIII	11	1,98	13	0,025	0,91	4	0,02
<b>HB3 + 0.8% Penetron + CNC 0.15%</b>	XIX	10,5	1,84	11	0,03	1,04	11	0,015
	XX	11	1,68	6	0,025	0,97	13	0,015

Table 25. HB3 mixes crack analysis results

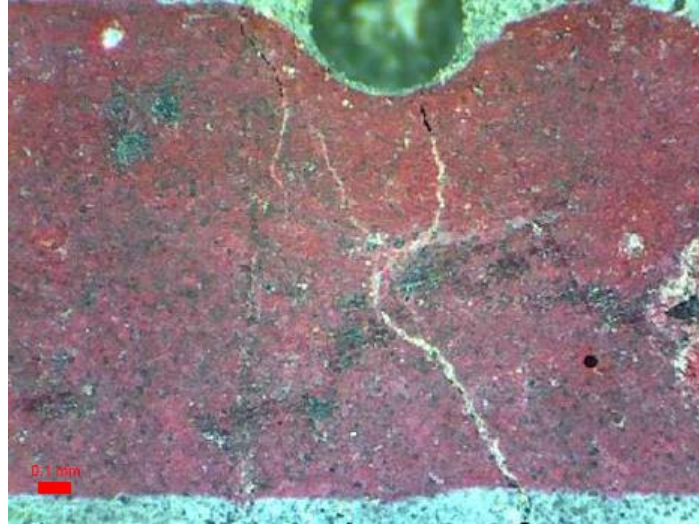
Concrete	Beam	Max. Load [ton]	DEMEC 1-5			DEMEC 6-10		
			$\epsilon_{avg}$ [‰]	N° Cracks	$\omega_{avg}$ [mm]	$\epsilon_{avg}$ [‰]	N° Cracks	$\omega_{avg}$ [mm]
<b>HB4</b>	VII	11	2,26	20	0,025	1,21	11	0,015
	VIII	11	2,19	14	0,05	1,56	10	0,03
<b>HB4 + 0.8% Penetron</b>	XXI	10	2,05	6	0,03	1,15	5	0,015
	XXII	10	1,63	6	0,025	0,86	4	0,015
<b>HB4 + 0.8% Penetron + NAFEN 0.25%</b>	XXIII	9,5	1,92	6	0,025	1,12	7	0,015
	XXIV	10	2,67	14	0,03	1,36	8	0,015
<b>HB4 + 0.8% Penetron + CNC 0.15%</b>	XXV	10	2,99	13	0,03	1,85	12	0,015
	XXVI	9,5	1,59	14	0,025	0,85	11	0,015

Table 26. HB4 mixes crack analysis results

As can be observed from the tables, in general HB4 mixes, compared to HB3 mixes, at the same maximum load reached or even lower, have always suffered greater deformations, due to their lower fibres content, but with a comparable value of average number of residual cracks and average crack width. As regard instead the addition of crystalline admixtures and nanomaterials in the HB3 and HB4 mixes, for similar deformation values, no appreciable variations have been detected in terms of number of cracks appeared and average crack width.

The analysis also found that even before the self-healing exposure in water, in the samples with the addition of crystalline admixtures and nanoparticles, part of the narrower cracks with a width <0,05 mm already appeared closed or semi-closed, characterized by a whitish precipitation possibly attributable to the calcium carbonate ( $\text{CaCO}_3$ ), as shown in the Figure 4–15 below.





*Figure 4–15. Crack closed before the healing exposure*

## 4.5 High-pressure water permeability test results

Water permeability was the condition upon which the subsequent low-pressure water permeability tests and chloride penetration tests were based, since these latter tests were carried out accordingly to the results obtained in the high-pressure water permeability tests.

All the UHPFRCs tested have shown excellent results in terms of permeability, with zero grams of water passed through the specimens in 5 minutes of testing time. Since the specimens are characterized by the same cracking level, after five tests with no results of water passed, it was decided to conclude the tests related to the UHPFRCs, stating that for all the specimens with "large cracking level" corresponding to an average crack width of 0.03 mm water does not pass. Figure 4–16 reports a photo taken from below during a high-pressure water permeability test where there are no signs of water passing through the sample.





Figure 4-16. Bottom of a UHPFRC specimen during a water permeability test in 2 bar pressure

Table 27 below shows the results of the tests performed on UHPFRC specimens.

<i>Specimen tested</i>	<i>Average Crack Width [mm]</i>	<i>High-pressure WPT results [g H<sub>2</sub>O]</i>
<b>V - A</b>	0,025	0
<b>V - B</b>	0,025	0
<b>VII - A</b>	0,025	0
<b>VII - B</b>	0,050	0 ÷ 10
<b>IX - A</b>	0,025	0

Table 27. High-pressure water permeability test results (UHPFRC)

None of the specimens showed clear signs of water passing through the cracks. Furthermore, no moisture was even detected at the base of the specimens at the end of the tests, proof that water was not able to cross the cracked section. Only in the case of the specimen VII - B, characterized by a slightly higher average crack width (see Table 27), some drops of water were observed came out, however, it was not possible to measure them due to the too small weight, approximately from 0 to 10 grams.

As proof of the fact that samples are actually cracked, Figure 4–17 shows the specimens condition at the end of the water permeability tests. Water pressure brought to light all the micro-cracks previously observed with the microscope.



Figure 4–17. Cracks made visible by the water permeability test

As explained in the methodology section "High-pressure water permeability test", with traditional and high-performance specimens it was not possible to perform the tests, consequently, as for UHPFRC, no quantifiable results have obtained (see Table 28).

<i>Specimen tested</i>	<i>Average Crack Width [mm]</i>	<i>High-pressure WPT results [g H<sub>2</sub>O]</i>
<b>I - A</b>	0,20	Not measurable
<b>I - B</b>	0,20	Not measurable
<b>III - A</b>	0,15	Not measurable
<b>III - B</b>	0,15	Not measurable

Table 28. High-pressure water permeability test results (traditional and high-performance concrete)

In conclusion, the outcomes of the water permeability tests in high-pressure conditions confirm the better behaviour in durability of a UHPFRC respect to a traditional concrete.

The former was able to totally prevent the entry of liquids in a cracked sample with average crack width of 0,025 mm, whereas the latter, with average crack width of 0,2 mm, let all the water run in a few seconds. Despite the considerable importance of these results, this type of test was not able to give back numerical values able to detect an improvement after the healing process, consequently, water permeability tests in low-pressure conditions and chloride penetration tests, respectively for traditional concretes and UHPFRCs, have been carried out, from which more tangible results have been achieved.

## 4.6 Low-pressure water permeability test results

The results obtained from the specimens tested demonstrate a direct correlation between crack width and water flow, without any external pressure induced. As the specimens were of traditional concrete and high-performance concrete, test was performed on a single localized crack. As supposed, larger was the crack width, lesser the time taken by the water column to empty. In fact, specimens with a higher cracking level have proved a faster water flow through the crack and they took less time to end the test. It was observed as well that water flow speed decreased in time due to the continuous decrement in pressure of the water column itself. Before starting the tests, a further crack analysis was made on the specimens, to verify if crack width was the same respect to the previous analysis, keeping in consideration that the sawing operation could have modified the crack width. From this analysis, it was noticed that cracks were wider in the inner section of the beam, namely, at the interface between the sample A and B, where the cut was made, whereas on the surface, cracks were approximately narrower of 0,01 mm.

The results related to the four specimens tested, two of conventional concrete (II - A and II - B) and two of high-performance concrete (IV - A and IV - B), are presented in the Table 29.

<i>Specimen tested</i>	<i>Crack Width [mm] - Superficial section</i>	<i>Crack Width [mm] - Inner section</i>	<i>Low-pressure WPT results</i>
<b>II - A</b>	0,05 ÷ 0,15	0,2	50 mm H <sub>2</sub> O (3:00 h)
<b>II - B</b>	0,05 ÷ 0,15	0,2	5 mm H <sub>2</sub> O (3:00 h)
<b>IV - A</b>	0,1 ÷ 0,15	0,3	2:10 h
<b>IV - B</b>	0,1 ÷ 0,15	0,3	2:30 h

*Table 29. Low-pressure water permeability test results*

In the previous Table 28 results are expressed in two different way. Regarding the high-performance concrete specimens, their results are expressed in terms of time, since the test could be terminated "quickly" within a few hours, with the complete emptying of the water column and the surface of the sample completely dry. Regarding the conventional concrete specimens, it was preferred to express the results in terms of length (mm), referred to the decrease of the water level respect to the initial 50 cm of column in 3 hours of testing time, since water flowed too slowly to be able to measure the time till when the column was totally empty. Furthermore, the fact that traditional concrete has shown a better behaviour in low-pressure permeability, clearly demonstrate that water permeability is much more correlated to the width of the single crack than to the type of concrete used. Figure 4–18 presents the condition of the specimens after the test, where it is possible to notice the single localized crack in the tested area. The same specimens have been tested again after the healing period in water, in order to evaluate the effectiveness of self-healing in recovery of the durability properties.



*Figure 4–18. Specimens after low-pressure water permeability test*

## 4.7 Chloride penetration test results

Results achieved from the chloride penetration tests provide evidence of the degree of durability guaranteed by the UHPFRCs. After 3 days in which the cracked specimens have been subjected to the chloride action, simulating the exposure conditions of a marine environments (exposure class XS), results have shown a considerable penetration of chlorides through the cement matrix. As it is possible to notice from Figure 4–19, thanks to the occurred reaction between the silver ions and the chloride ions, chloride has clearly penetrated through the concrete thickness where cracks are located (white part in the surface).



*Figure 4–19. Visible chloride penetration in UHPFRC specimens after the spray of silver nitrate*

Furthermore, analysing the results obtained from the tests, HB4 mixes (including those with the addition of functionalities) showed a greater chloride penetration through the concrete matrix than the HB3 ones, testified by the bigger visible chloride area (Figure 4–20, Figure 4–21, Figure 4–22, Figure 4–23). This is due to the different composition of the aggregates only made of fine silica sand, and to the lower amount of fibres which are contained in the HB4 dosage. Moreover, while in the HB3 mixes there is a much more widespread penetration of chloride, in the mixes of HB4 it is possible to note the clear presence of localized cracks through which chloride has penetrated. Below, various comparisons between the results obtained for the HB3 mixes and the HB4 mixes with the same concentrations of additives are reported, reflecting the fact that HB3 mixes showed greater resistance to chloride penetration, thus a better durability.

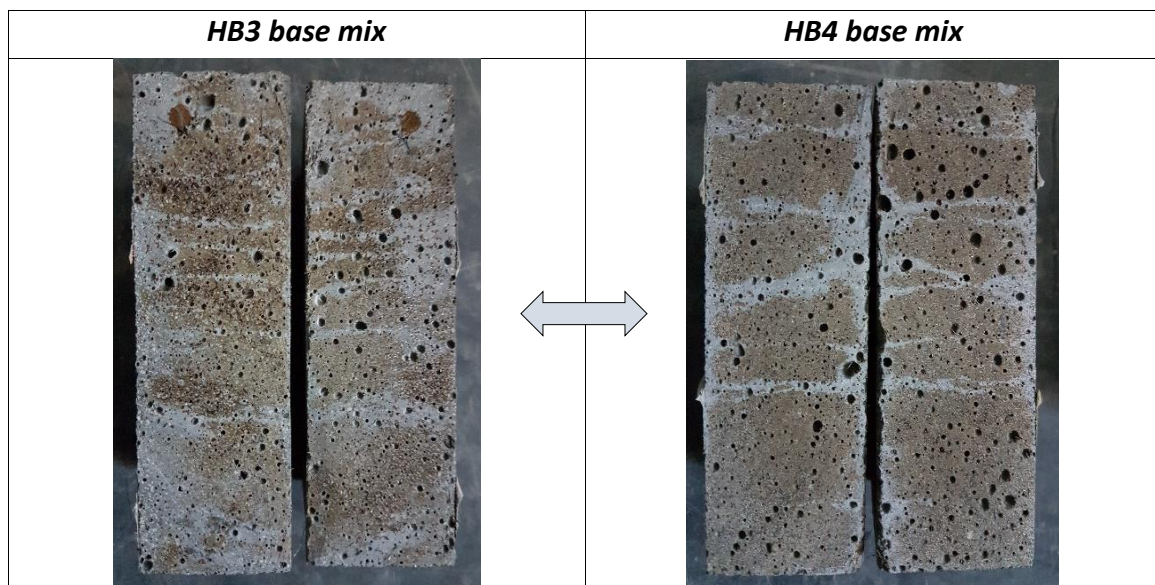


Figure 4–20. Comparison between chloride penetration in HB3 and HB4



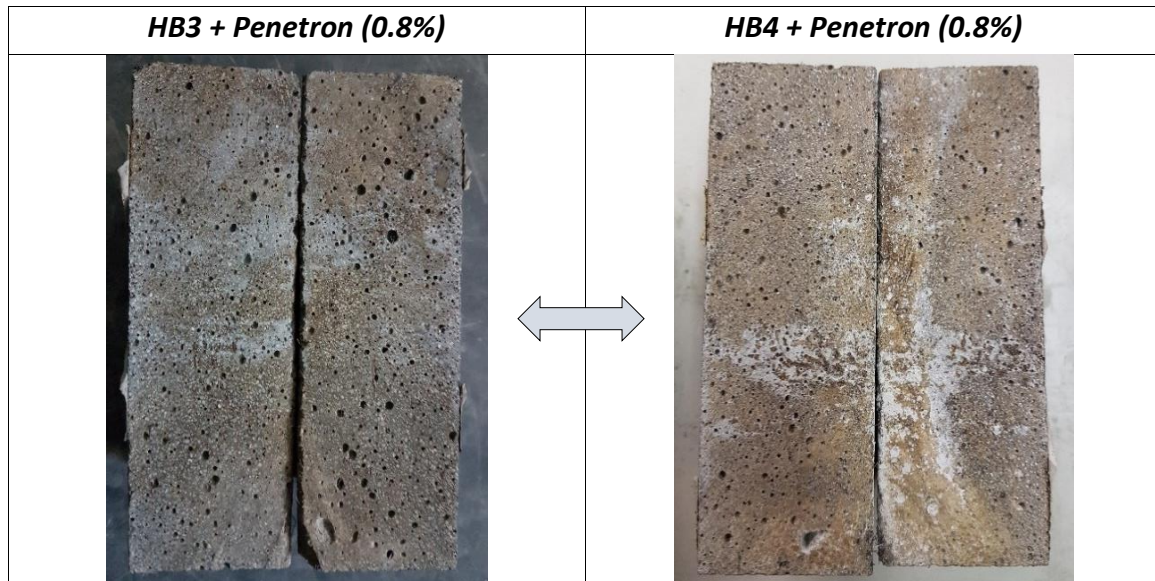


Figure 4–21. Comparison between chloride penetration in HB3 and HB4 with addition of Penetron

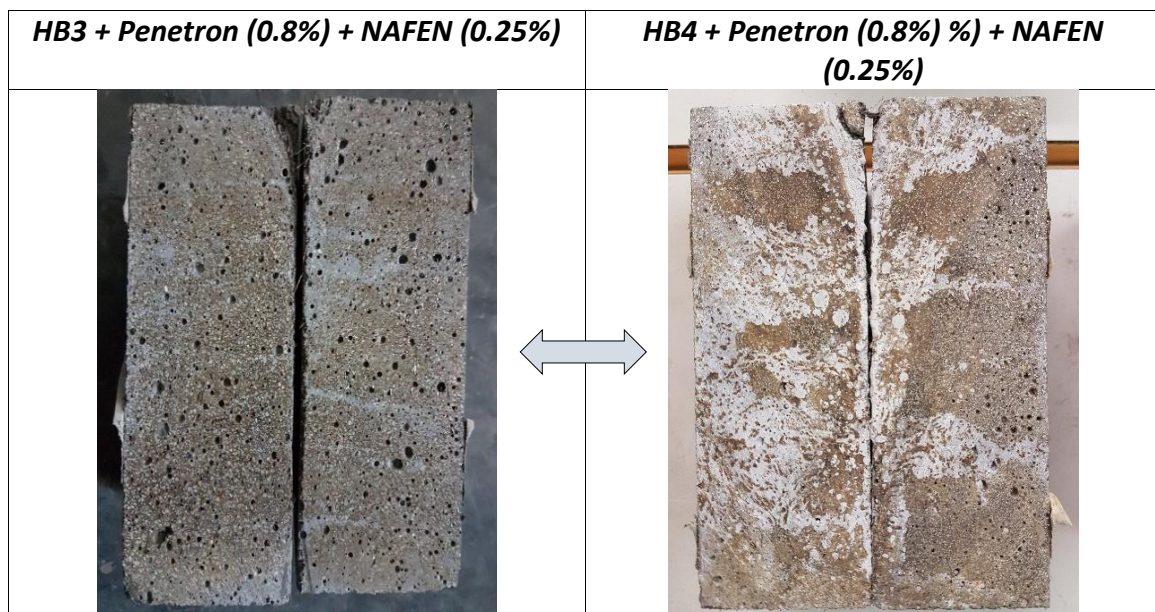


Figure 4–22. Comparison between chloride penetration in HB3 and HB4 with addition of Penetron and Alumina Nano-Fibres

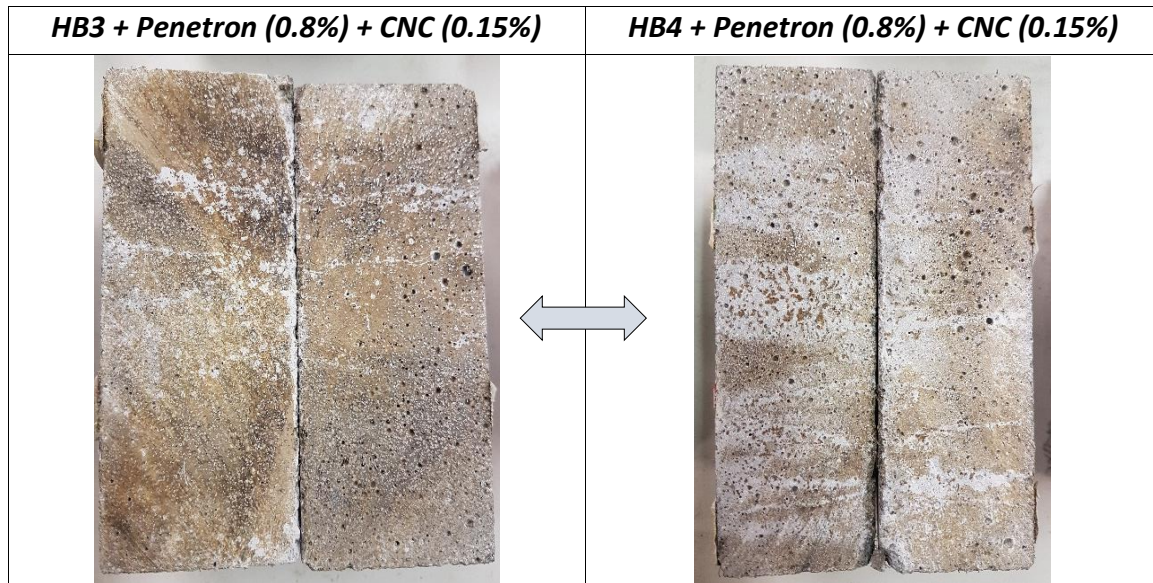


Figure 4–23. Comparison between chloride penetration in HB3 and HB4 with addition of Penetron and Cellulose Nano-Crystals

With specific regard to the degree of improvement induced by the addition of additives in HB3 mix, mixes with the addition of Nanocellulose or Nafen showed a degree of protection slightly higher to chloride penetration than the base ones. Mixtures with the addition of Penetron have shown the best results among all the samples instead, demonstrating even before the healing exposure a remarkable capability in preventing chloride penetration, owing to the waterproofing feature provided by the addition of these crystalline admixtures. Below, two comparisons between the HB3 and HB4 base mixes with the ones with 0.8% of Penetron are reported (Figure 4–24, Figure 4–25), where is possible to observe the clear improvement induced by the addition of Penetron. In the base concrete mixes chloride has penetrated through easily localizable cracks, whereas with the addition of Penetron chloride penetration appears reduced and much more widespread.



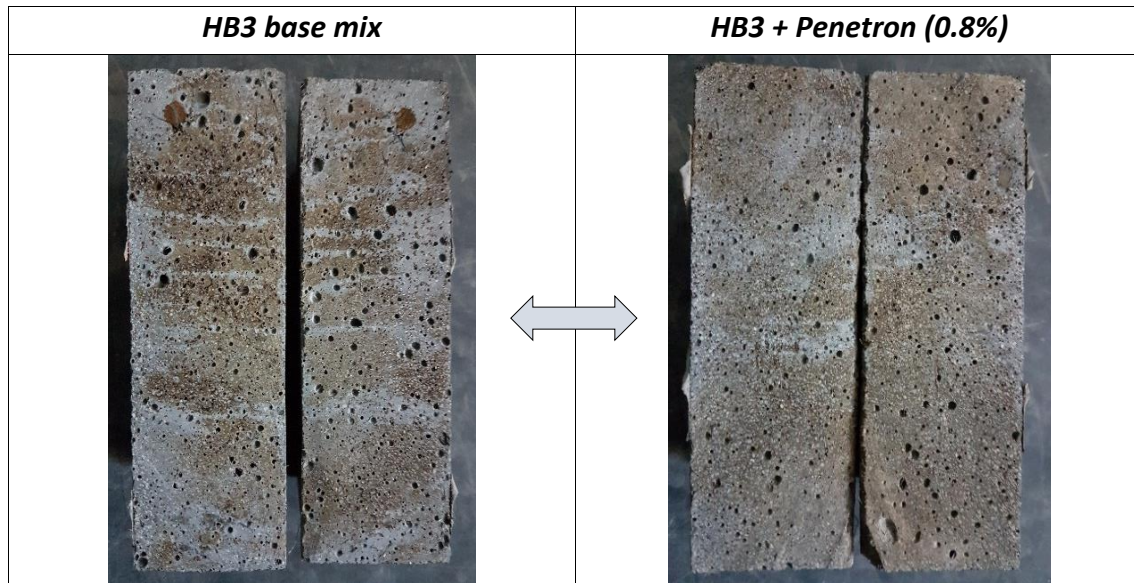


Figure 4-24. . Comparison between chloride penetration in HB3 and HB3 with addition of Penetron

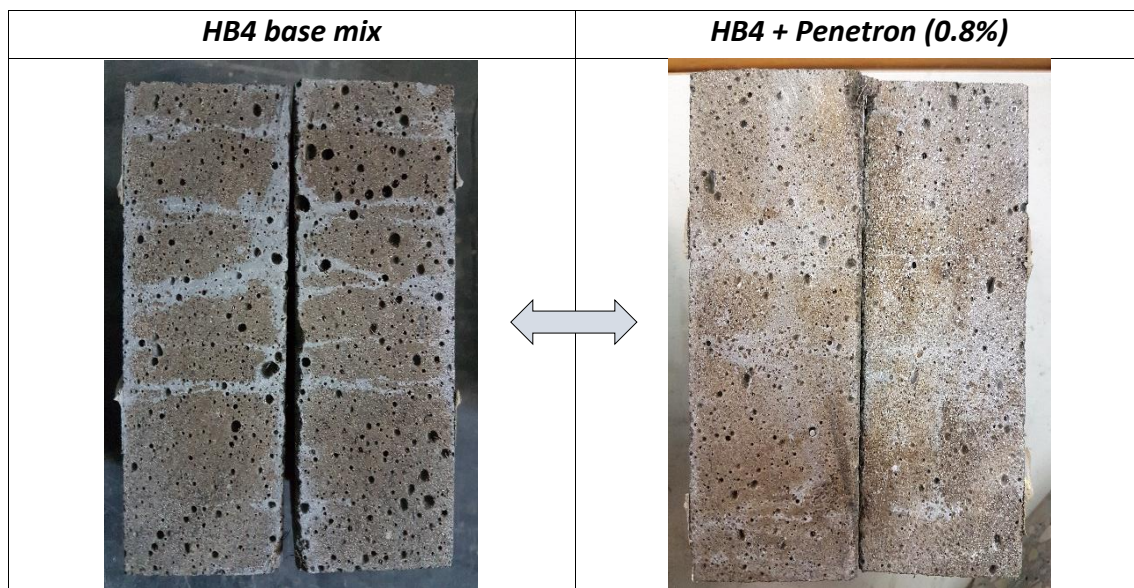
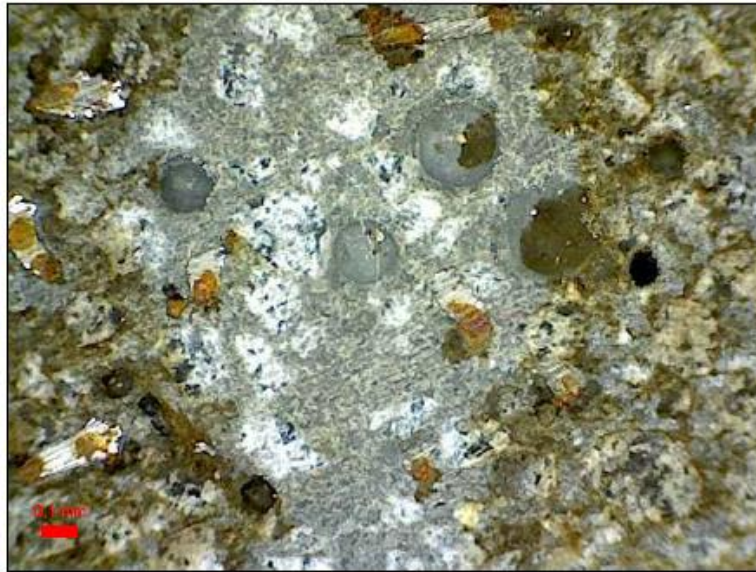


Figure 4-25. Comparison between chloride penetration in HB4 and HB4 with addition of Penetron

The whitish area, where cracks are located and where chloride is penetrated, has been observed with the optical microscope, however no open cracks have been found (Figure 4-26).



*Figure 4–26. Photo of chloride penetration taken with the optical microscope at a 200X magnification*

Although all the UHPFRC samples have suffered a chloride penetration, it can be clearly seen that some specimens present a more sizeable penetration than others. This is attributable to two main factors, the internal cracks width, which should be analysed to have a more reliable data on the average level of damage of each sample, and above all the chemical reactions inside the concrete matrix caused by the addition of waterproofing products such as crystalline admixtures capable of sealing capillary cracks and thus improving durability of UHPFRC elements.

## 4.8 Outcomes after Self-healing

In this section, the results related to the tests performed after the self-healing exposure are discussed. First of all, after 28 days of immersion in water, specimens were analysed with the optical microscope, to evaluate the surface crack closure. From the analysis was noticed that in the UHPFRCs most of the narrower cracks ( $< 0.1$  mm) were closed or partially closed, with a yellow precipitate inside the cracks due to the corrosion of the steel fibres (Figure 4–27). In the traditional and high-performance concretes, no visual cracks closure has been detected instead, due to the greater cracks' width. These results are consistent with those found in the literature.

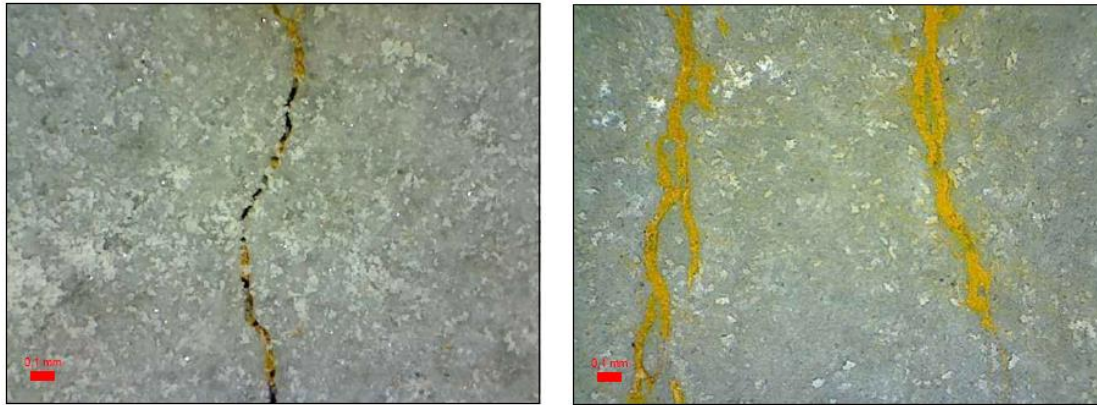


Figure 4-27. Cracks closure detected in UHPFRCs after 28 days of healing exposure

Regarding the recovery of durability properties, traditional and high-performance concretes did not show noteworthy improvements in low-pressure water permeability tests, with results closely comparable to those previously obtained in the tests before self-healing (Table 30). A slight improvement has been noted in the specimens II - B and IV - B with a decrease in water flow passed through the cracked specimens. However, on the other hand, specimens II - A and IV - A have shown a worsening in the degree of permeability provided, with a greater water flow able to cross the crack.

<i>Specimen tested</i>	<i>Crack Width [mm] - Superficial section</i>	<i>Crack Width [mm] - Inner section</i>	<i>LPWPT result before healing</i>	<i>LPWPT result after healing</i>
<b>II - A</b>	0,05 ÷ 0,15	0,2	50 mm H <sub>2</sub> O (3:00 h)	60 mm H <sub>2</sub> O (3:00 h)
<b>II - B</b>	0,05 ÷ 0,15	0,2	5 mm H <sub>2</sub> O (3:00 h)	0 mm H <sub>2</sub> O (3:00 h)
<b>IV - A</b>	0,1 ÷ 0,15	0,3	2:10 h	1:45 h
<b>IV - B</b>	0,1 ÷ 0,15	0,3	2:30 h	460 mm H <sub>2</sub> O (3:00 h)

Table 30. Low-pressure water permeability test results after 28 days of healing exposure

Concerning the chloride penetration tests in UHPFRCs, results showed remarkable effects. Results have been analysed comparing the area of the chloride penetration in the twin specimens (A and B) belonging to the same beam before and after 28 days of healing exposure, both for the base mixes HB3 and HB4 and for the mixtures with the addition of Crystalline Admixtures and Nanoparticles, in order to evaluate the level of enhancement achieved thanks to the addition of these functionalities.

From the analysis it is possible to state that:

- A clear decrease in chloride penetration has been detected in the base mixes HB3 and HB4 due to autogenous healing. The former showed a greater decrease compared to the latter (Figure 4–28, Figure 4–29);
- The addition of Penetron Admix at a concentration of 0.8% of the binder materials promoted a further improvement in chloride penetration protection in most of the specimens (Figure 4–30), major in the HB3 mixes respect to the HB4 ones. However, at greater concentrations (1.6%) Penetron did not show relevant effects (Figure 4–32);
- The addition of Cellulose Nano-Crystal and Cellulose Nano-Fibres at a concentration of 0.15% of the binder materials did not produce significant improvements (Figure 4–31);
- The combined addition of Penetron Admix and Nanocellulose showed mostly scattered results (Figure 4–33);
- The combined addition of Penetron Admix and Alumina Nano-Fibres (NAFEN) showed slight improvements, even if Nano Alumina has not been actually used as self-healing promoter, but as enhancer of durability through a better cracking mechanism; for this reason, there is no expectation of improvement on its part after the healing exposure, but only from Penetron also used as healing promoter.



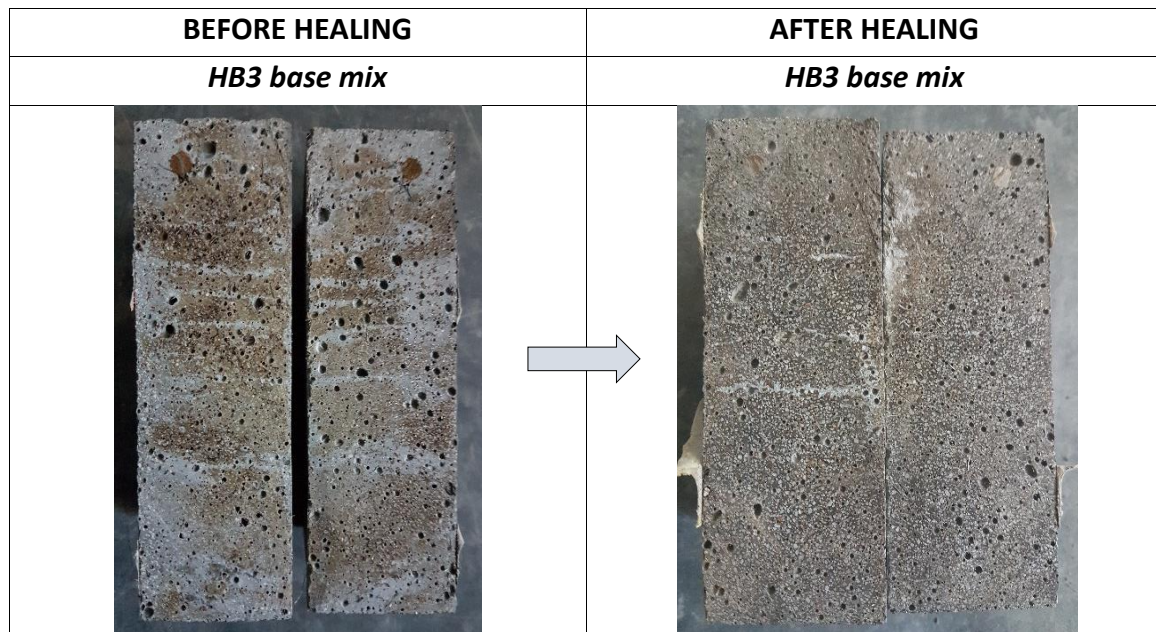


Figure 4–28. Comparison between chloride penetration in HB3 before and after the healing exposure

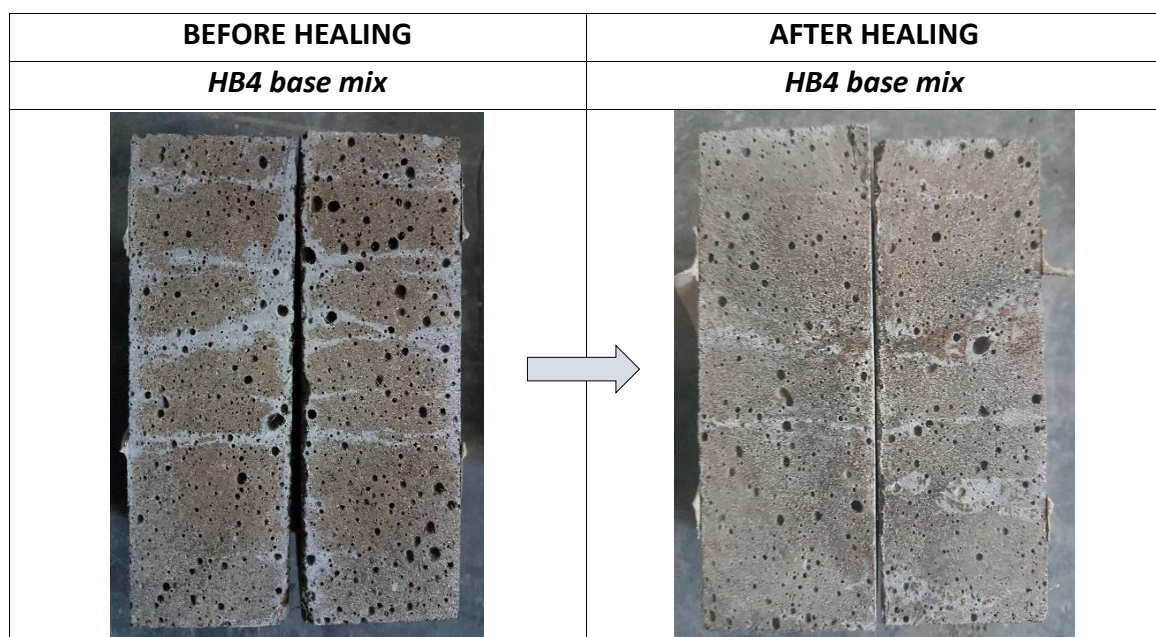


Figure 4–29. Comparison between chloride penetration in HB4 before and after the healing exposure

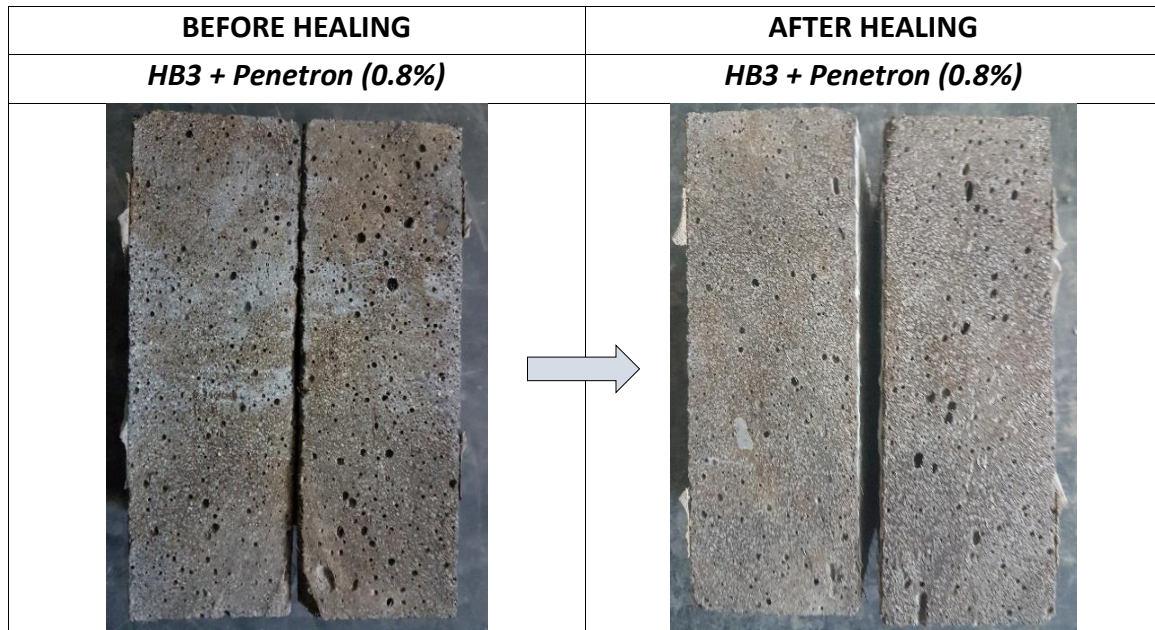


Figure 4–30. Comparison between chloride penetration in HB3 with addition of Penetron (0.8%) before and after the healing exposure



Figure 4–31. Comparison between chloride penetration in HB3 with addition of Nanocellulose before and after the healing exposure





Figure 4–32. Comparison between chloride penetration in HB3 with addition of Penetron (1.6%) and Alumina Nano-Fibres before and after the healing exposure

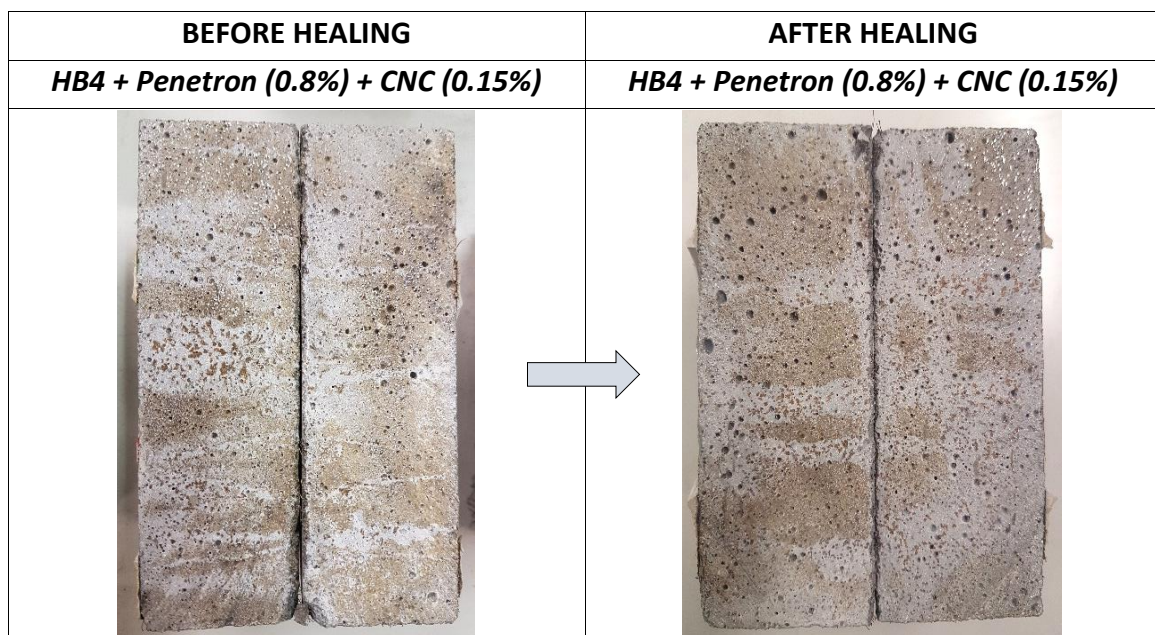


Figure 4–33. Comparison between chloride penetration in HB4 with addition of Penetron (0.8%) and Cellulose Nano-Crystal before and after the healing exposure

All comparisons between specimens before and after healing can be consulted in Appendix 2. Chloride penetration results.

## 5. Conclusions and Future lines

### 5.1 Conclusions

This work aimed to achieve the targets described in the section 1.2 Objectives. The following conclusions related to each point can be drawn from this thesis:

1. The methodology provided for studying the self-healing capability of Ultra-High-Performance Fibre-Reinforced Concretes proved to be efficient, allowing to reach the pre-set goals. As said above, this methodology is made of standard steps easy to implement in laboratory, which broadly are: the phase of pre-cracking, where the ability to control the cracking procedure reaching the desired level of strain has been demonstrated; the phase of crack analysis, where by means of optical microscope together with software for the image analysis it is possible to detect and measure every crack, even up to widths of 10  $\mu\text{m}$ ; and finally the permeability tests, which have proved to be able to detect the variation in durability properties due to the crack healing.
2. With reference to the level of damage induced, water permeability in high-pressure conditions has proved to be ineffectual in the study of durability of Ultra-High-Performance Fibre-Reinforced Concrete, with zero grams of water passed across the samples for average crack width of 0.03 mm, but it proved to be effective in low-pressure conditions for traditional concrete. On the other hand, chloride penetration turned out to be very effective in the evaluation of durability of Ultra-High-Performance Fibre-Reinforced Concrete, with results which have allowed to qualitatively analyse and compare the amount of chloride penetrated through the specimens for the different types of concrete mixtures. Overall, all the HB3 mixes have shown a superior durability to chloride penetration compared to the HB4 ones. Furthermore, the addition of crystalline admixtures (Penetron) at a concentration of 0.8% by cement content has guaranteed the best protection against chloride penetration among all the specimens.



3. The results of the analysis of the cracking pattern of the two concrete classes have highlighted the peculiar differences between the Ultra-High-Performance Fibre-Reinforced Concrete and the traditional concrete. The former presents a cracking pattern characterized by multi micro-cracks (up to 20) in the order of hundredth of a millimetre ( $0.01 \div 0.05$  mm), while the latter a cracking behaviour characterized by few localized cracks (2 or 3) in the order of tenth of a millimetre ( $0.1 \div 0.3$  mm). This cracking pattern is the factor that most affects their performance in terms of durability and self-healing capability. Accordingly, results affirm the superior durability and self-healing performance of Ultra-High-Performance Fibre-Reinforced Concrete elements.
4. The products used in addition to the Ultra-High-Performance Fibre-Reinforced Concrete base mixes have provided scattered results. However, the HB3 mixes functionalized with crystalline admixtures have proved to guarantee from the beginning (before healing) the best degree of durability, with the lowest penetration of chloride among all the samples, thanks to the waterproofing property provided by Penetron. Moreover, the addition of Penetron has shown further long-term improvements after 28 days of healing in water. Conversely, the addition of Nano-cellulose did not provide clear improvements, as well as the addition of Nano-alumina.

## 5.2 Future lines

This research has opened the doors to new possible investigations. Firstly, since for each concrete batch four reinforced beams were casted and, in this work, only two of these have been tested, the first future investigation consists in testing the remaining beams. The initial purpose was to create two level of damage, namely, "small crack" and "large crack", described in the section "Pre-cracking" of the Methodology. In this research only the "large" level of damage was generated, consequently, the investigation is going to continue using the same methodology described in this thesis but working with a "smaller" level of damage, to assess the degree of durability provided and the potential

improvement of self-healing performance. The self-healing evaluation method that will be used is the standardized chloride penetration test. Regarding the chloride penetration issue, one of the next investigations will be to quantify the concentration of chloride penetrated, since in this work only a qualitative analysis was done. Concerning the healing promoters used in this thesis, more in-depth analyses on the effectiveness of crystalline admixtures and nanoparticles in affecting durability, self-healing and mechanical properties are recommended. In this regard, a study on mixing at different speeds is already underway, to evaluate the effects of a better dispersion of addition products like nanocellulose. Finally, the analysis of the corrosion of the steel fibres is an interesting topic of investigation that will have to be faced.

## References

- Akhavan A., F. Rajabipour, *Evaluating ion diffusivity of cracked cement paste using electrical impedance spectroscopy*, Mater. Struct. 46 (2013) 697–708.
- Aldea C.M., S.P. Shah, A. Karr, *Permeability of cracked concrete*, Mater. Struct. 32 (1999) 370–376.
- Behfarnia K. and Salemi N., *The effects of nano-silica and nano-alumina on frost resistance of normal concrete*, Cement and Concrete Composites 94 (2018) 327–340.
- Borg R. P., E. Cuenca, E. M. Gastaldo Brac, L. Ferrara, J. Sustainable Cem. -Based Mater., *Crack sealing capacity in chloride-rich environments of mortars containing different cement substitutes and crystalline admixtures*, 2017.
- Brinchi, L., Cotana, F., Fortunati, E., and Kenny, J. M. (2013). “Production of nanocrystalline cellulose from lignocellulosic biomass: Technology and applications.” Carbohydr. Polym., 94(1), 154–169.
- Cailleux E., Pollet V., *Investigations on the development of self-healing properties in protective coatings for concrete and repair mortars*. In Proceedings of 2nd International Conference on Self-Healing Materials, Chicago, IL, USA, 28 June–1 July 2009.
- Cao, Y., Zavatterri, P., Youngblood, J., Moon, R., and Weiss, J. (2015). “The influence of cellulose nanocrystal additions on the performance of cement paste.” Cem. Concr. Compos., 56, 73–83.
- Cuenca E., A. Tejedor, L. Ferrara, presented at Proc. HAC 2018, Valencia, Spain, July 2018.
- Cuenca E., G. Cislighi, M. Puricelli, L. Ferrara, presented at DSCS2018, Moscow, June 2018.
- De Belie N., E. Gruyaert, A. Al-Tabbaa, P. Antonaci, C. Baera, D. Bajäre, A. Darquennes, R. Davies, L. Ferrara, A. Jefferson, C. Litina, B. Miljevic, A. Otlewska, J. Ranogajec, M. Roig, K. Paine, P. Ludowski, P. Serna, J.M. Tulliani, S. Vucetic, J. Wang, H. Jonkers. *A review on*

*self-healing concrete for damage management of structures*, Materials Interface Sci. (2018).

De Nardi C., Bullo, S., Cecchi, A. & Ferrara, L., 2016. *Self-healing capacity of advanced lime mortars*. Advances in Materials and Processing Technologies, 2(3), pp.349-60.

De Rooij M.R., Schlangen, E. & Joseph, C., 2013. Introduction. In M. De Rooij, K. Van Tittelboom, N. De Belie & E. Schlangen, eds. *Self-healing Phenomena in Cement-based Materials: State-of-the-art Report of RILEM Technical Committee 221-SHC*. Springer RILEM State-of-the-Art Reports. pp.1-17.

Desmettre C. & Charron, J.-P., 2012. *Water permeability of fiber reinforced concrete subjected to constant and cyclic loading*. In BEFIB2012 – Fibre reinforced concrete. UM, Guimarães, 2012. Joaquim Barros et al. (Eds).

Edvardsen C., 1996. Wasserdurchlässigkeit und Selbstheilung von Trennrissen in Beton. Berlin: Beuth.

Edvardsen C., 1999. *Water Permeability and Autogenous Healing of Cracks in Concrete*. ACI Materials Journal, 96(4), pp.448-454.

Eichhorn, S. J., et al. (2010). "Review: Current international research into cellulose nanofibres and nanocomposites." J. Mater. Sci., 45(1), 1–33.

Ferrara L., E. Cuenca, *Effects of self-healing promoted by crystalline admixture on the concrete resistance to chloride penetration*. Accepted for publication to DSCS 2018, 2nd International Workshop on Durability and Sustainability of Concrete Structures, Moscow, Russia, 6-7 June 2018 (2018).

Ferrara L., Krelani, V. and Moretti, F., 2016. *On the use of crystalline admixtures in cement based construction materials: from porosity reducers to promoters of self-healing*. Smart Materials and Structures, 25, p.084002.

Ferrara Liberato, Tim Van Mullem, Maria Cruz Alonso, Paola Antonaci, Ruben Paul Borg, Estefania Cuenca, Anthony Jefferson, Pui-Lam Ng, Alva Peled, Marta Roig-Flores,

Mercedes Sanchez, Christof Schroefl, Pedro Serna, Didier Snoeck, Jean Marc Tulliani, Nele De Belie. *Experimental characterization of the self-healing capacity of cement based materials and its effects on the material performance: A state of the art report by COST Action SARCOS WG2. Construction and Building Materials* 167 (2018) 115–142.

Ferrara, L., Ferreira, S.R., Della Torre, M., Krelani, V., Silva, F. and Toledo Filho, R.D.: “*Effect of cellulose nanopulp on autogenous and drying shrinkage of cement based composites*”, in *Nanotechnology in Construction, Proceedings Nicom 5*, K. Sobolev and S.P. Shah, eds., Springer, Chicago, 26-28 May 2015, pp. 325-330.

Ferrara, L., Krelani, V. and Moretti, F.: “*Autogenous healing on the recovery of mechanical performance of High Performance Fibre Reinforced Cementitious Composites (HPFRCCs): part 2 – correlation between healing of mechanical performance and crack sealing*”, *Cement and Concrete Composites*, 73, October 2016, pp. 299-315.

Ferrara, L., Krelani, V., Moretti, F., Roig Flores, M. and Serna Ros, P.: “*Effects of autogenous healing on the recovery of mechanical performance of High Performance Fibre Reinforced Cementitious Composites (HPFRCCs): part 1*”, *Cement and Concrete Composites*, 83, October 2017, pp. 76-100.

Gagné, R. & Argouges, M., 2012. *A study of the natural self-healing of mortars using air-flow measurements*. *Materials and Structures*.

Ghosh S. K., *Self-Healing Materials: Fundamentals, Design Strategies, and Applications*, John Wiley and Sons, Weinheim, Germany 2009.

Gowda R., H. Narendra, Dinesh Rangappa, R. Prabhakar, *Effect of nano-alumina on workability, compressive strength and residual strength at elevated temperature of Cement Mortar*, *Materials Today: Proceedings* 4 (2017) 12152–12156.

Hearn N. & Morley, C., 1997. *Self-sealing property of concrete - Experimental evidence*. *Materials and Structures/Matériaux et Constructions*, 30, pp.404-11.

Homma D., H. Mihashi, T. Nishiwaki, *Self-healing capability of fibre reinforced cementitious composites*, *J. Adv. Concr. Technol.* 7 (2) (2009) 217–228.

Huang H., G. Ye, D. Damidot, *Cem. Concr. Res.* 2014, 60, 68.

Ismail M., A. Toumi, R. Francois, R. Gagne, *Effect of crack opening on the local diffusion of chloride in cracked mortar samples*, *Cem. Concr. Res.* 38 (2008) (2008) 1106–1111.

Jacobsen S., J. Marchand, H. Homain, *SEM observations of the microstructure of frost deteriorated and self-healed concretes*, *Cem. Concr. Res.* 25 (8) (1995) 1781–1790.

Jaishankar P. and C. Karthikeyan, *Characteristics of Cement Concrete with Nano Alumina Particles*, *Earth and Environmental Science* 80 (2017) 012005.

Jiang Z., Li, W. & Yuan, Z., 2015. *Influence of mineral additives and environmental conditions on the self-healing capabilities of cementitious materials*. *Cement and Concrete Composites*, 57, pp.116-27.

Jongvisuttisun, P., Negrello, C., and Kurtis, K. E. (2013). “*Effect of processing variables on efficiency of eucalyptus pulps for internal curing.*” *Cem. Concr. Compos.*, 37, 126–135.

Kim D.J., Kang, S.H. & Ahn, T.-H., 2014. *Mechanical Characterization of High-Performance Steel-Fiber Reinforced Cement Composites with Self-Healing Effect*. *Materials*, 7, pp.508-26.

Kim D.J., Kang, S.H. & Ahn, T.-H., 2014. *Mechanical Characterization of High-Performance Steel-Fiber Reinforced Cement Composites with Self-Healing Effect*. *Materials*, 7, pp.508-26.

Kim Van Tittelboom and Nele De Belie. *Self-Healing in Cementitious Materials—A Review*. *Materials* 2013. Magel Laboratory for Concrete Research, Department of Structural Engineering, Faculty of Engineering, Ghent University, Technologiepark Zwijnaarde 904, Ghent B-9052, Belgium.

Lauer K. R., F. O. Slate, *ACI Mater. J.* 1956, 52, 1083.

Li Z, Wang H, He S, Lu Y, Wang M. *Investigations on the preparation and mechanical properties of the nano-alumina reinforced cement composite*. *Mater Lett* 2006;60(3):356–9.

- Ma H., Qian, S. & Zhang, Z., 2014. *Effect of self-healing on water permeability and mechanical property of Medium-Early-Strength Engineered Cementitious Composites*. Construction and Building Materials, (68), pp.92-101.
- Maes M., D. Snoeck, N. De Belie, *Chloride penetration in cracked mortar and the influence of autogenous crack healing*, Constr. Build. Mater. 115 (2016) 114–124.
- Moon, R. J., Martini, A., Nairn, J., Simonsen, J., and Youngblood, J. (2011). “*Cellulose nanomaterials review: Structure, properties and nanocomposites.*” Chem. Soc. Rev., 40(7), 3941–3994.
- Nazari A, Riahi S, Riahi S, Shamekhi SF, Khademno A. *Influence of Al<sub>2</sub>O<sub>3</sub> nanoparticles on the compressive strength and workability of blended concrete*. J Am Sci 2010;6(5):6–9.
- Neville A., *Autogenous healing—A concrete miracle*, Concr. Int. 24 (2002) 76–82.
- Nishiwaki T., Koda, M., Yamada, M., Mihashi, H. & Kikuta, T., 2012. *Experimental Study on Self-Healing Capability of FRCC Using Different Types of Synthetic Fibers*. Journal of Advanced Concrete Technology, 10, pp.195-206.
- Olivier K., A. Darquennes, F. Benboudj, R. Gagne, J. Adv. Concr. Technol. 2016, 14, 217.
- Onuaguluchi, O., Panesar, D., and Sain, M. (2014). “*Properties of nanofibre reinforced cement composites.*” Constr. Build. Mater., 63, 119–124.
- Ousmane A. Hisseine, Ahmed F. Omran and Arezki Tagnit-Hamou, *Influence of Cellulose Filaments on Cement Paste and Concrete*, J. Mater. Civ. Eng., 2018, 30(6): 04018109.
- Ousmane A. Hisseine, N. Basic, Ahmed F. Omran, Arezki Tagnit-Hamou, *Feasibility of using cellulose filaments as a viscosity modifying agent in selfconsolidating concrete*, Cement and Concrete Composites 94 (2018) 327–340.
- Peters, S. J., Rushing, T. S., Landis, E. N., and Cummins, T. K. (2010). “*Nanocellulose and microcellulose fibers for concrete.*” Transp. Res. Rec., 2142, 25–28.

Reinhardt H.W., M. Jooss, *Permeability and self-healing of cracked concrete as a function of temperature and crack width*, Cem. Concr. Res. 33 (2003) 981–985.

Roig-Flores M., Moscato, S., Serna, P. & Ferrara, L., 2015. *Self-healing capability of concrete with crystalline admixtures in different environments*. Construction and Building Materials, 86, pp.1-11.

Roig-Flores M., Pirritano, F., Serna, P. & Ferrara, L., 2016. *Effect of crystalline admixtures on the self-healing capability of early-age concrete studied by means of permeability and crack closing tests*. Construction and Building Materials, 114, pp.447-57. M. Wu, B. Johannesson, M. Geiker, Constr. Build. Mater. 2012, 28, 571.

Sahmaran M., M. Li, V. Li, *Transport properties of engineered cementitious composites under chloride exposure*, ACI Mater. J. 104 (6) (2007) 604–611.

Scrivener K.L., 1984. *Development of Microstructure during the Hydration of Portland*. Ph. D Thesis University of London.

Shekari AH and Razzaghi MS. *Influence of nanoparticles on durability and mechanical properties of high performance concrete*. Procedia Eng. 2011; 14:3036–41.

Sisomphon K., Copuroglu, O. & Koenders, E.A.B., 2012. *Self-healing of surface cracks in mortars with expansive additive and crystalline additive*. Cement & Concrete Composites, 34, pp.566–74.

Sisomphon K., Copuroglu, O. & Koenders, E.A.B., 2013. *Effect of exposure conditions on self-healing behaviour of strain hardening cementitious composites incorporating various cementitious materials*. Construction and Building Materials, 42, pp.217–24.

Snoeck D., Ph.D. Thesis, Ghent University 2015

Speck O., Schlechtendahl, M., Schmich, F. & Speck, T., 2013. *Self-healing processes in plants – A treasure trove for biomimetic self-repairing materials*. Ghent, 2013. Fourth International Conference on Self-Healing Materials.



Ter Heide N., 2005. *Crack healing in hydrating concrete*. Delft, The Netherlands: Delft University of Technology, Faculty of Civil Engineering and Geosciences. Master Thesis.

Torregrosa E. C., 2013, *Dosage optimization and bolted connections for UHPFRC ties*. Ph.D. Thesis, Instituto de Ciencia y Tecnología del Hormigón (ICITECH), Universitat Politècnica De València.

Van Breugel K., 2007. *Is there a market for self-healing cement-based materials? Proceedings of the First International Conference on Self-Healing Materials*, Noordwijk aan Zee, The Netherlands.

Van Tittelboom K., Gruyaert, E., Rahier, H. & de Belie, N., 2012. *Influence of mix composition on the extent of autogenous crack healing by continued hydration or calcium carbonate formation*. Construction and Building Materials, (37), pp.349–59.

Wang K., D.C. Jansen, S.P. Shah, et al., *Permeability study of cracked concrete*, Cem. Concr. Res. 27 (3) (1997) 381–393.

White S.R., Sottos, N.R., Geubelle, P.H., Moore, J.S., Kessler, M.R., Sriram, S.R., Brown, E.N. & Viswanathan, S., 2001. *Autonomic healing of polymer composites*. NATURE, 409.

Win P.P., M. Watanabe, A. Machida, *Penetration profile of chloride ion in cracked reinforced concrete*, Cem. Concr. Res. 34 (2004) 1073–1079

Yang Y., Lepech, M.D., Yang, E.-H. & Li, V.C., 2009. *Autogenous healing of engineered cementitious composites under wet–dry cycles*. Cement and Concrete Research, 39, pp.382–90.

Yang Y., Yang, E.-H. & Li, V.C., 2011. *Autogenous healing of engineered cementitious composites at early age*. Cement and Concrete Research, 41, pp.176-83.

## Appendix 1. Pre-cracking results

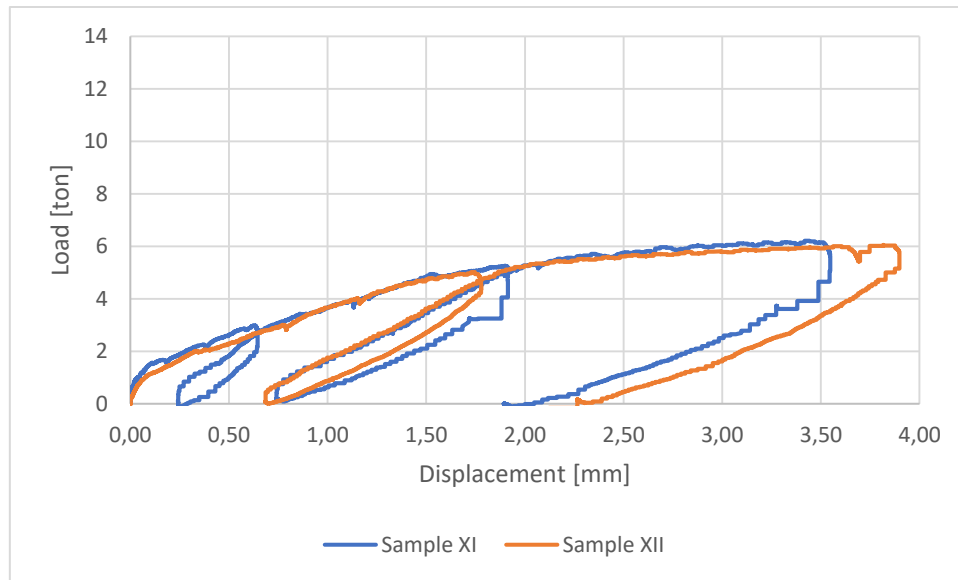


Figure 0-1. Load-displacement graph H0

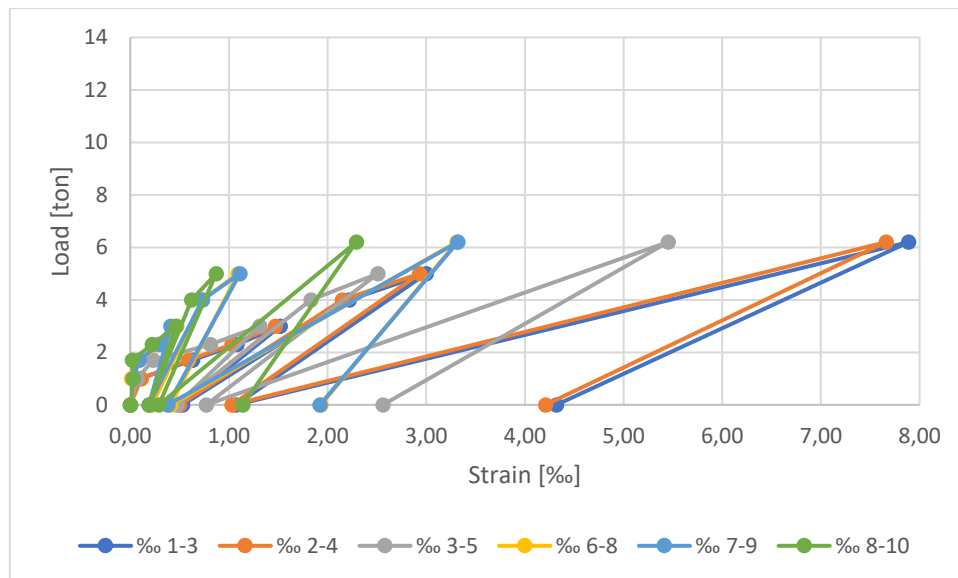


Figure 0-2. Load-strain graph H0 Beam I

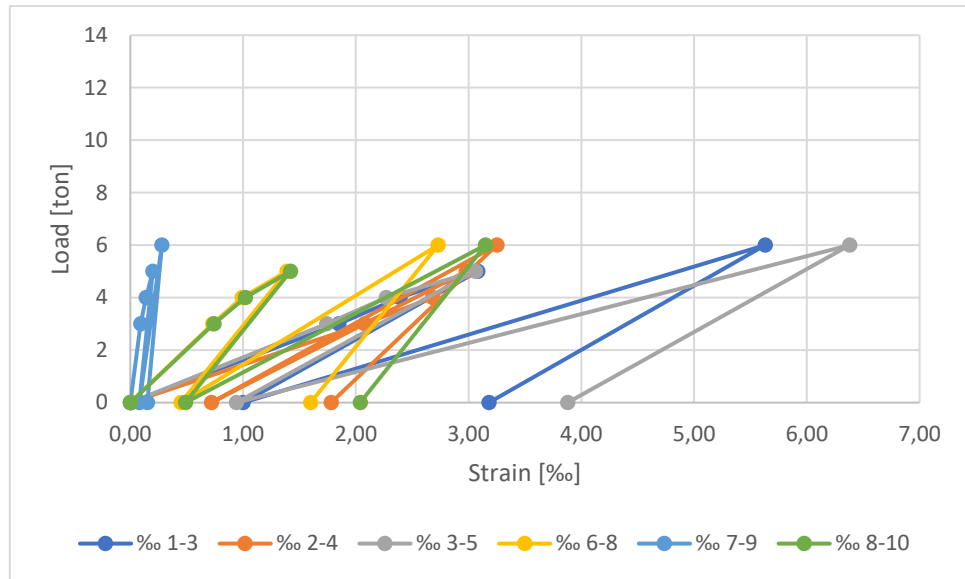


Figure 0-3. Load-strain graph H0 Beam II

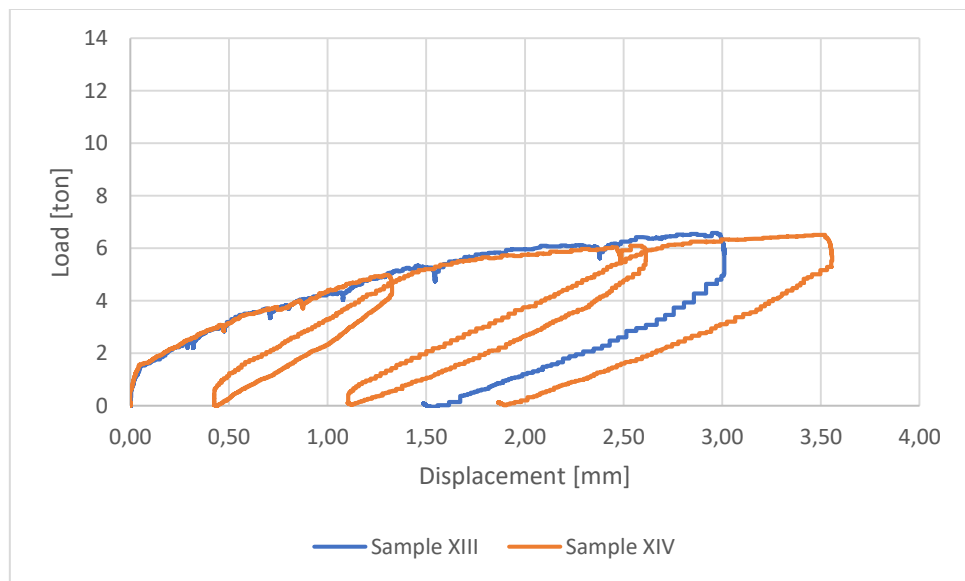


Figure 0-4. Load-displacement graph H1

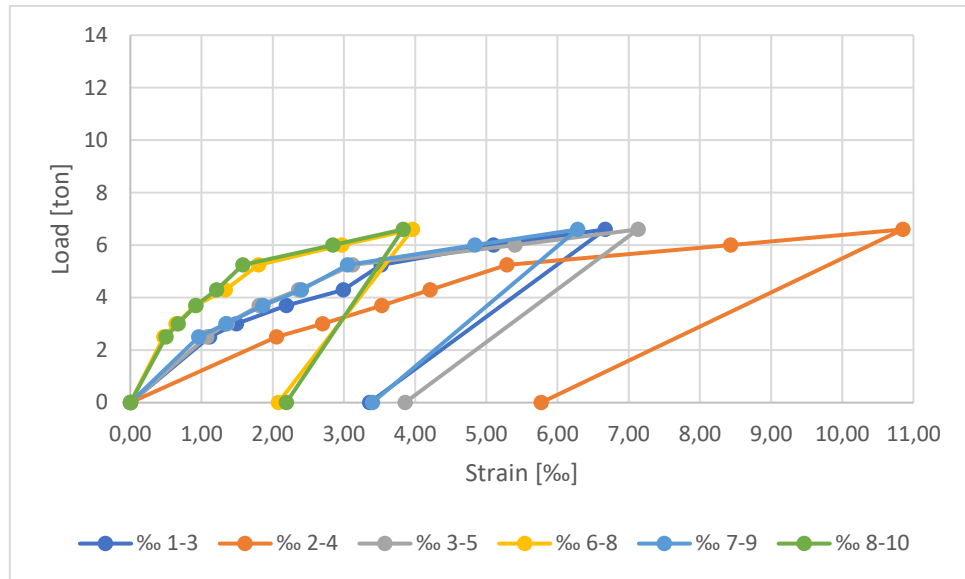


Figure 0-5. Load-strain graph H1 Beam III

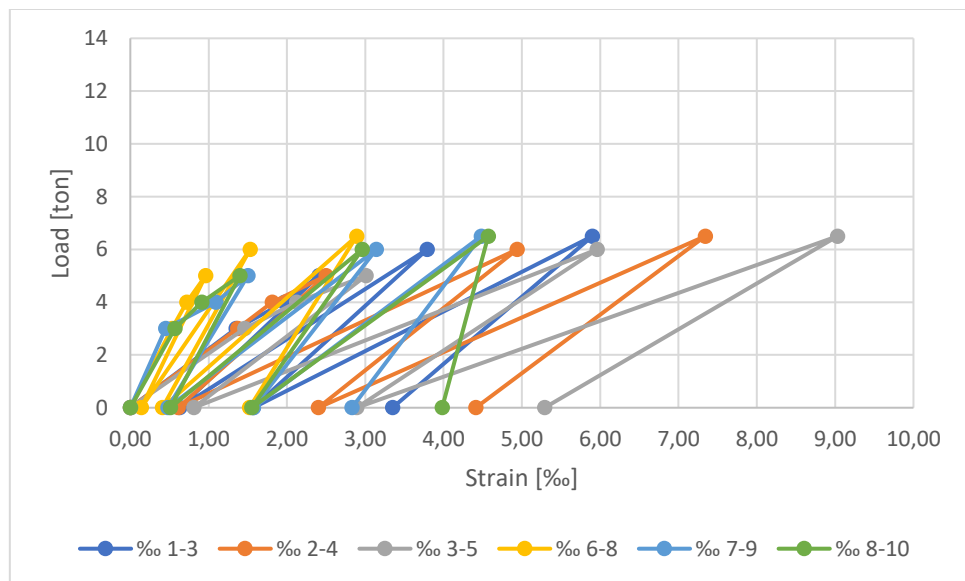


Figure 0-6. Load-strain graph H1 Beam IV

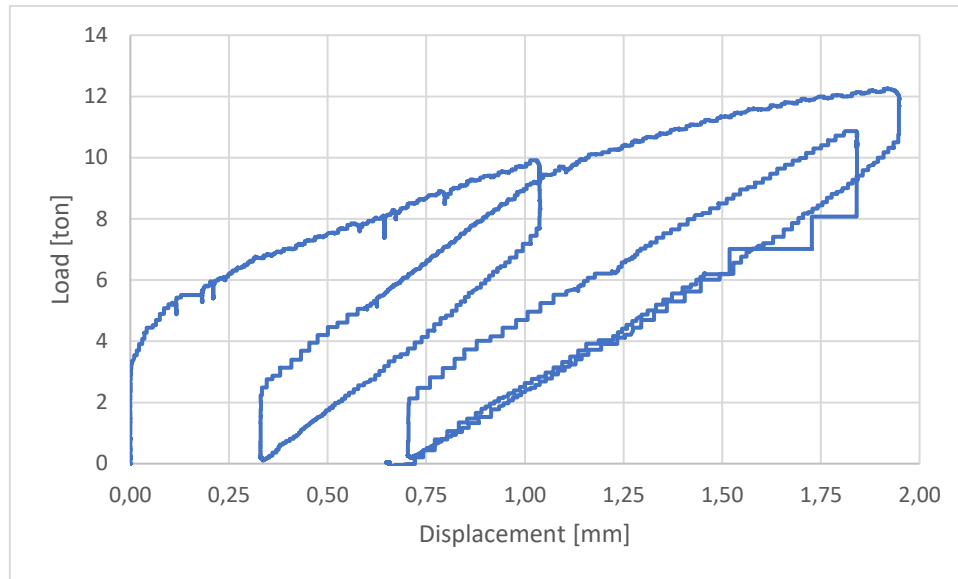


Figure 0-7. Load-displacement graph HB3

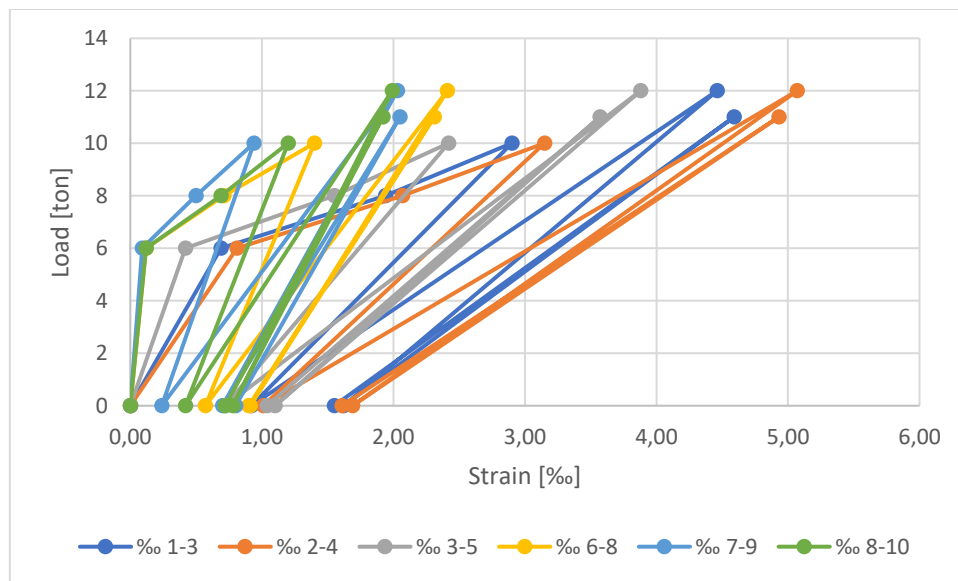


Figure 0-8. Load-strain graph HB3 Beam V

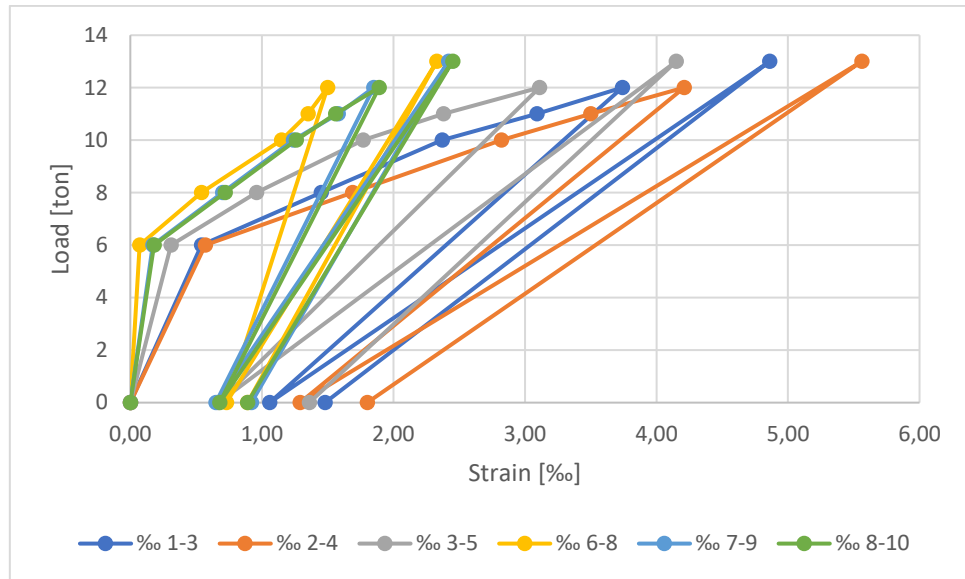


Figure 0-9. Load-strain graph HB3 Beam VI

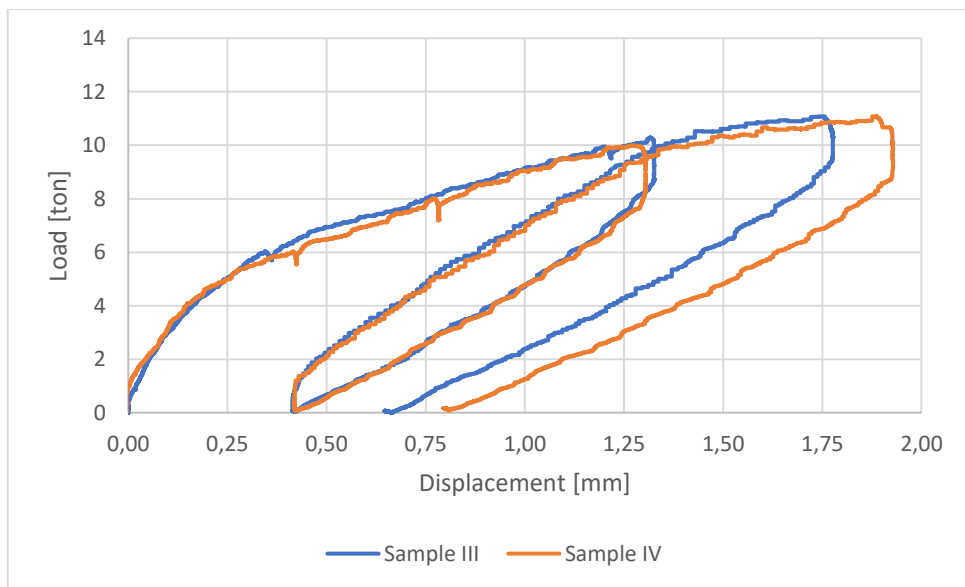


Figure 0-10. Load-displacement graph HB4

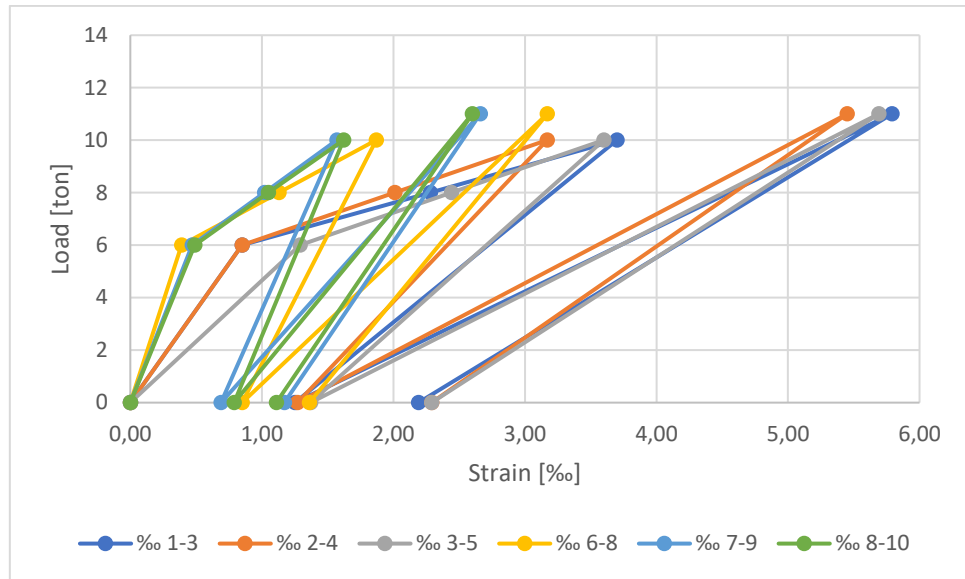


Figure 0-11. Load-strain graph HB4 Beam VII

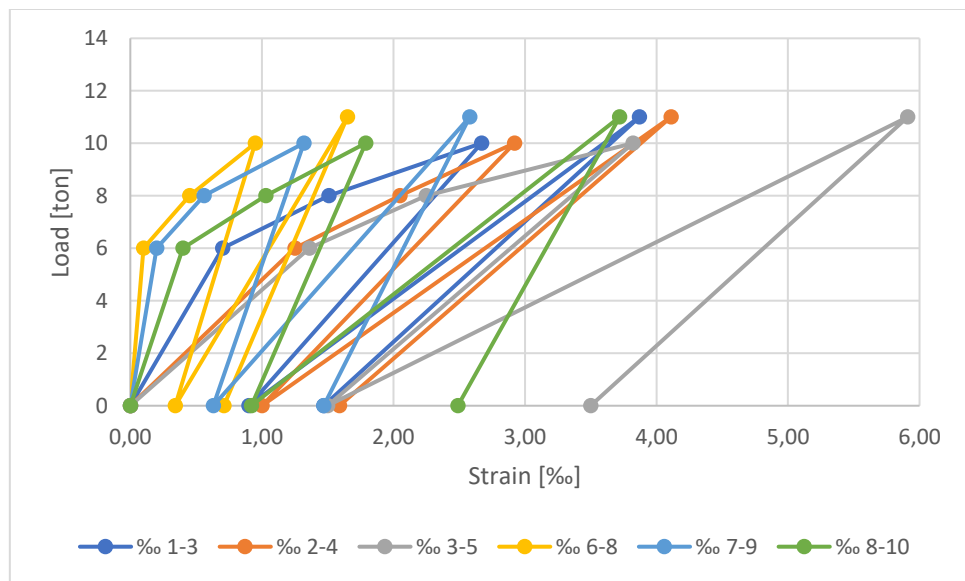


Figure 0-12. Load-strain graph HB4 Beam VIII

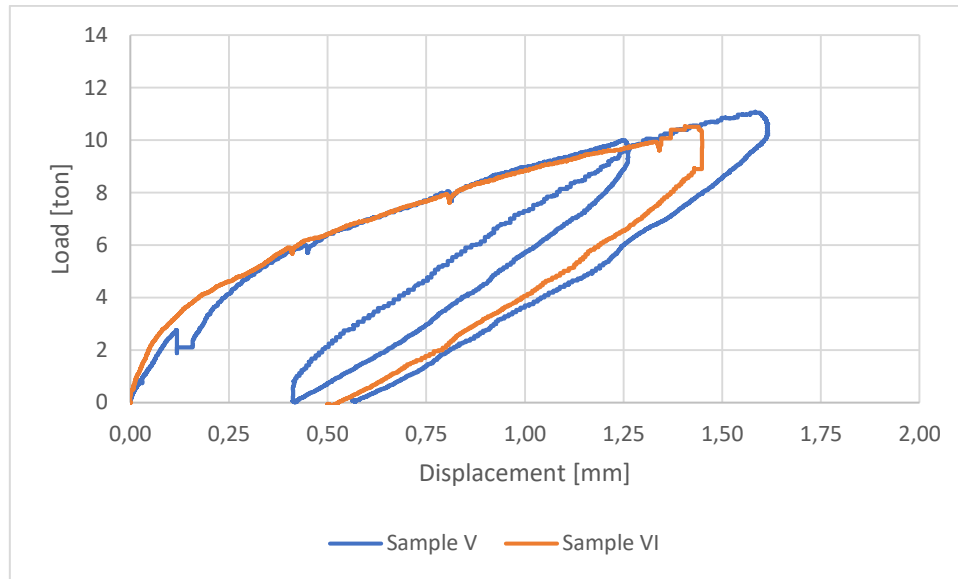


Figure 0-13. Load-displacement graph HB3 + Penetron (0.8%)

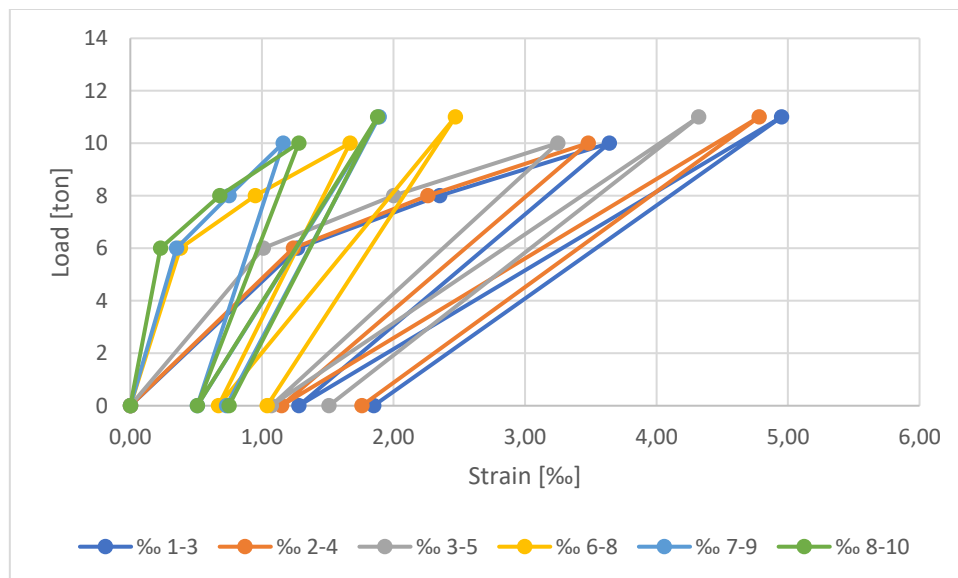


Figure 0-14. Load-strain graph HB3 + Penetron (0.8%) Beam IX



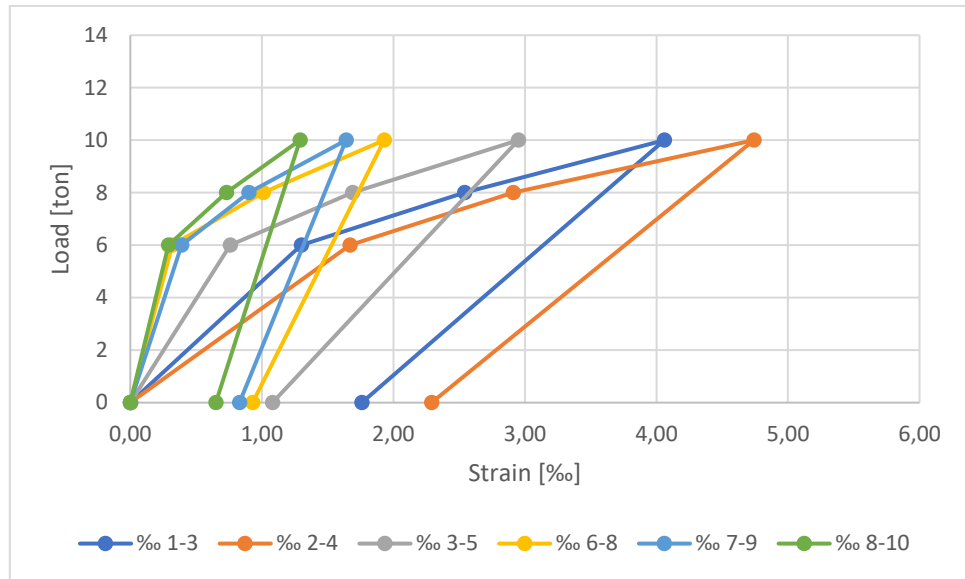


Figure 0-15. Load-strain graph HB3 + Penetron (0.8%) Beam X

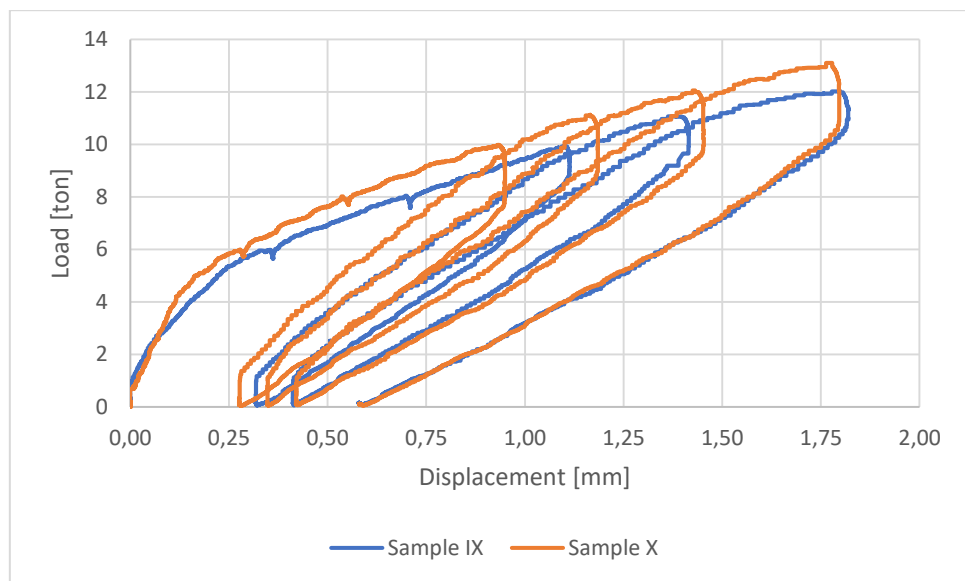


Figure 0-16. Load-displacement graph HB3 + NAFEN (0.25%) + Penetron (0.8%)

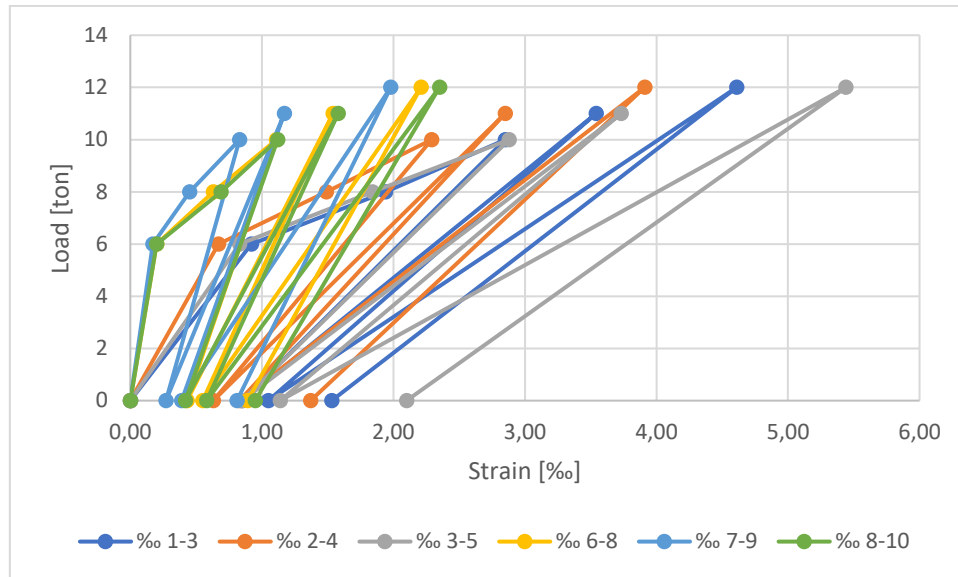


Figure 0-17. Load-strain graph HB3 + NAFEN (0.25%) + Penetron (0.8%) Beam XI

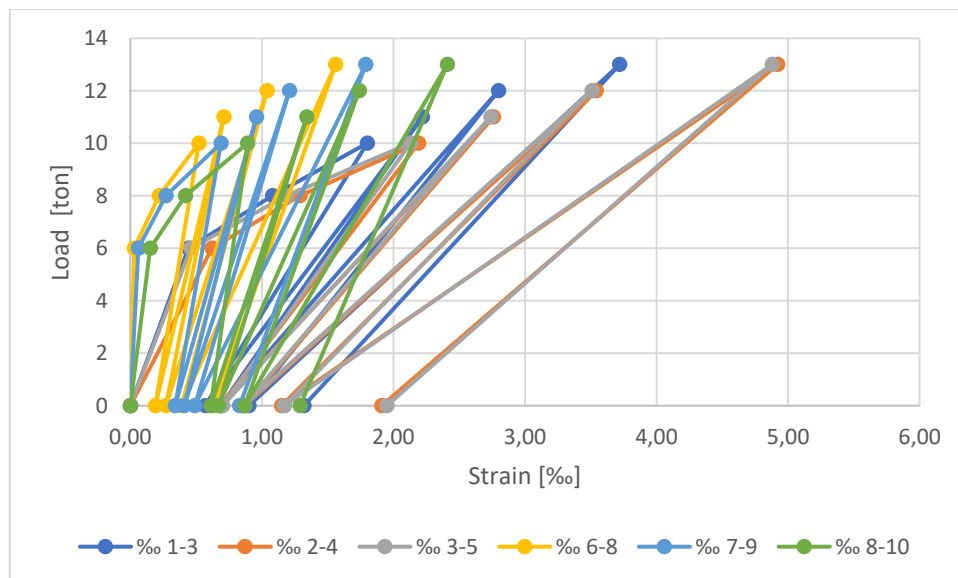


Figure 0-18. Load-strain graph HB3 + NAFEN (0.25%) + Penetron (0.8%) Beam XII

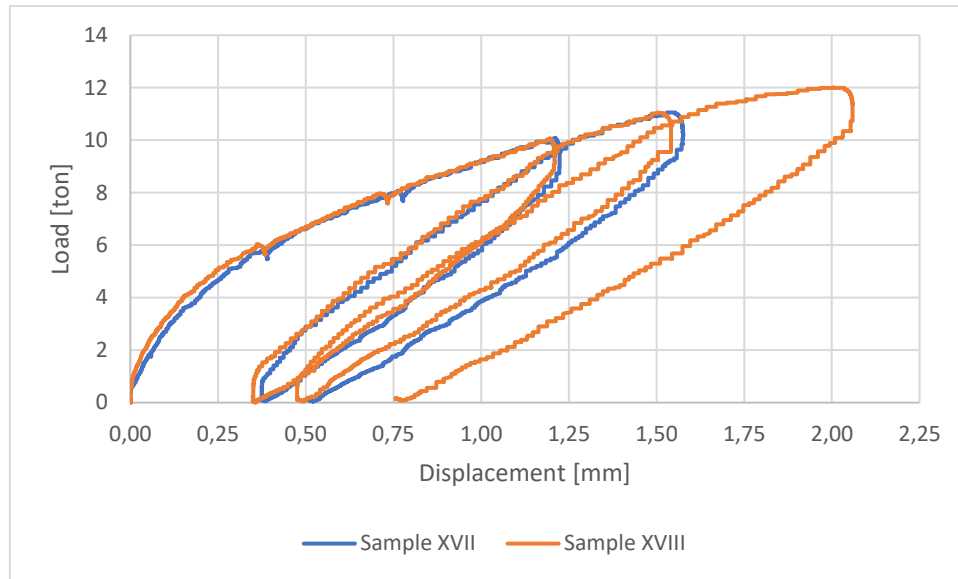


Figure 0-19. Load-displacement graph HB3 + NAFEN (0.25%) + Penetron (1.6%)

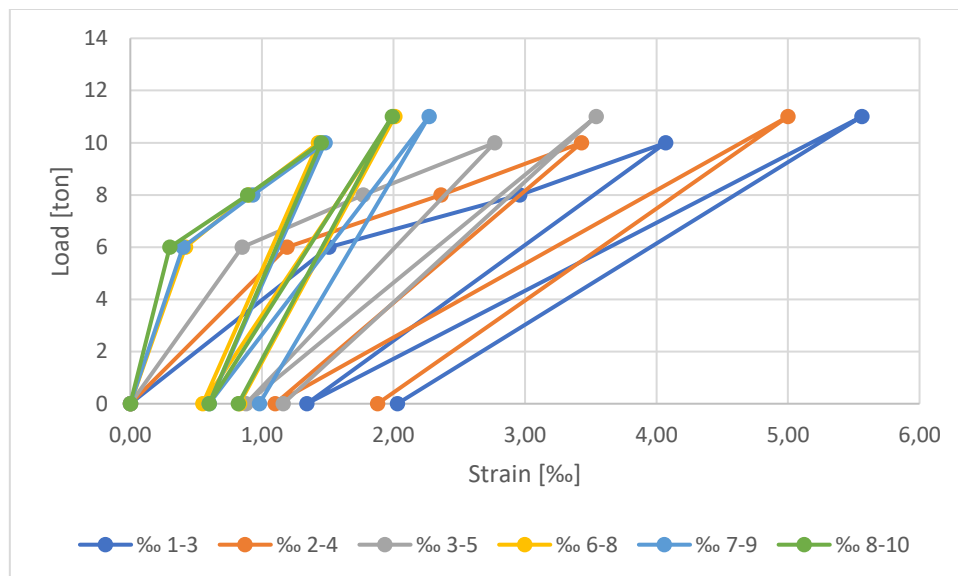


Figure 0-20. Load-strain graph HB3 + NAFEN (0.25%) + Penetron (1.6%) Beam XIII

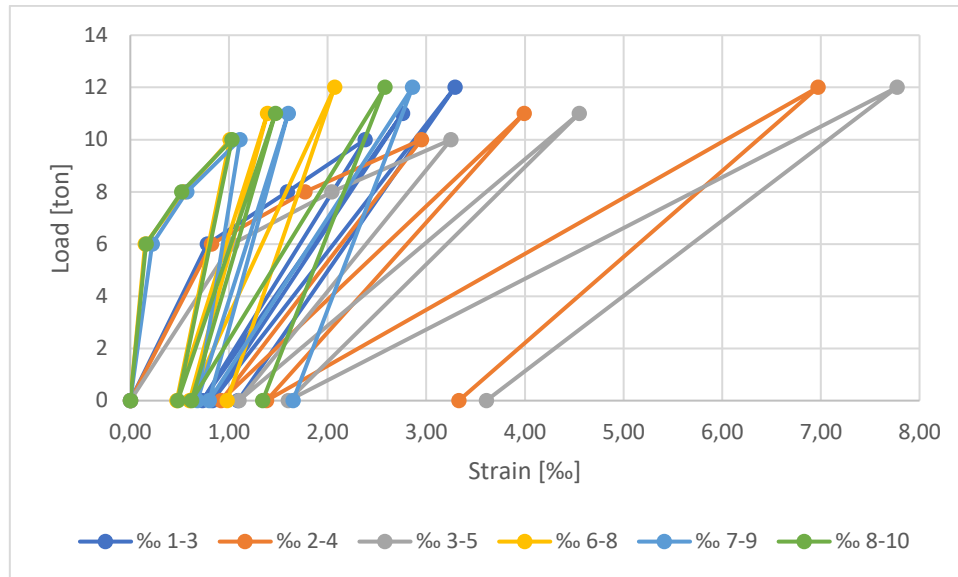


Figure 0-21. Load-strain graph HB3 + NAFEN (0.25%) + Penetron (1.6%) Beam XIV

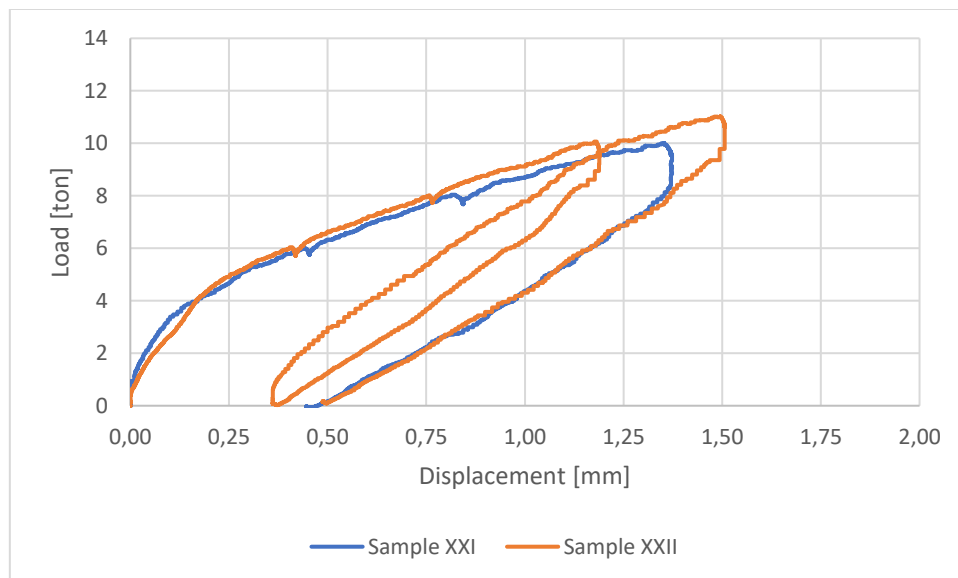


Figure 0-22. Load-displacement graph HB3 + CNF/CNC (0.15%)

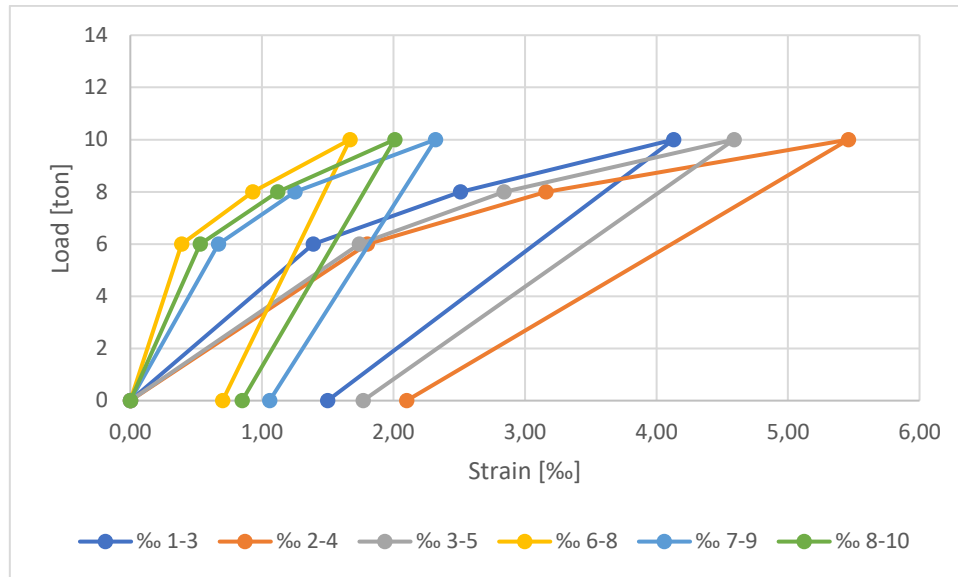


Figure 0-23. Load-strain graph HB3 + CNF/CNC (0.15%) Beam XV

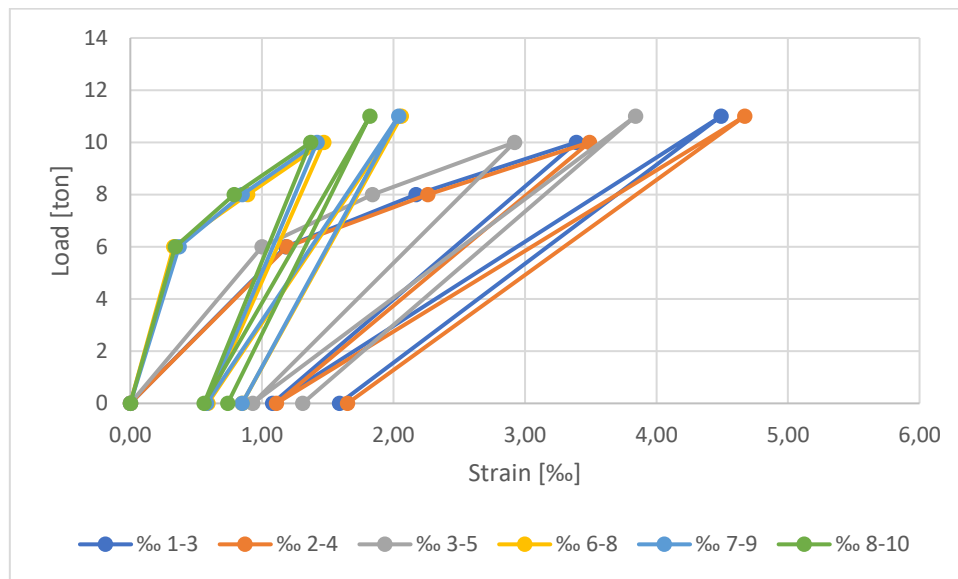


Figure 0-24. Load-strain graph HB3 + CNF/CNC (0.15%) Beam XVI

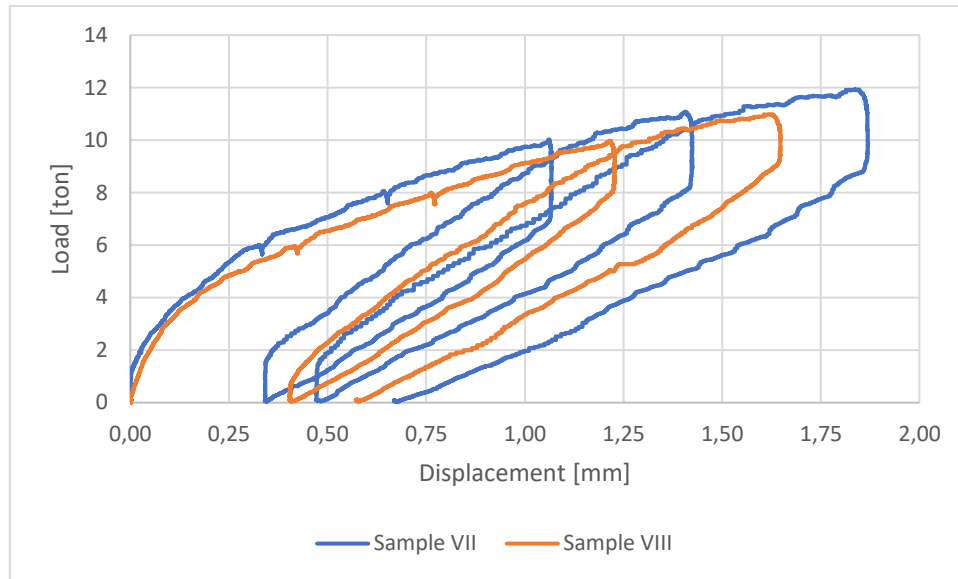


Figure 0-25. Load-displacement graph HB3 + CNF/CNC (0,15%) + Penetron (0,8%)

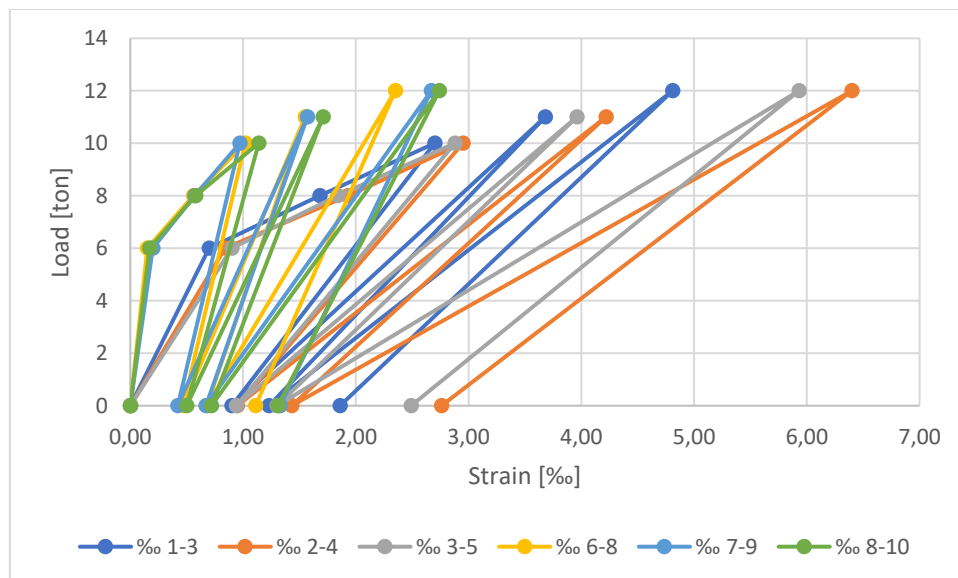


Figure 0-26. Load-strain graph HB3 + CNF/CNC (0.15%) + Penetron (0.8%) Beam XVII

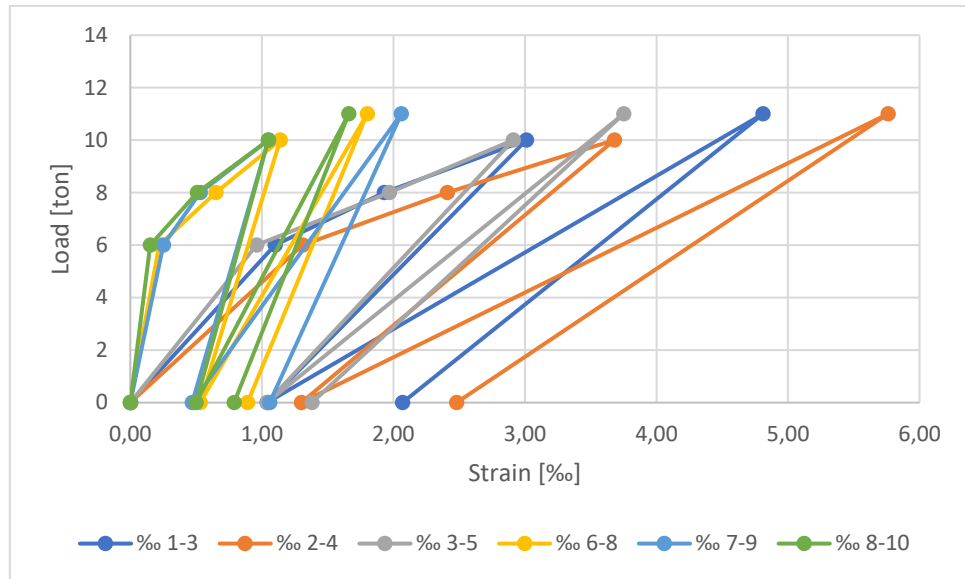


Figure 0-27. Load-strain graph HB3 + CNF/CNC (0.15%) + Penetron (0.8%) Beam XVIII

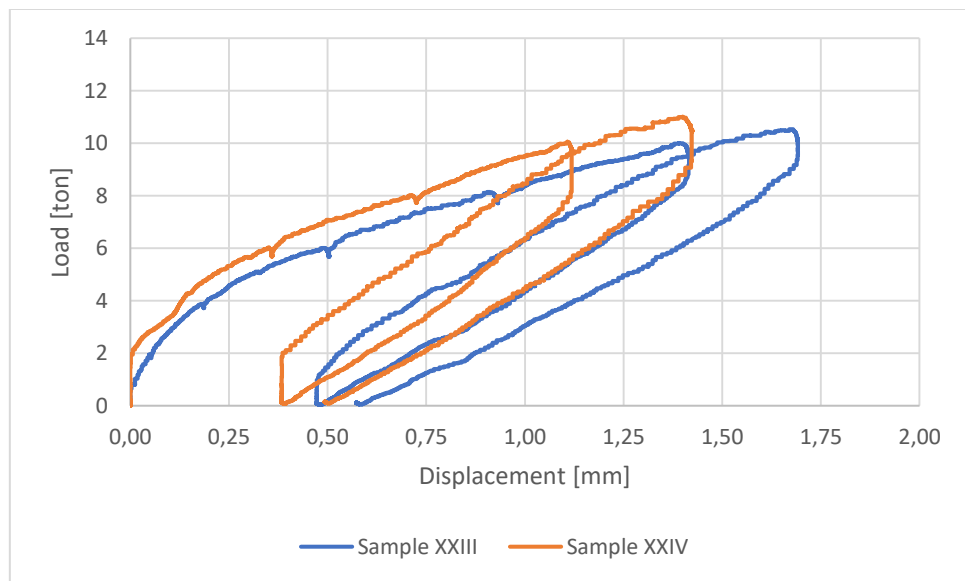


Figure 0-28. Load-displacement graph HB3 + CNC (0,15%) + Penetron (0,8%)

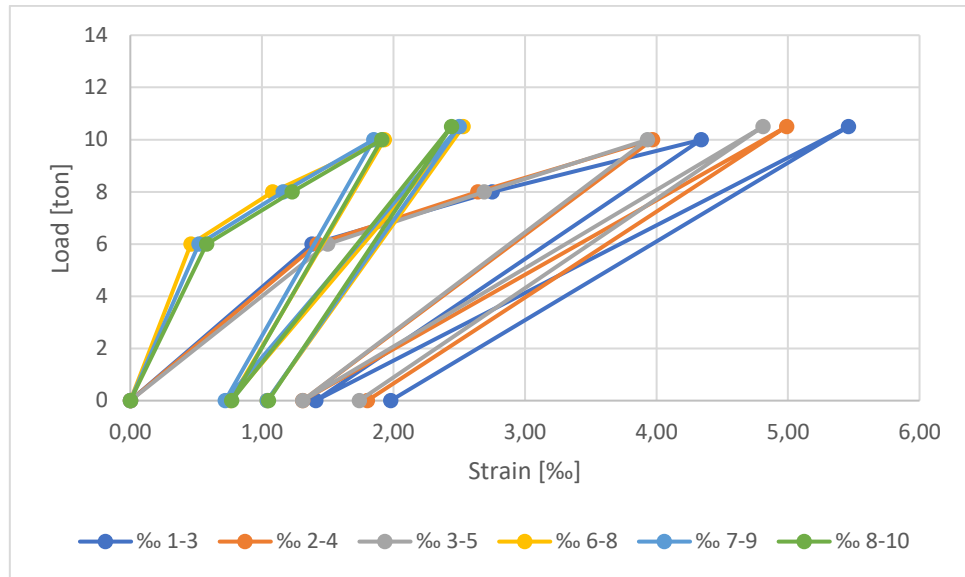


Figure 0-29. Load-strain graph HB3 + CNC (0.15%) + Penetron (0.8%) Beam XIX

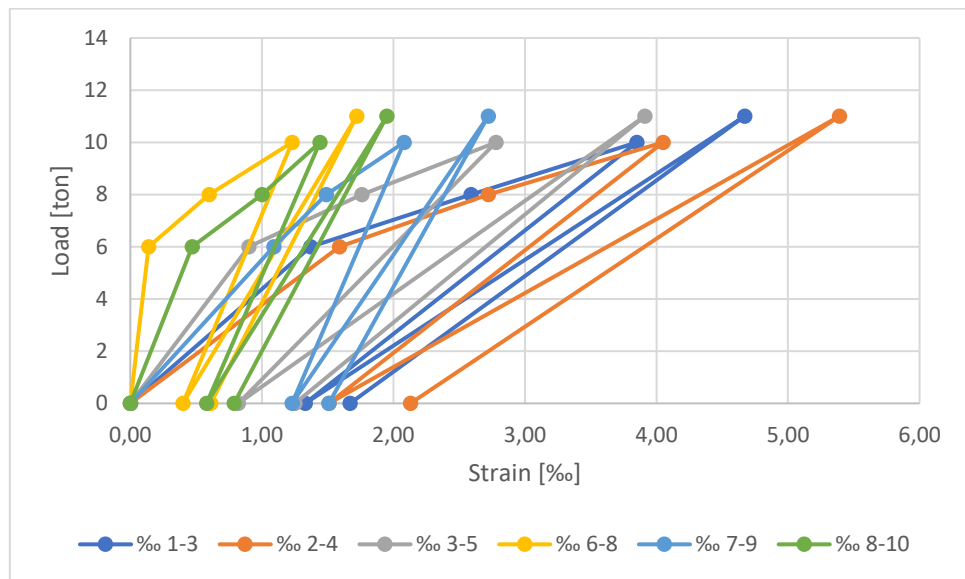


Figure 0-30. Load-strain graph HB3 + CNC (0.15%) + Penetron (0.8%) Beam XX



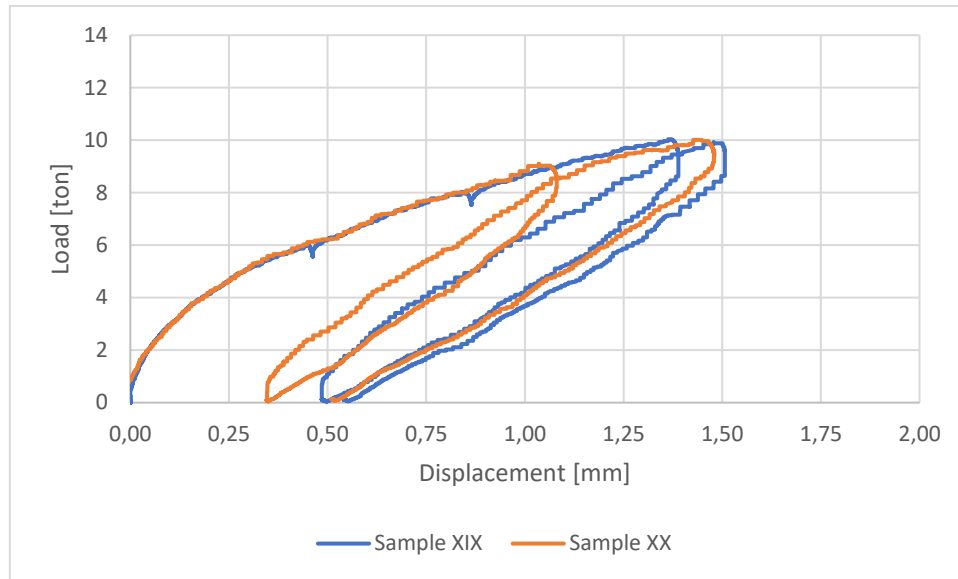


Figure 0-31. Load-displacement graph HB4 + Penetron (0,8%)

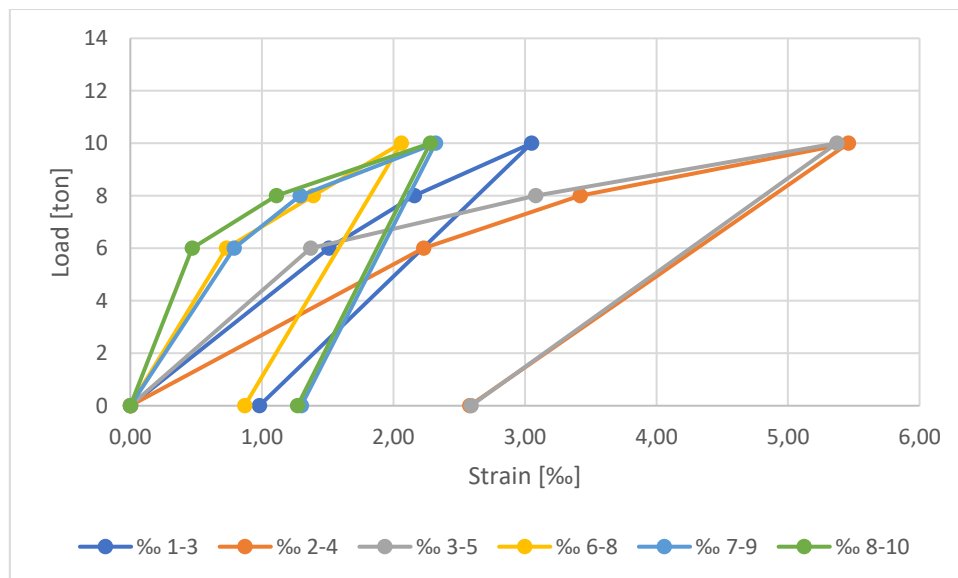


Figure 0-32. Load-strain graph HB4 + Penetron (0.8%) Beam XXI

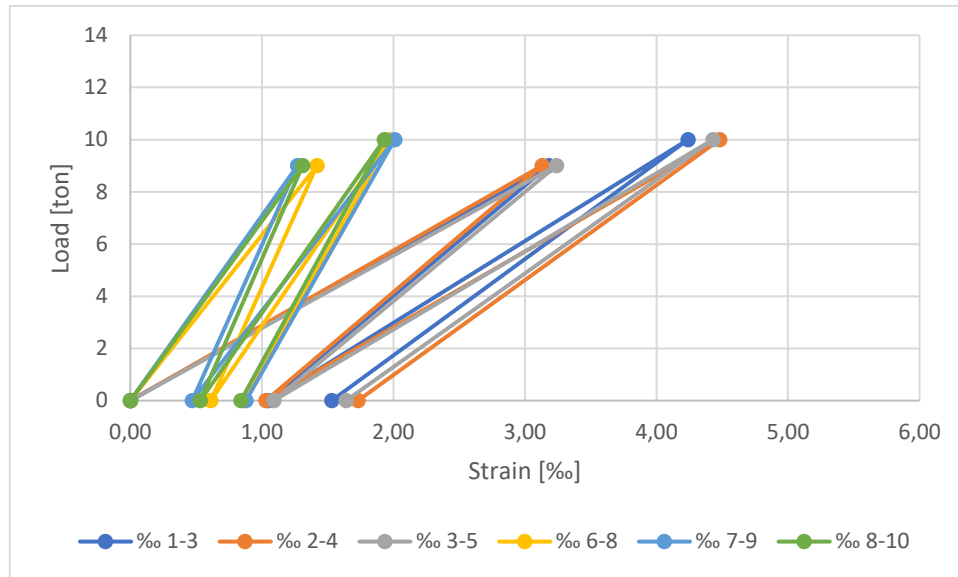


Figure 0-33. Load-strain graph HB4 + Penetron (0.8%) Beam XXII

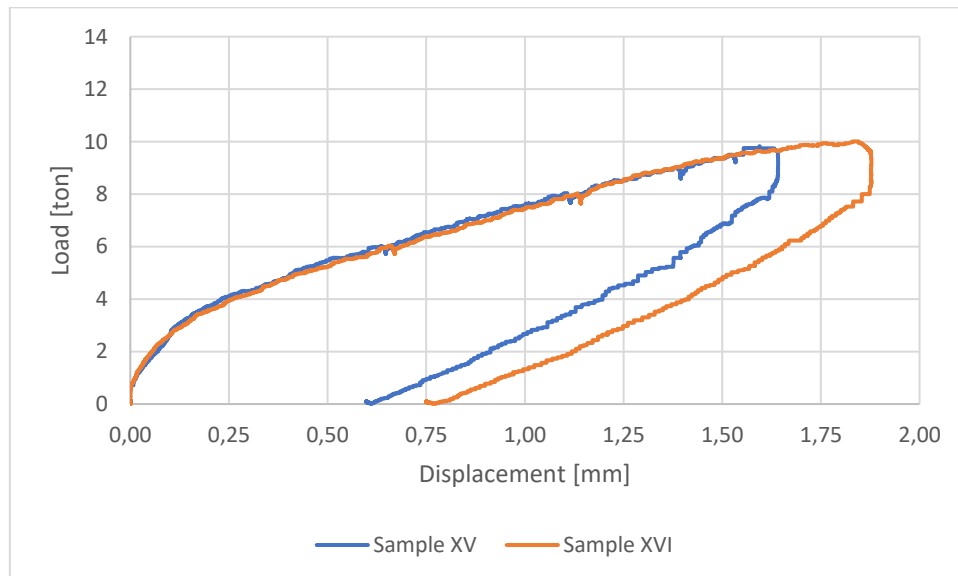


Figure 0-34. Load-displacement graph HB4 + NAFEN (0,25%) + Penetron (0,8%)

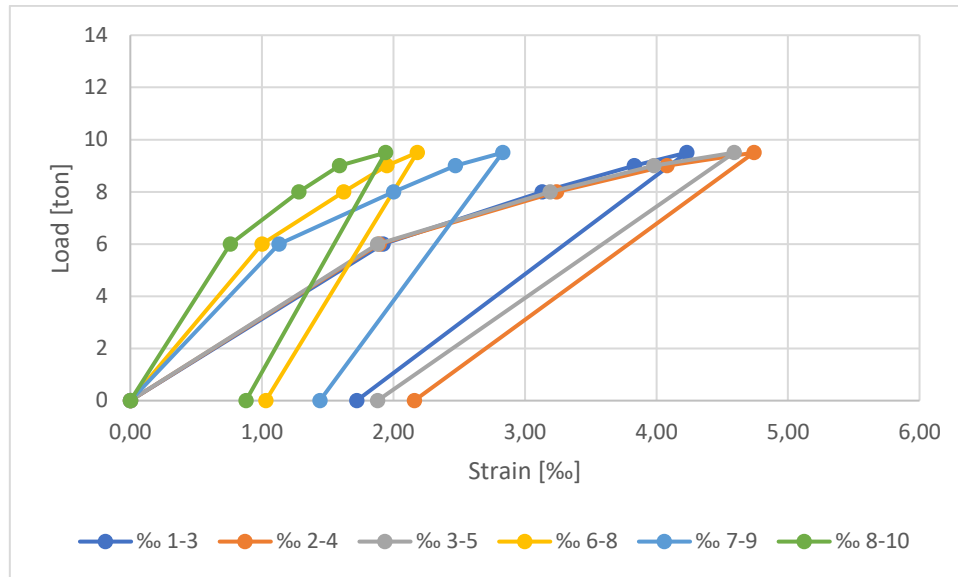


Figure 0-35. Load-strain graph HB4 + NAFEN (0,25%) + Penetron (0,8%) Beam XXIII

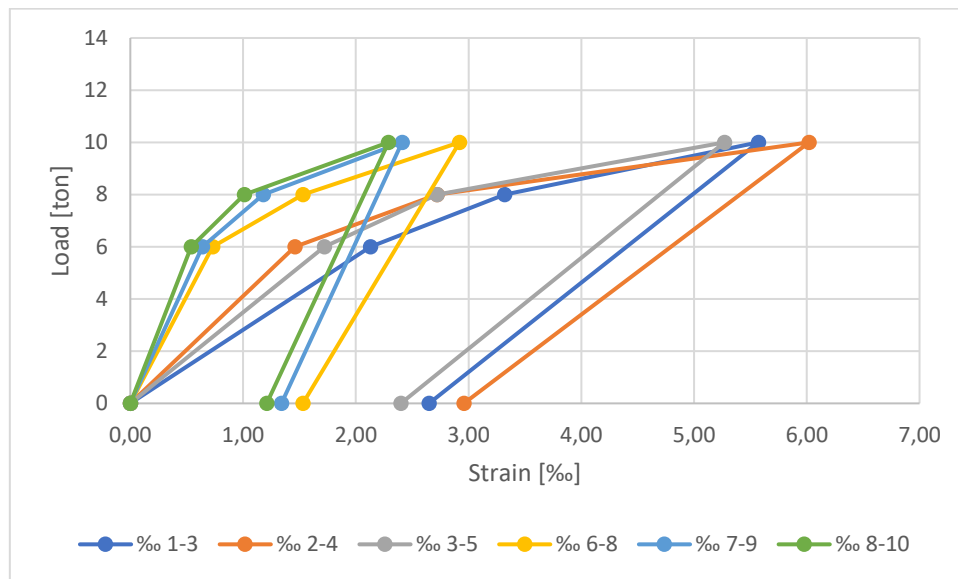


Figure 0-36. Load-strain graph HB4 + NAFEN (0,25%) + Penetron (0,8%) Beam XXIV

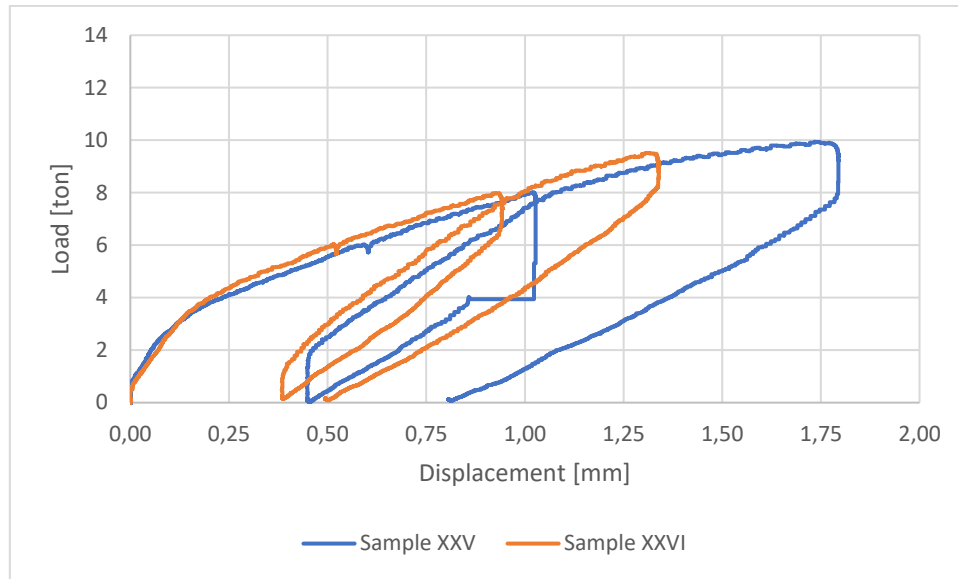


Figure 0-37. Load-displacement graph HB4 + CNC (0,15%) + Penetron (0,8%)

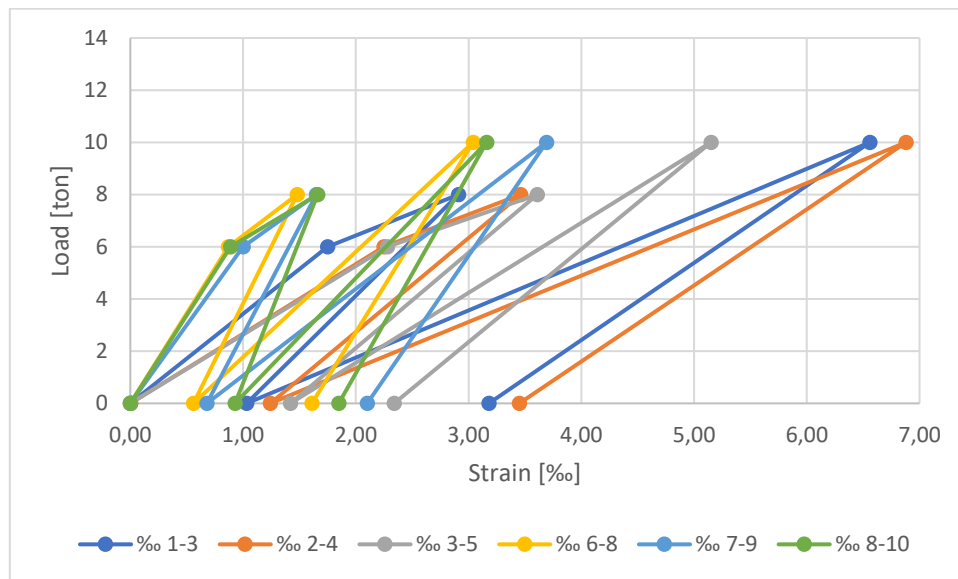


Figure 0-38. Load-strain graph HB4 + CNC (0,15%) + Penetron (0,8%) Beam XXV

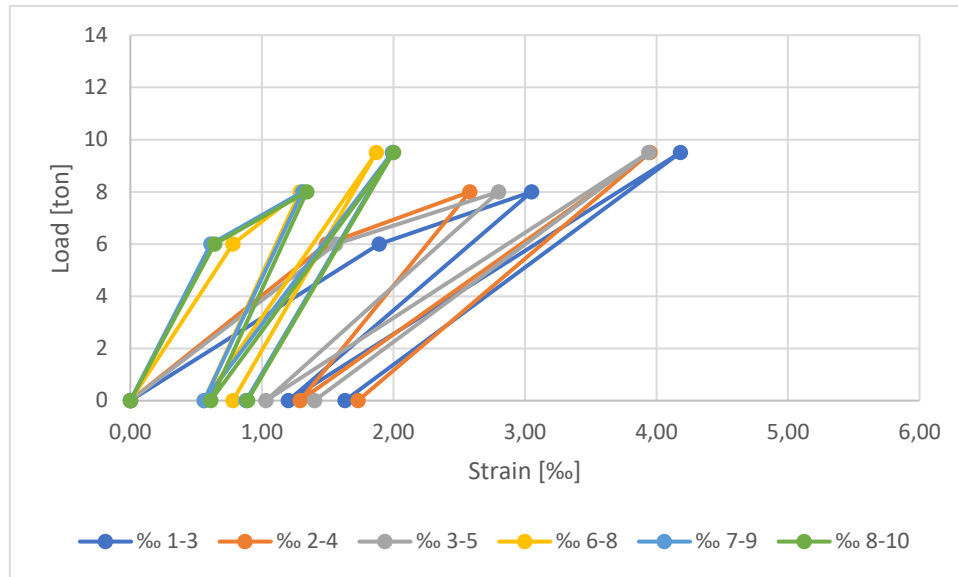


Figure 0–39. Load-strain graph HB4 + CNC (0,15%) + Penetron (0,8%) Beam XXVI

## Appendix 2. Chloride penetration results

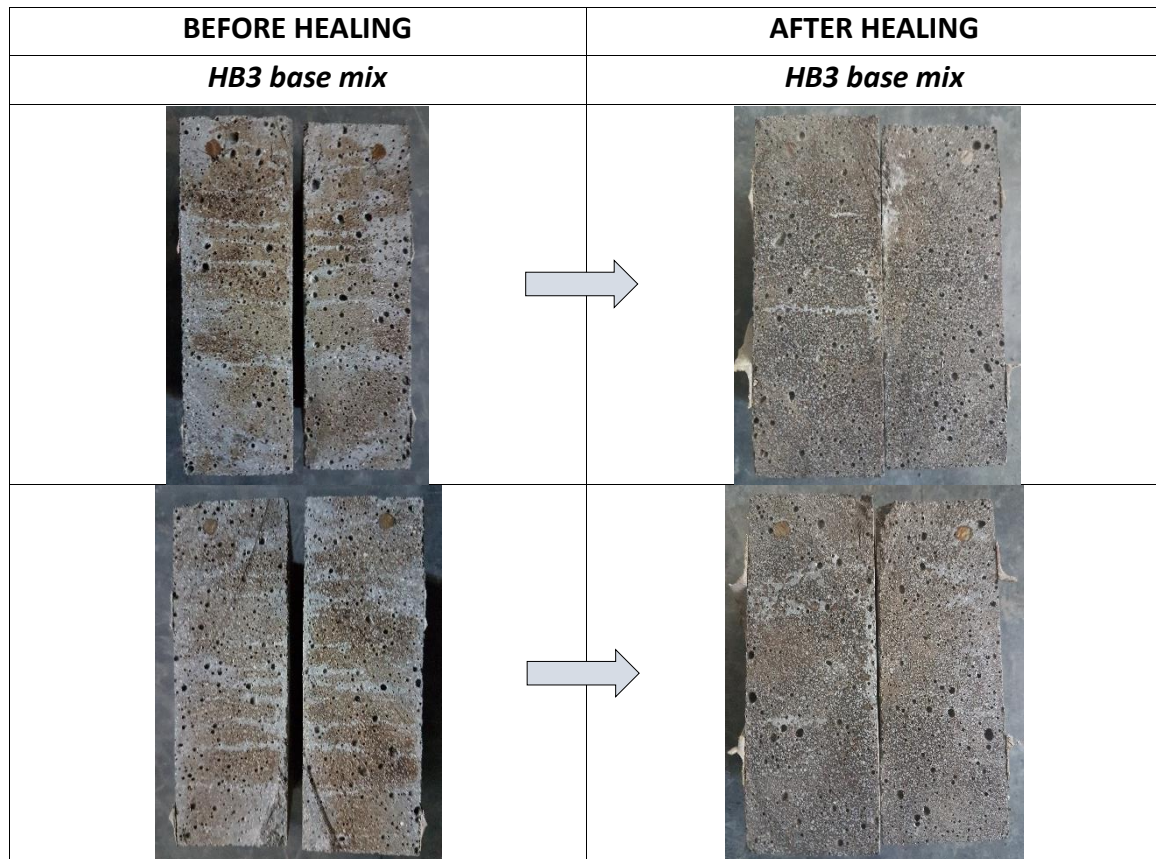
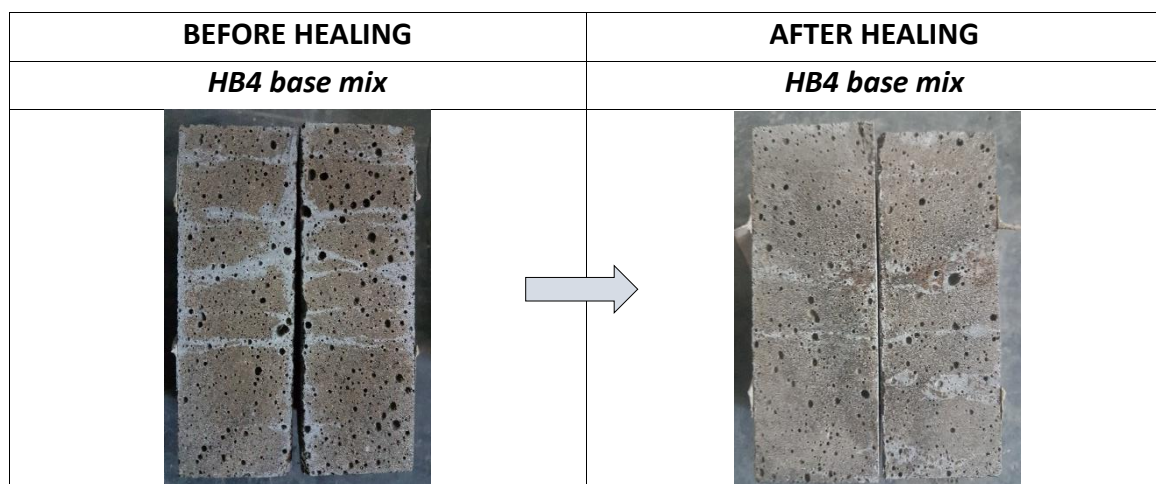


Figure 0-1. Self-healing outcome HB3



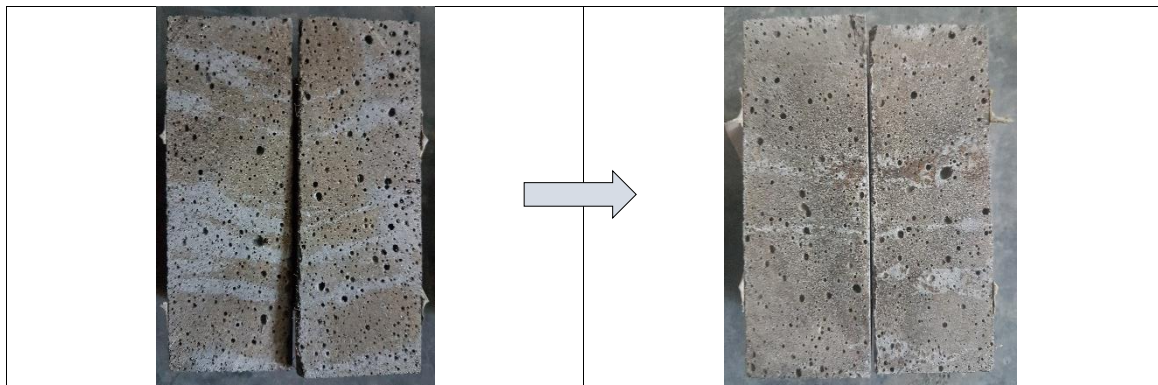


Figure 0-2. Self-healing outcome HB4

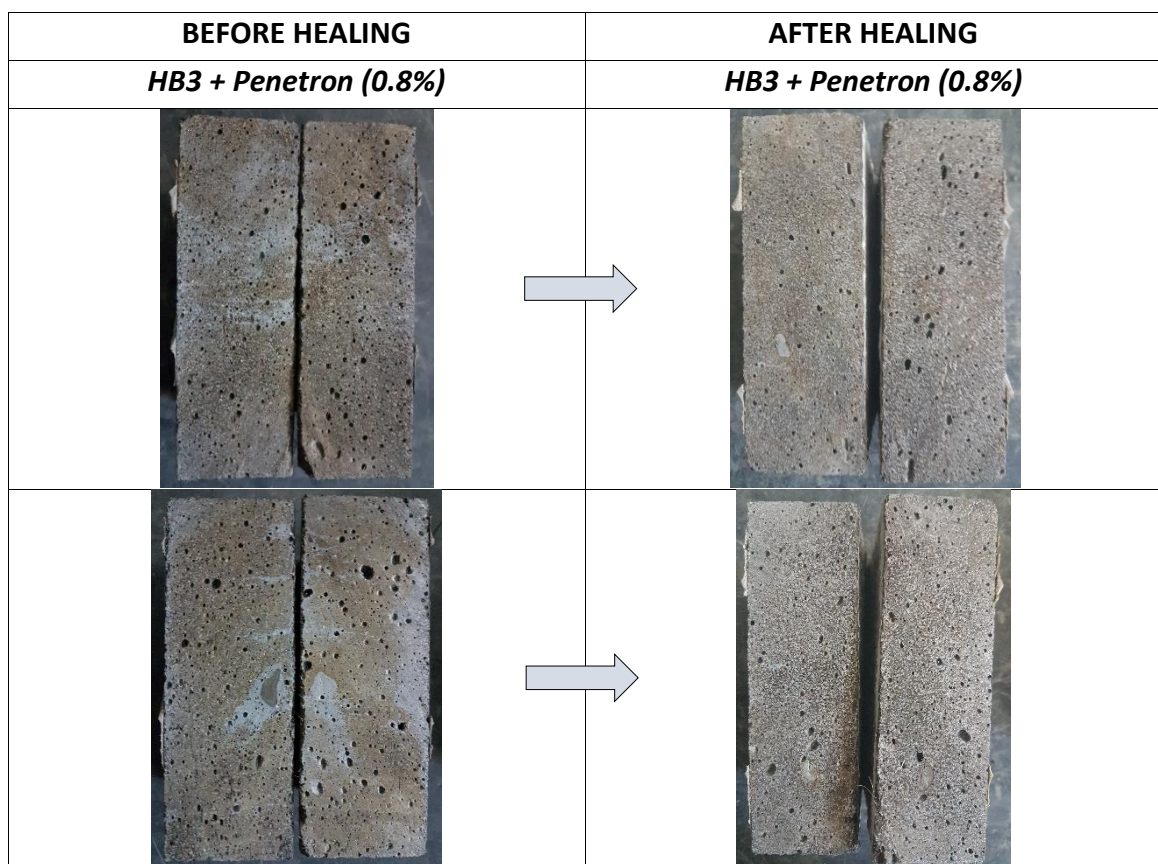


Figure 0-3. Self-healing outcome HB3 + Penetron (0.8%)









BEFORE HEALING		AFTER HEALING	
<b>HB3 + NAFEN (0.25%) + Penetron (0.8%)</b>		<b>HB3 + NAFEN (0.25%) + Penetron (0.8%)</b>	
			
			

Figure 0–4. Self-healing outcome HB3 + NAFEN (0.25) + Penetron (0.8%)

BEFORE HEALING		AFTER HEALING	
<b>HB3 + NAFEN (0.25%) + Penetron (1.6%)</b>		<b>HB3 + NAFEN (0.25%) + Penetron (1.6%)</b>	
			



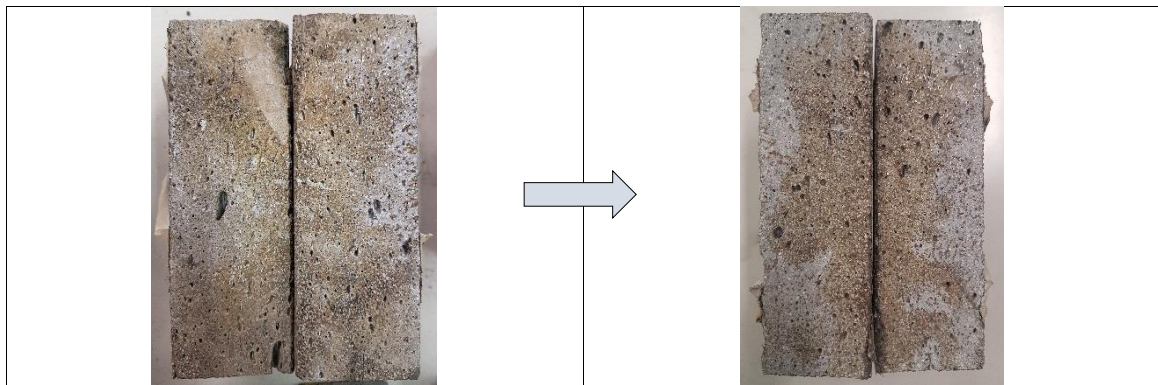


Figure 0-5. Self-healing outcome HB3 + NAFEN (0.25) + Penetron (1.6%)

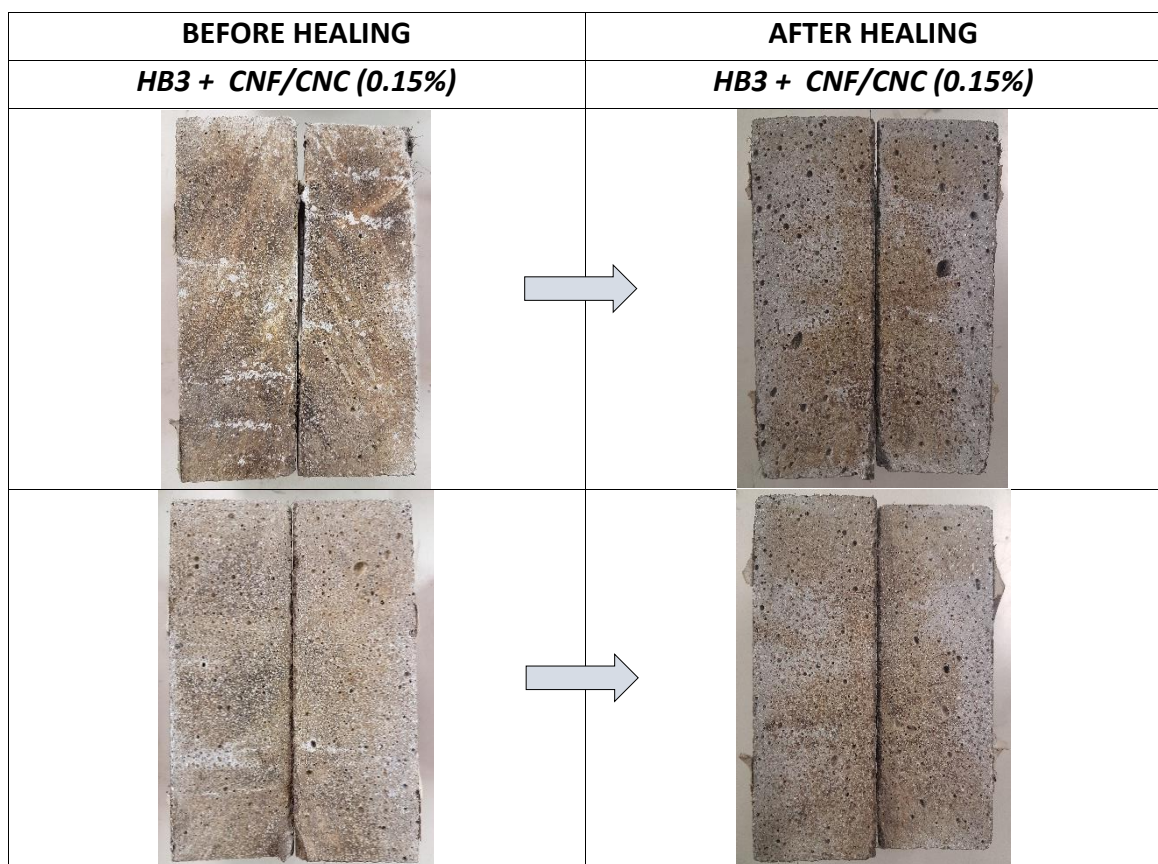


Figure 0-6. Self-healing outcome HB3 + CNF/CNC (0.15%)



Figure 0-7. Self-healing outcome HB3 + CNF/CNC (0.15%) + Penetron (0.8%)

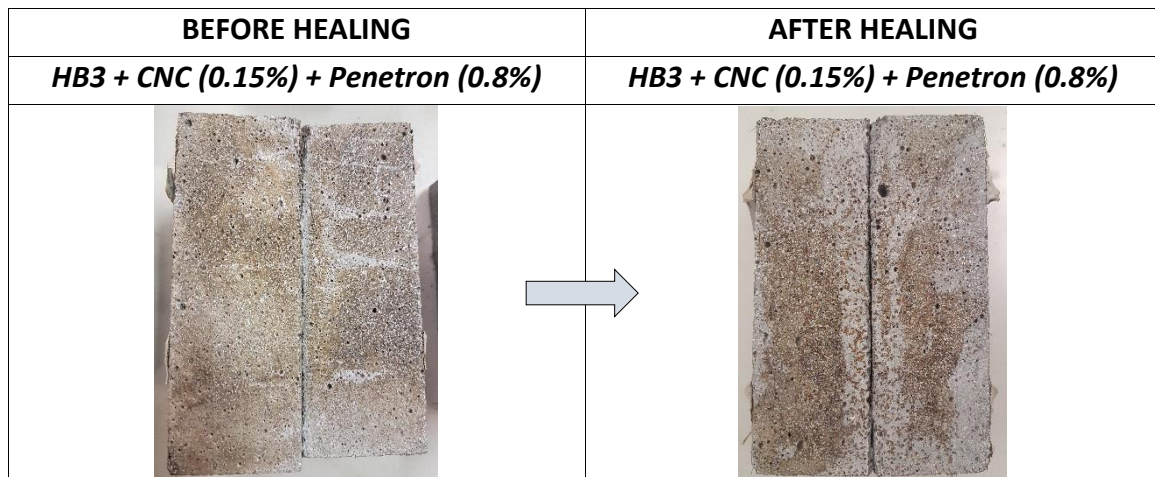




Figure 0-8. Self-healing outcome HB3 + CNC (0.15%) + Penetron (0.8%)



BEFORE HEALING		AFTER HEALING	
<b>HB4 + Penetron (0.8%)</b>		<b>HB4 + Penetron (0.8%)</b>	
			
			

Figure 0–9. Self-healing outcome HB4 + Penetron (0.8%)

BEFORE HEALING		AFTER HEALING	
<b>HB4 + NAFEN (0.25%) + Penetron (0.8%)</b>		<b>HB4 + NAFEN (0.25%) + Penetron (0.8%)</b>	
			

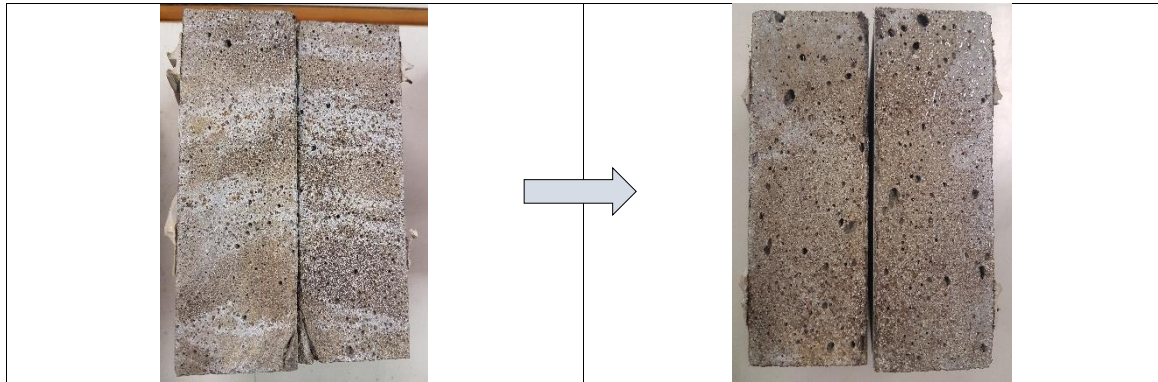


Figure 0-10. Self-healing outcome HB4 + NAFEN (0.25%) + Penetron (0.8%)




BEFORE HEALING		AFTER HEALING	
HB4 + CNC (0.15%) + Penetron (0.8%)		HB4 + CNC (0.15%) + Penetron (0.8%)	
			
			

Figure 0-11. Self-healing outcome HB4 + CNC (0.15%) + Penetron (0.8%)